SEMICONDUCTOR-BASED HYBRID PLASMONICS

by

Mohamed Eldlio

Submitted in partial fulfillment of the requirements
for the degree of Doctor of Philosophy

at

Dalhousie University
Halifax, Nova Scotia
May 2017

This thesis is dedicated to the soul of my father, Saad Eldlio, for whom I call on Allah for forgiveness and mercy.

Table of Contents

List of Tables

List of Figures

Abstract

As the typical size of electronic devices approaches the nanometer range, the size mismatch between such devices and optical components—which are typically in the micrometer range—poses a challenge for the two technologies integration on the same chip. For conventional dielectric waveguides, the mode cannot be confined to sizes smaller than half the wavelength due to the diffraction limitation. One possible and promising technological development to resolve this issue is the so-called surface plasmon polaritons (SPPs). Given the growing importance of optical plasmonics in semiconductors for a wide variety of applications; it is essential to devise a modal which is directly interpretable in physical terms. In the optical regime metals have a complex permittivity, which means that SPPs suffer from large propagation loss.

To mitigate this loss, semiconductors can be used instead of metal, but their application is limited in the far-infrared regime because the permittivity has a negative real part. Semiconductors are therefore promising materials for developing efficient terahertz (THz) waveguides. The frequency of a THz wave occupies the electromagnetic spectra between microwave and infrared ranges and acts as a bridge. As a result THz semiconductor-based hybrid plasmonics has become one of the most promising applications in the plasmonics field.

This thesis presents a theoretical study and develops the physics and mathematics of SPPs in semiconductors at optical frequencies, taking into account the different properties of these semiconductors. It also investigates the modal properties of a hybrid plasmonic waveguide operating at a THz regime in different types of structures. The analytical results are compared to conventional hybrid waveguides previously reported. Numerical solutions are also obtained for proposed novel hybrid terahertz plasmonic waveguide structures. Moreover, a theoretically study of the optical properties of a superconductor-insulator-superconductor waveguide both at THz and telecommunication frequencies were performed.

These novel studies provide insight into the fundamental nature of optical plasmon semiconductors. A primary focus of the thesis is geometries which exhibit the capability of supporting SPPs.

List of Abbreviations Used

A	Normalized mode area
CVD	Chemical Vapor Deposition
CMOS	Complementary metal–oxide–semiconductor
CMT	Coupled Mode Theory
D	Diameter
FEM	Finite Element Method
FoM	Figure of merit
FDTD	Finite-Difference Time-Domain
FEM	Finite Element Method
HMC	Hybrid mode characteristics
HPTWG	Hybrid plasmonic terahertz waveguide
HPW	Hybrid Plasmonic Waveguides
HSPP	Hybrid Surface Plasmon Polariton
Si	Silicon
SPPs	Surface Plasmon Polaritons
STHSPPs	Semiconductor terahertz hybrid Surface Plasmon Polaritons
A_0	Diffraction-limited area in free space
A_{eff}	Effective mode area
e	Electron charge
$\hbar$	Plank's constant
TC	Telecommunication
TIR	Total Internal Reflection
W(r)	Energy density
β	Propagation constants
ω	Angular frequency
ω_p	Plasma frequency
λ_0	Wavelength
γ	The damping
μ	Mobility of the carriers

LR-HTSPPs	Long-range hybrid terahertz SPPs
IMI	Insulator-metal-insulator
IPC	Integrated Photonic Circuits
T_0	Room temperature
1D	One Dimensional
2D	Two Dimensional
3D	Three Dimensional
$Im(\beta)$	Imaginary part of the complex propagation constant
k_0	Wavenumber
k'	Real part of the wave number
k"	Imaginary part of the wave number
k_{spps}	Wave number of SPPs
L_c	Coupling length
L_p	Propagation length
L_{Np}	Normalized propagation length
L_{Nm}	Normalized mode length
L_m	Mode length
N	Carrier density
n	Carrier density
n_c	Refractive index of silica
n_{eff}	Effective mode index
NIR	Near infrared
NSERC	Natural Sciences and Engineering Research Council
PECs	Perfect electric conductor boundary conditions
PMC	Perfect magnetic boundary condition
r	Radius / diameter of ridge
SC	Superconductor
SCISC	Superconductor-insulator-superconductor
SiO_2	Silica
SPs	Surface Plasmonics
T	Temperature
T_m	Thickness of metal
TPX	Polymethylpentene
W_m	Total mode energy
YBCO	Yttrium-Barium-Copper-Oxide
β_e	Even propagation constants
β_0	Odd propagation constants
γ_c	Field decay coefficient in the cladding
ε_d	Permittivity of a dielectric
ε_d	Permittivity of a dielectric
ε_0	Permittivity of free space

ε'	Real part of a permittivity
ε''	Imaginary part of a permittivity
θ	Angle
v_g	Group velocity
v_p	Phase velocity
ω_o	ω_o

Acknowledgement

First and foremost, I wish to thank Allah for everything given to me. I would also like to express my sincere gratitude to my supervisor, Dr. M. Cada, for his continuous support of my Ph.D. studies and related research, and for his patience, motivation, and profound knowledge. I appreciate all of his contributions of time, ideas, and funding during my Ph.D studies. His guidance helped me throughout the research and writing of this thesis, and his demanding questions gave me the incentive to broaden my research from various perspectives.

As well, I would like to thank my committee members, Dr. Guy Kember and Dr. Mo. El-Hawary, for their insightful comments, encouragement and dedication, and for all of the invaluable things that I learned from them.

Thank you also to Dr. Youqiao Ma for the stimulating discussions and camaraderie during the evenings we were working together before deadlines, for always being there to help and encourage me, and for all the fun we had together. I would also like to thank Dr. Tatjana Gric and Franklin Che for their contributions to some of my papers, and Dr. Cada's photonics group, especially Runaqu, Vistal, Yousef Alattar, and Amal, who helped me with the writing and gave me the incentive to strive toward my goal. Also, I would like to thank Ahmed Alqallaf for introducing me to the LYX document processor, with which this thesis was written. In particular, I am grateful to Dr. Maeda Horishi for enlightening me concerning waveguide theory research. I am deeply grateful to Dr. S. Ponomarenko for his discussions and explanations of physics terms. I would like to thank Mohand Abdulahafed for helping me to get Libyan funding.

Additionally, I wish to thank my previous supervisor, Prof. Jerzy Siuzdak, at the Warsaw University of Technology, Faculty of Electronics and Information Technology (Poland), for his dedication and all of the valuable things I learned from him, as well as for his encouragement during my master's researcsh.

Special thanks is due to my mother, sisters, and brothers for supporting me emotionally and spiritually in the writing of this thesis and in my life in general. I cannot thank you enough for encouraging me, and I know that your prayers helped sustain me throughout this journey. I will never, ever forget my beloved daughters, Mariam, Masouda, and Asma, and my beloved sons, Muftah, Saad, and Mohammed. I would like to express my thanks to you for being such good girls and boys and always cheering me up. Last but not least, I would like to express appreciation to my beloved wife, Fatema, who helped me during many sleepless nights and was always my support in moments when there was no one to answer my queries.

This thesis is partially funded by NSERC (Natural Sciences and Engineering Research Council) CREATE (Collaborative Research and Education Training Experience) ASPIRE (Applied Science in Photonics and Innovative Research in Engineering) program.

Chapter 1

INTRODUCTION

1.1 INTRODUCTION

There has been significant growth recently in theoretical and experimental work related to Surface Plasmon Polaritons (SPPs). SPPs can be understood as electromagnetic waves coupled to the collective oscillation of free electrons along a dielectric-metal interface [1, 2, 3]. From the optics view, SPPs are optical modes of an interface, from an electrodynamics view, SPPs are a particular case of a surface wave, and from the solid-state physics view, SPPs are collective excitation of electrons [4]. Moreover, SPPs is longitudinal electron density waves propagating along the interface, exponentially decaying between different media. An SPP wavelength is always smaller than an incident wavelength, λ_0, due to SPP modes having a greater momentum than light of the same frequency. Therefore, SPP devices are termed as subwavelength components. The idea is to merge electronics and photonic phenomena at the nanoscale level, but at optical frequencies. To achieve this, plasmonic chips could be implemented for high data rate processing or very effective sensing applications [5].

Physically, waves arise from the interaction of the mechanical inertia of quasi-free electrons in metals and their electrostatic repulsion [6]. Mathematically, a surface plasmon is a solution to a wave equation at a planar metal-dielectric interface, taking into account that the exponential decay at optical frequencies is large (a few hundred nanometers) and positive

in a dielectric interface, whereas it is smaller (a few tens of nanometers) at metal interfaces. Therefore, the electromagnetic energy of SPPs is strongly localized in the vicinity of the surface, allowing the confinement of optical waves to the nanoscale, as illustrated in Fig. 1.1.

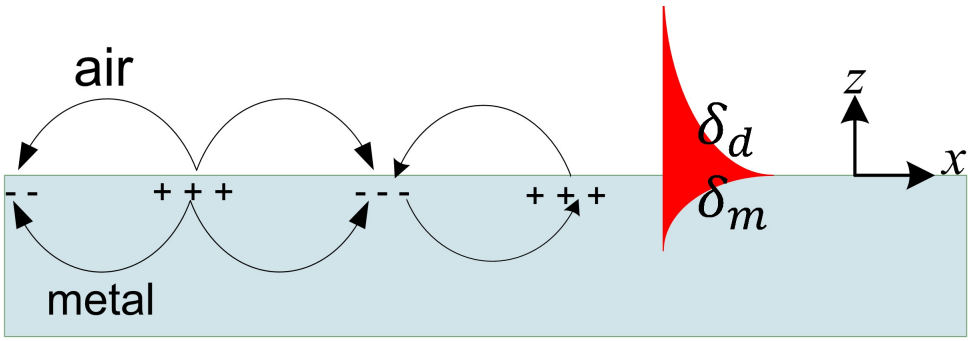

Figure 1.1: Schematic of the charges and the electromagnetic field of surface plasmon polariton propagating along a metal-dielectric interface in the x-direction together with the exponential dependence of the field, E, in the z-direction.

Moreover, the interaction between free carrier concentrations and an electromagnetic photon [7, 8] causes a phenomenon known as a Surface Plasmon (SP). The term "plasmon" is used when a metal's free electron gas carries surface charge density oscillations at optical/THz frequencies. SPs result from coupled modes, which can be used to confine light and increase electromagnetic fields at an interface between two media where at least one is conducting [9, 10]. However, real applications of plasmonics are limited by large propagation loss [11], due to the fact that in the optical regime, the noble metals (such as silver and gold) have a complex permittivity. An additional challenge is that it is difficult to deposit a crystalline superstrate onto a metal substrate. Because of imperfections in the metal film, the superstrate formed is usually polycrystalline or amorphous, which in turn increases the plasmonic loss [12]

To mitigate the issue of propagation loss a semiconductor can be used instead of a metal, because it has a smaller negative real part of permittivity. Another technique would be to

excite the SPPs at interfaces, for instance in prism geometries [2], gratings [2], structures that support SPPs such as slot waveguides [13], cavities [14], or hybrid plasmonic waveguides [15]. The hybrid plasmonic waveguide is the main focus of this work, and will be investigated in detail later.

There is enormous potential for advanced SPP applications in fields such as physics [16], biology [17], and photonics [18]. Moreover, in fact, prism-based SPP sensors are already commercially successful products [19]. However, more work needs to be done to design new types of plasmonic devices before it can be seen which applications will benefit from plasmonics.

1.2 OBJECTIVES AND CONTRIBUTIONS

The objectives of this thesis are three-fold: To find a suitable model for the dielectric function that can work especially for semiconductors; to study and develop the theoretical concept of plasmonics by using semiconductors at optical/THz frequencies instead of metals; and to design new plasmonic waveguide structures by using THz frequencies, which can be useful for practical applications. As well, comparisons using both frequencies are discussed and investigated in detail in this work. The sub-objectives are to develop different methods for optimizations and applications, and to study different structures in addition to plasmonic hybrid waveguides by using various semiconductor-dielectric structures.

To excite and propagate SPPs at low frequencies, several researchers have used semiconductors instead of metals, due to their higher permittivity [9, 10]. By changing the carrier density in a semiconductor, the permittivity can also easily change [20]. To control SPP transmission characteristics, the dielectric materials can be made of a semiconductor in all semiconductor plasmonic structures [20] for semiconductor gratings. Later in this work, I will focus on a new plasmonic device that emerged from a system that is very different

from those discussed in earlier literature. In so doing, I will analyze and investigate the system using a semiconductor without a metal interface. This system may be useful for commercial nanophotonic applications.

Consequently, the focus and interest will be concerned with controlling SPP propagation and dispersion at the semiconductor-dielectric interface. First, I will study and develop the physics and mathematics of SPPs in semiconductors at optical frequencies, taking into account the different properties of these semiconductors with losses included. Second, I will study different hybrid plasmonic waveguide structures, beginning with metal as a starting point, and then using a semiconductor instead of metal to achieve an optimal trade-off between propagation loss and small mode area. Because metals have greater permittivity at low frequencies, use of a semiconductor leads to weakly bound SPPs, limiting the use of low frequency plasmonics [7, 21, 20, 22].

The objectives of this research will be achieved through performance of the following:

1. Carrying out a detailed analysis to clarify the physical theoretical solutions for the propagation of electromagnetic waves at optical frequencies along a semiconductor/dielectric interface when losses are taken into account in the form of a complex dielectric function. A combined method using the Drude and Lorentz models for the dielectric function is proposed.

2. Investigating the modal properties of a hybrid plasmonic waveguide operating in the THz regime, composed of a silver film near which two silicon rods are placed. A detailed analysis is made of the propagation length, the effective indices, and the modal area of the supported modes. A preliminary investigation of a directional coupler is also made based on the proposed waveguides.

3. Proposing and numerically investigating a Semiconductor THz Hybrid SPPs (STH-SPPs) waveguide. A novel THz waveguide comprised of a micro-ridge placed on top of a substrate is reported. By using finite element simulation, I showed that the waveguide can achieve high confinement as well as low propagation loss, which is promising for THz circuits and sensor applications.

4. Theoretically studying the optical properties of a superconductor-insulator-superconductor (SCISC) waveguide at both terahertz (THz) and telecommunication (TC) frequencies. For the superconductor (SC), Yttrium-Barium-Copper-Oxide (YBCO) has been chosen, since YBCO shows better plasmonic behavior in the THz range as compared to other SCs. The simulation results clearly show long propagation length and deep subwavelength mode length, which are two important parameters for the SCISC waveguide. This also indicates that the SCISC waveguide has the potential to solve some problems of the conventional metal-insulator-metal waveguide, such as large attenuation loss.

In this thesis, the above objectives have been achieved. Published papers itself are attached in each relevant chapter as following:

- Drude-Lorentz Model of Semiconductor Optical Plasmons (Chapter 3).
- A long-range hybrid THz plasmonic waveguide with low attenuation loss (Chapter 4).
- A THz semiconductor hybrid plasmonic waveguide with fabrication-error tolerance (Chapter 5).

- Plasmonic properties of superconductor-insulator-superconductor waveguide (Chapter 6).

1.3 PROBLEM STATEMENT

With the growing importance of optical plasmons in semiconductors [9] across a wide variety of applications, it is essential to devise a model which is directly interpretable in physical terms and also applicable to the area of photonics. This work is focused on a topic currently being actively researched, namely optical and THz SPPs in semiconductors. In this thesis, numerical solutions and several software programs (e.g., MATLAB and COMSOL) will be used to explore the potential use of semiconductors instead of a metal-dielectric interface at optical frequencies.

By optimizing the geometrical parameters, ultra-deep confinement can be obtained. The compact form of the dispersion relation enables us to achieve affordably close to a complete understanding of what would normally be computationally costly studies involving the dispersion relation in optical plasmon semiconductors. From a physics perspective, the solutions of the dispersion relation can be used to study plasmonic pulses propagating along the material interface by integrating the corresponding wave equation.

Two of the more difficult tasks are to confine light and to increase the electromagnetic fields near the interfaces, both of which present a challenge. Understanding of the semiconductor and waveguide theory are required to gauge and design a structure with complex propagation.

In order to conduct in-depth research in this area, greater knowledge of the fields associated with SPPs is required before moving into the core of the research. I will also investigate the following problems, which I believe represent a noteworthy research gap:

1. The use of the semiconductor/dielectric interface remains challenging in the field of plasmonics because it depends on the doping concentration of the semiconductor, which also determines the number of bound and free charge carriers in the material. By considering loss in certain complex models that work for semiconductors, the plasma frequency can be determined by the effective carrier mass as well as the doping concentration. The plasma dispersion are related to the losses and affect the shape of the plasma dispersion curve.

2. The trade-off between the mode propagation length with low loss and mode confinement is not well-balanced. A tighter mode confinement means that a more transverse mode (TM) of the electromagnetic radiation field will be distributed near the conducting surface, resulting in large attenuation loss. The modal loss is quite high because the metallic structure could support the propagation of large loss plasmonic modes. This challenge limits the advantages of plasmonic devices and has delayed the use of plasmonic waveguides in practical applications, which is affecting the progress of plasmonic technology.

3. The temperature at which the superconductor-insulator-superconductor waveguide operates is disadvantageous. For instance, biologically, cells cannot survive in an environment of such low temperatures, which imposes a critical challenge in biosensor applications. Even dead cells cannot be detected at these temperatures which further impedes the progress of biosensor applications.

1.4 OUTLINE OF THE THESIS

Concerning the modeling and simulation of THz/optical semiconductor plasmonics, the thesis will proceed as follows:

- In Chapter 2, I will explore and review the fundamental theory of plasmonics, including the properties of SPPs and SP excitation. This chapter also describes the theoretical analysis of the waveguide and gives an introduction to the hybrid plasmonic waveguide. As well, a rigorous analytic model of confined light between different dielectric interfaces is investigated, based on coupled mode theory, for optical and terahertz frequencies in terms of a hybrid wave propagation. This approach provides a clear picture of the behavior of slot waveguides, concerning the permittivity of materials or effects of varying semiconductor parameters. Terahertz waves are also addressed in detail.

- In Chapter 3, I explore the idea of the propagation of electromagnetic waves at optical frequencies along a semiconductor/dielectric interface, when losses are taken into account in the form of a complex dielectric function by using the Drude-Lorentz model.

- In Chapter 4, the concept of a long-range hybrid THz plasmonic waveguide with low attenuation loss is introduced and studied analytically with a coupled mode theory. Various structures and modes in waveguides with 1D and 2D confinement are examined and the dynamics of SPPs mode, hybrid mode, and microwire mode properties are demonstrated. I numerically examine a hybrid terahertz plasmonic waveguide using two silicon microwires separated by a thin metal film. I have extended this study to double pairs of microwire in an attempt to improve waveguiding properties.

The effects of various parameters on propagation length and normalized mode area are examined in order to achieve optimal parameters. Efficient waveguide transmission is crucial for several applications and therefore the analysis is highly relevant to ongoing efforts of developing efficient terahertz waveguides.

- In Chapter 5, I design a novel semiconductor THz hybrid SPP (STHSPP) structure to optimize the trade-off between mode confinement and propagation length (L_p). An investigation into the effect of structural perturbations indicates that our proposed waveguide has good tolerance for fabrication errors (i.e., for the normalized mode, the error is less than 10% when the shift of the microwire increases from 0 to $5\mu m$. Conversely, for the propagation length, the error is less than 3%). Similarly to Chapter 4, numerous modes in waveguides with 1D and 2D confinement are examined and the dynamics of SPP mode, hybrid mode, microfluidic channel, and microwire mode properties are investigated.

- Chapter 6 presents work for a plasmonic waveguide using superconductor claddings in planar waveguide geometry. The main finding of this work is the long plasmonic mode propagation length in SC-dielectric-SC waveguide geometry (e.g., a propagation length of more than $400mm$ is emphasized for YBCO claddings at a temperature of $T = 20\ K$ and an operating frequency of about 1THz). Compared to the propagation length with other works ($\sim$tenth of mm), this propagation length shows a forty-fold improvement, which is highly significant in this field of research.

- Chapter 7 presents a conclusion of the results and contributions as well as some suggestions for future research work.

Chapter 2

THEORETICAL BACKGROUND

This chapter is an introduction to the plasmonic and THz wave. It explores the fundamental theory of plasmonics, including the properties of SPPs at optical frequencies, SP excitation and waveguides, and reviews hybrid plasmonic applications. The purpose here is to cover essential material on the topic in order to familiarize the reader with the novel properties of optical/THz plasmonics and the potential advantages of incorporating semiconductors into photonic devices. Thus, it is important to describe how SPPs could potentially support plasmonics at an interface, which has a deep confinement of light with low propagation loss. The chapter concludes with a consideration of alternative electromagnetic radiation (i.e., THz using plasmonic waveguides).

2.1 FUNDAMENTALS OF SURFACE PLASMON POLARITON

The fundamental optical excitation that is confined to a metal/dielectric interface is the SPPs as described by Ritchie [23]. The term SPPs comes from the coupled mode, which can be used to confine light and increase electromagnetic fields at an interface between two media, of which at least one is conducting [1, 2, 3]. SPPs was considered first as a ground wave or radio wave propagation by Sommerfeld in 1899 [24]. Then, in 1907, the propagation of SPPs along a surface of finite conductivity was described mathematically by Zenneck [25]. In 1902, Wood observed and explained visible light reflecting at metallic gratings [26], a phenomenon which was later established by Fano in 1941 [27].

In 1960, Ritchie provided a clear definition experimentally [23], while in 1968, Otto, [28], Kretschmann and Raether [29] proposed optical excitation of this phenomenon on metal films.

As mentioned in the previous chapter, a semiconductor can be replaced with metal to support SPPs at the interface. Plasmonics in semiconductors are taking an increasingly prominent role in the design of future silicon-based optoelectronic chips [30]. SPPs, also known as plasmonics, is a new branch of nanophotonics research [2, 10] that is sometimes confused with SP. The two can be distinguished as follows. SP is a plasmon excitation at the interface of materials, whereas SPPs is the quasiparticles of the coupled modes of EM field and a surface plasmon oscillation.

Plasmonics technology has clear advantages over electronic or photonic technologies due to the fact that plasmonics combines the benefits of both technologies (i.e., it is in the optical frequency range and at the nanoscale diameter). The field deals with the interaction of light with metal or semiconductor structures and is driven by interest in fundamental questions and their applications. Despite its promising potential, the plasmonics field still needs extensive work before it can be deemed suitable for commercialization.

In the meantime, optical plasmons have prompted widespread interest in various applications [1, 2], and plasmonic-based geometry provides important usage of metal/dielectric interfaces due to the high concentration of charge carriers in metals. This high concentration allows plasmonics to be generated in metals. In reality, however, we are not limited to metals [31, 3], as every material with a high free carrier density (e.g., semiconductors) will support plasmonics. For example, recently published papers have shown support for optical plasmons in semiconductor/dielectric interfaces [10, 9]. One of these papers is our work, which I have included in this thesis (see Chapter 3).

The optical excitation of plasmonics in semiconductors is a subject of considerable experimental and theoretical interest, as demonstrated by the rapid increase in the number of applications related to, for instance, solar cells [32], biosensors [33], physics [34], photonics [18], and engineering [35]. Unlike metals, for semiconductor the permittivity theory can be extremely complex [10], since it depends on the doping concentration of the semiconductor, which also determines the number of bound and free charge carriers in the material.

In a semiconductor, plasma frequency can be determined by the effective carrier mass as well as the doping concentration. However, the electron densities and plasma frequency of metals are much higher than those of semiconductors due to the higher permittivity that metals possess. As described above, SPPs in semiconductor/dielectric interfaces have recently received considerable interest, and the use of a semiconductor/dielectric interface to support optical plasmons has been shown numerically in [10, 9, 36].

2.2 BASIC PROPERTIES OF SURFACE PLASMON POLARITONS AT METAL-DIELECTRIC INTERFACES

This section considers a plane interface between two different media, the permittivity of a metal (ε_m), and the permittivity of a dielectric ε_d, respectively. Starting from Maxwell's equations, the wave equation can be rewritten as:

$$\frac{\partial^2 \vec{E}(x)}{\partial x^2} + \left(k\varepsilon - \beta^2 \vec{E}\right) = 0 \tag{2.1}$$

$$\frac{\partial^2 \vec{H}(x)}{\partial x^2} + \left(k\varepsilon - \beta^2 \vec{H}\right) = 0 \tag{2.2}$$

By expanding the two Maxwell source-free curl equations for the time-dependent field, one can obtain the following set of coupled equations:

$$\frac{\partial E_z}{\partial y} - \frac{\partial E_y}{\partial z} = j\omega\mu_0 H_x \tag{2.3}$$

$$\frac{\partial E_x}{\partial z} - \frac{\partial E_z}{\partial x} = j\omega\mu_0 H_y \tag{2.4}$$

$$\frac{\partial E_y}{\partial x} - \frac{\partial E_x}{\partial y} = j\omega\mu_0 H_z \tag{2.5}$$

$$\frac{\partial H_z}{\partial y} - \frac{\partial H_y}{\partial z} = -j\omega\varepsilon_0\varepsilon_r E_x \tag{2.6}$$

$$\frac{\partial H_x}{\partial z} - \frac{\partial H_z}{\partial x} = -j\omega\varepsilon_0\varepsilon_r E_y \tag{2.7}$$

$$\frac{\partial H_y}{\partial x} - \frac{\partial H_x}{\partial y} = -j\omega\varepsilon_0\varepsilon_r E_z \tag{2.8}$$

If a propagating wave is considered, a solution confined to the interface exponentially decaying in the perpendicular z-direction on both sides of the interface is given by:

$$H_y(z) = H_2 exp(i\beta x - k_2 z), z > 0 \tag{2.9}$$

$$H_y(z) = H_1 exp(i\beta x - k_1 z), z < 0 \tag{2.10}$$

Now there is sufficient information available to determine the fields within a scale factor. Let us consider the transverse magnetic (**TM**) wave, only with a magnetic field parallel to

the interface, because no solution exists for transverse electric (**TE**) waves [2, 3]. By using Equations 2.9 and 2.10 and assuming that the metal-dielectric interface lies in the *xy* plane at z=0, surface waves in the x-direction can be shown, as illustrated in Fig. 1.1.

By applying the boundary conditions at the interface, one can solve for **E** as expressed by the following relation:

$$k_m/k_d = -\varepsilon_m/\varepsilon_d \tag{2.11}$$

where, ε_d, and ε_m are the permittivity of the dielectric and metal respectively. The above expression shows that the condition for SPP existence is that it propagates at the interface of two different media, with opposite signs of dielectric permittivity. The expression for **H**y yields [2]:

$$k = \beta^2 - k\varepsilon_m \tag{2.12}$$

$$k = \beta^2 - k\varepsilon_d \tag{2.13}$$

Combining Equation 2.3 with Equations 2.12 and 2.13, and performing some simple algebraic operations finally yields the complex parallel wave vector in the x-direction and in the z-direction, given by:

$$k_x = k_x^{'} + jk_x^{''} = \frac{\omega}{c}\left(\frac{\varepsilon_m\varepsilon_d}{\varepsilon_m+\varepsilon_d}\right)^{1/2} \tag{2.14}$$

where, ω is the angular frequency, c is the speed of light in a vacuum, and ε_m and ε_d are the relative permittivities of the conductor and the dielectric respectively. The $k_x^{'}$ is a real part

which accounts for the surface plasmon wavelength and is taken to be positive. Conversely, $k_x^{''}$ is responsible for the damping decay. By replacing k_x with k_{spps} in the above equations, one can rewrite the complex wave number of SPPs as: $k_{spps} = k_{spps}^{'} + jk_{spps}^{''}$.

If $\left|\varepsilon^{''}m\right| \ll \left|\varepsilon^{'}m\right|$ by using the square root Taylor expansion to the first order, Equation 2.14 can be written as:

$$k_{spps} = k_{spps}^{'} + jk_{spps}^{''} = k_0\sqrt{\frac{\varepsilon_d\varepsilon_m}{\varepsilon_d\varepsilon_m}}.\frac{\left[1+\frac{j\varepsilon^{"}m}{\varepsilon^{'}m}\right]}{\left[1+\frac{j\varepsilon^{''}m}{2\left(\varepsilon^{'}m+\varepsilon_d\right)}\right]} \tag{2.15}$$

Then the real part that indicates the wave vector of the SPPs is:

$$k_{spps}^{'} = k_0\sqrt{\frac{\varepsilon_d\varepsilon_m}{\varepsilon_d\varepsilon_m}} \tag{2.16}$$

and the imaginary part of the wavevector that provides information about their propagation loss is:

$$k_{spps}^{''} = \frac{k_0}{2}\frac{\varepsilon_m^{''}}{\sqrt{\varepsilon_m^{'}}}\left(\frac{\varepsilon_d}{\varepsilon_m+\varepsilon_d}\right)^{3/2} \tag{2.17}$$

Equation 2.14 shows the dispersion relation, whereas ω/c is the light line. It is assumed that the near medium is a perfect dielectric, ignoring the imaginary part for the moment. From Fig. 1.1, it can be seen that the evanescent damping decay of the fields is away from the interface. As shown, at the dielectric interface the amplitude is larger than at the metal interface; in fact, it is a few hundred nanometers at the dielectric interface and tens of nanometers at the metal interface. In other words, when the imaginary part of the SPPs increases, the propagation length will decrease. Thus, the wavelength of SPPs can be written as:

$$\lambda_{spps} = \frac{2\pi}{k'_{spps}} = \frac{2\pi}{k_0}\sqrt{\frac{\varepsilon_m + \varepsilon_d}{\varepsilon_m \varepsilon_d}} \tag{2.18}$$

and the propagation length of SPPs as:

$$L_{spps} = \frac{1}{2k''_{spps}} \tag{2.19}$$

Next, it is important to consider the k vector. If ε_m is very close to ε_d, this indicates that we are close to zero. In reality, however, zero is never reached due to the imaginary part. Instead, this means that k becomes very large and ω is close to what is called surface plasmon excitation, with ω being the precise frequency. Furthermore, when k approaches infinity, then k approaches the SPPs frequency.

The question here is: Why is this so important in the optical frequency range? The answer is that when k is large, the wavelength is very short. Thus, these particular SPPs have extremely short wavelengths. They still have an optical frequency, but the wavelength becomes smaller up to the total of the magnetic field, which is extremely important for nanophotonic applications. Again, as ε_d becomes larger, the SPPs become smaller, which is part of the reason why ω_p falls below the light line for glass and air, as shown in Fig. 2.1. In other words, for higher frequencies, the SPP dispersion moves away from the light line toward larger wave vectors and shorter SPPs wavelengths. Fig. 2.1 shows ω_p, which is the plasma frequency; the light line which is $\omega = c\,k_x$; $\omega_{spp}\,air$, which is the metal/air interface; and, finally, $\omega_{spp}\,\varepsilon_d$, which is clear from Fig. 2.1 that it is a different plasma frequency than at the air/metal interface.

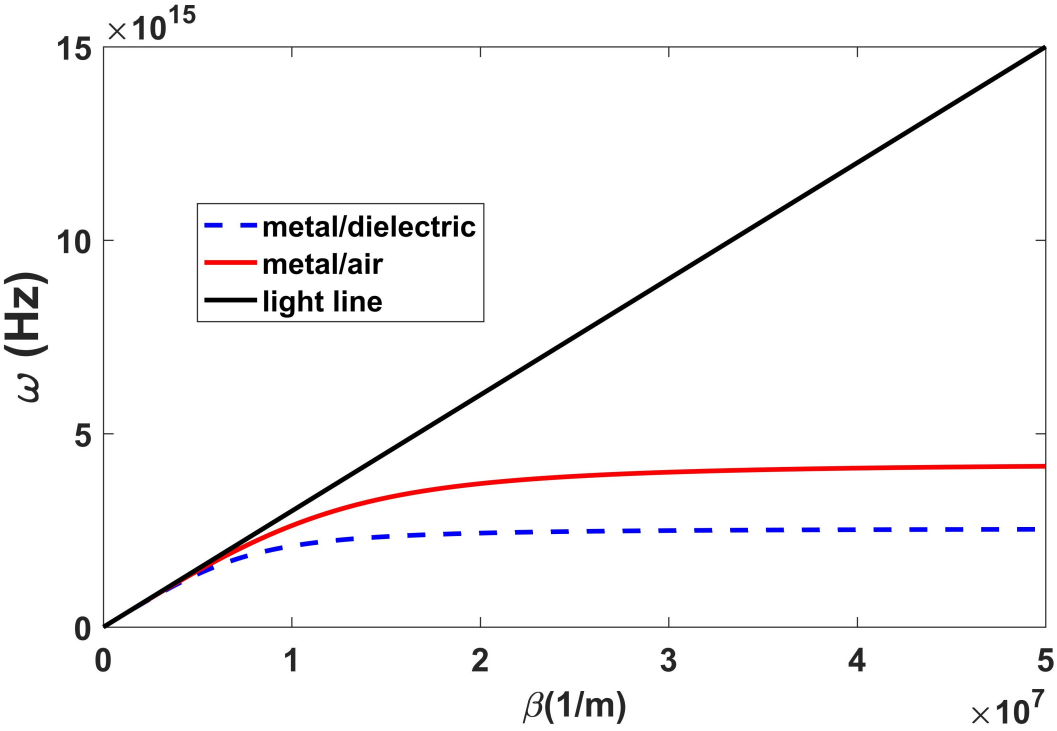

Figure 2.1: Dispersion relation of SPPs in metal/air (red curve) and in metal-dielectric (blue dash curve). The black line indicates the light line.

2.2.1 Dispersion Relation

Let us now examine the dispersion relation of SPPs. According to the Drude model for free electron gases, the Drude dielectric function is given by:

$$\varepsilon_r = \varepsilon_\infty - \frac{\omega_p^2}{\omega\,(\omega + j\gamma)} \tag{2.20}$$

where, ε_∞ is the high frequency permittivity, γ is the damping term, and ω_p is the plasma angular frequency given by [37]:

$$\omega_p = \sqrt{\frac{ne^2}{\varepsilon_0 m^* m_0}} \tag{2.21}$$

where m^*, e, and n are the electron effective mass, the electron charge, and the carrier density, respectively, and ε_0 is the permittivity of free space. To be able to account for losses for semiconductors, for example, we used a dielectric constant in the form, $\varepsilon_r = \varepsilon^{'} + j\varepsilon^{''}$. The Drude model in the z-direction will then be in the form:

$$\varepsilon(\omega, z) = \varepsilon^{'} + j\varepsilon^{''} = \varepsilon_\infty \left(1 - \frac{\omega_p^2}{(\omega^2 + \gamma^2)} + j\frac{\omega_p^2}{\omega(\omega^2 + \gamma^2)}\right) \tag{2.22}$$

For large frequencies close to ω_p, damping is negligible, so the Drude dielectric function can be stated as:

$$\varepsilon_r = \varepsilon_\infty - \frac{\omega_p^2}{\omega^2} \tag{2.23}$$

In addition, the SPP propagation velocities are different from the speed of light accrued by the SPP dispersion. It is well-known that the phase velocity is defined as $\upsilon_p = \omega/k$ and the group velocity as $\upsilon_g = \partial\omega/\partial k$. The phase velocity can then be written as $\upsilon_g = c\sqrt{\frac{\varepsilon_m+1}{\varepsilon_m}}$. The focus should thus be on the relationship between the wavelengths. However this means that the dispersion relation plasma mode cannot be matched below the light line. To match and excite these, some techniques must be performed, which will be discussed in the next section.

2.3 SURFACE PLASMON EXCITATION

As mentioned above, to generate the SPPs we need to solve the problem of the wave vector mismatch. In this section some techniques are used to excite the light below the light line. The goal is to excite the SPPs below the light line, in order to couple the light with a long wavelength at a metal-air interface. The metal must be thin enough (tens of nanometers) to allow the energy from light to be transferred into the metal.

To excite the SPPs using light, several techniques are required that make the wave vector match possible. As can be seen in Fig. 2.1, the red and blue curves are the SPP modes below the light line, indicating that there is no coupling between the far field and the SPP modes. What does this mean? If a laser (which is a far-field system) shines into a system which is typically excited or supports SPPs, these will not couple unless certain techniques are introduced.

The first technique is to excite the SPPs from a high index medium to a lower index medium. In Fig. 2.1 there is a line which is $\omega/k = c$ with respect to an equal frequency. We also have ω, which is an excitation frequency across several dispersion lines. It is now clear that we can use a high index medium that is larger than k_{spps}, which can permit excitation of a higher medium in the metal, but not directly. Indeed, it is not as easy as it sounds, and requires a specific technique.

The most widely used method is based on the direct coupling of light waves into SPP modes by using various configurations and geometries to achieve a wave vector between the matching fields [2]. Geometries which are commonly used are the Kretschman method and the Otto configuration, as illustrated in Fig. 2.2. They are different geometries for prism coupling. In 1968, Kretschmann and Raether deposited a metal directly onto a prism to solve the problem of the Otto configuration, which is an air gap between the prism and the metal [1, 2, 3]. However, before performing this geometry, we should be sure (using Kretschmann geometry) that the metal is sufficiently thin.

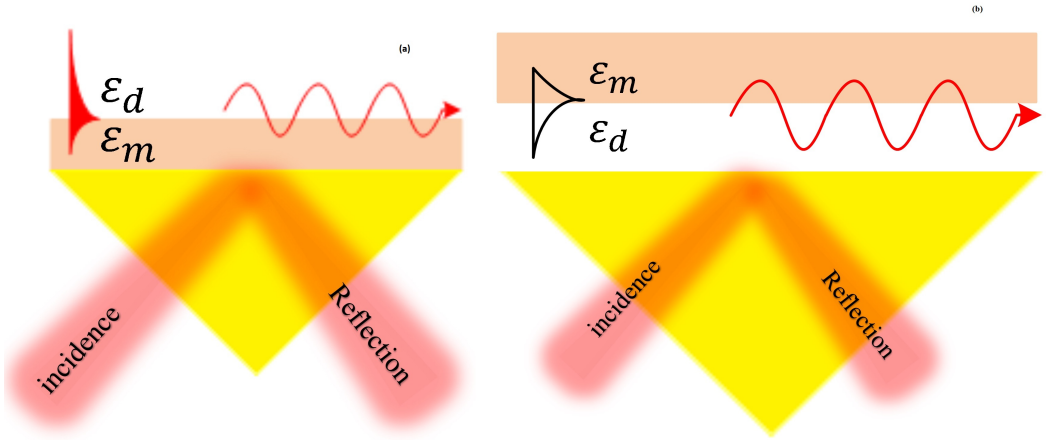

Figure 2.2: Two schematics illustrating commonly used geometries. a) Kretschmann configuration and b) the Otto configuration.

It is expected that shining light through the dielectric face of a prism toward the metal-dielectric interface (but only at the metal-air interface), will allow SPPs to be seen as the angle is changed, which in Fig. 2.2 is the angle θ. In the range of Total Internal Reflection (TIR), one can see a complete reflection of these angles. Once this is achieved, at some point we will see SPPs in a metal receiving energy, as the energy comes from the incidence of the laser beam. The prism coupling technique is also suitable for exciting coupled SPP modes in metal–insulator–metal (MIM) or in insulator-metal-insulator (IMI) three-layer systems [2].

An alternative method, when the surface is too rough for coupling the light, is to use a grating coupler [1, 2, 3]. Increasing the momentum is achieved by adding a reciprocal [2] grating lattice mode to the free space wave number. The periodicity of the represented surface is illustrated in Fig. 2.3. From this figure, it can be seen that a metal grating has a period of τ, and the polar angle is θ. Here, θ is used to describe the angle of incidence measured from the incident light of the grating. The idea is that shining the laser light on a period surface will cause the light to be diffracted by the grating if the condition [2]

$$\beta = k\sin\theta \pm mg \tag{2.24}$$

is fulfilled, where m= (1, 2, 3...) and $g = {}^{2\pi}/_{\tau}$.

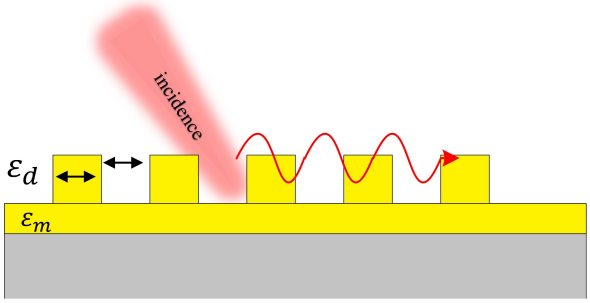

Figure 2.3: Phase-matching of light to SPPs using a grating.

2.4 Coupled Mode Theory

In light of the description of the basics of SPPs in previous sections, what will happen if the substrate is infinite and the metal is thin? From this point onward, SPP properties will be discussed in terms of Coupled Mode Theory (CMT). To provide a better understanding of CMT, the simplest example will be used, i.e., symmetric and asymmetric modes. With reference to the modes shown in Fig. 2.4, the field distributions should be either symmetric or asymmetric with respect to the center of the material chosen. The mode is symmetric (i.e., Long Range-SPPs (LR-SPPs) when the dielectric permittivity is the same in regions 1 and 3 (i.e.$\varepsilon_1 = \varepsilon_3$), and the fields are decaying exponentially into both regions. If the asymmetric mode profile has one zero crossing (i.e. ε_2), one of the modes may start to leak into the medium with a higher refractive index. In contrast, the symmetric mode profile has non-zero crossing within the material, as shown in Fig. 2.4.

Another example is illustrated in Fig. 2.5. Fig 2.5 shows the mode confinement in the slots, by setting the gap (SiO_2) as 50 nm. In the simulation, we used the measured refractive indices of 1.42 and 3.4 for SiO_2 and Si with width of 100 nm, respectively at optical frequency. Fig. 2.5 (a, c) shows the symmetric mode, while Fig.2.5 (b, d) shows the asymmetric mode. Lower indices within the gaps causes strong field enhancement in the gap region, in accordance with slot waveguide theory. As the SiO_2 gap decreases in size, the stronger mode coupling between the two slots leads to an increase in effective mode (n_{eff}) and a decrease in L_p.

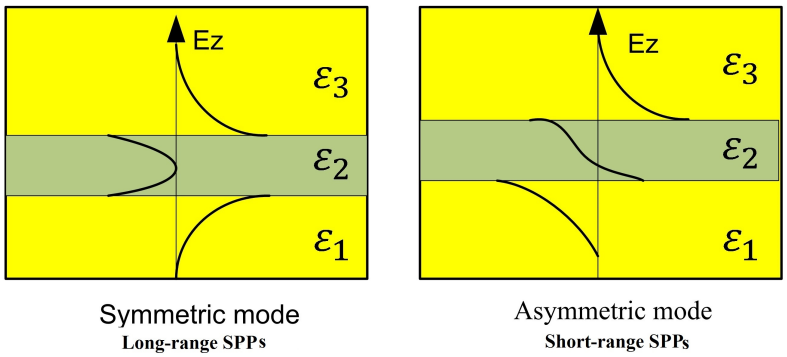

Figure 2.4: Field distributions for short-range and long-range SPPs together with the comparative behavior of the real part of the propagation constant and loss with decreasing metal.

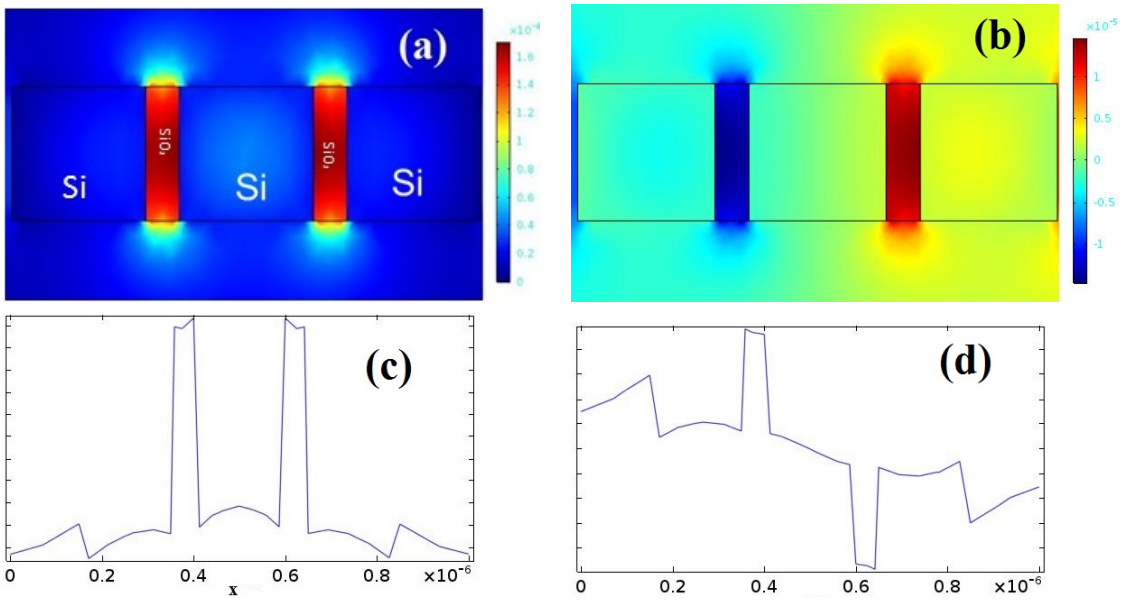

Figure 2.5: 2D energy density distributions of the proposed structure for (a) symmetric mode, (b) asymmetric mode, and (c and d) normalized *Ex* distributions along the *x*-direction.

The propagation length between two even and odd modes (symmetric and asymmetric, respectively) and the coupling length (L_c) can be expressed as:

$$L_c = \frac{\pi}{Re\{\beta_e\} - Re\{\beta_o\}} = \frac{\lambda}{2\left(Re\left\{n_{eff}^{even}\right\} - Re\left\{n_{eff}^{odd}\right\}\right)} \tag{2.25}$$

Here, λ is the wavelength, and β_e and β_o are the propagation constants (basically effective indices) of the even and odd modes, respectively. As an example, the relation between the coupling length and the size is plotted and explained in detail in Chapter 4. This shows that the mode could be supported by Hybrid Plasmonic Terahertz Waveguides (HPTWG), which is the result of coupling between SPPs and microwire waveguide modes.

2.5 PLASMONIC WAVEGUIDES

In physics, a waveguide can be understood as any guided wave structure that can confine and guide electromagnetic power efficiently from one destination to another, such as an optical fiber or a metal tube. The earliest theoretical studies of hollow tube waveguides were carried out by Lord Rayleigh in 1897 [38]. Then, 40 years later, G. C. Southworth and W. L. Barrow rediscovered the concept [39]. Interestingly, Southworth and Barrow worked for several years with no knowledge of one another. A few other types of waveguide will be discussed briefly in the following sections.

2.5.1 Dielectric Waveguides

Over the past decade, waveguides have been one of the most widely studied components of THz technology [40]. For instance, SPPs are considered to be promising waveguides for the THz regime [15, 41], but the theory of guiding electromagnetic waves has been known for a long time [24]. In 1899, the idea of guiding a circularly symmetric TM wave along a conducting wire with a small surface was considered. A complete analysis that provides a foundation for dielectric waveguides can be found in ref. [42] and is based on Maxwell's equations. There are many types of waveguide, some of which, including the slot waveguide, will be discussed below.

2.5.2 Slot Waveguide

The first work performed with the slot waveguide was done in 2003 [13, 43]. Since then, extensive research has been carried out on such waveguides as alternative candidates for integrated circuits. Fig. 2.6 (a) depicted a slot waveguide is composed of two materials that have a high refractive index separated by a low refractive index gap of a few tens of

nanometers. The electric field is greatly enhanced and confined at the high-index interfaces of the optical field in the slot region as shown in Fig. 2.6 (b). In the slot structure, the guiding mechanism is based on TIR in a high-index material surrounded by a low-index material. The typical structure of a slot waveguide, with symbols, is shown in Fig. 2.6 (a). Fig 2.6 (a) shows the mode confinement in the slots with the SiO_2 gap set to $50\,nm$, while the gap height is $100\,nm$, and the width of Si is $100\,nm$. This waveguide is described further in Chapters 4 and 5.

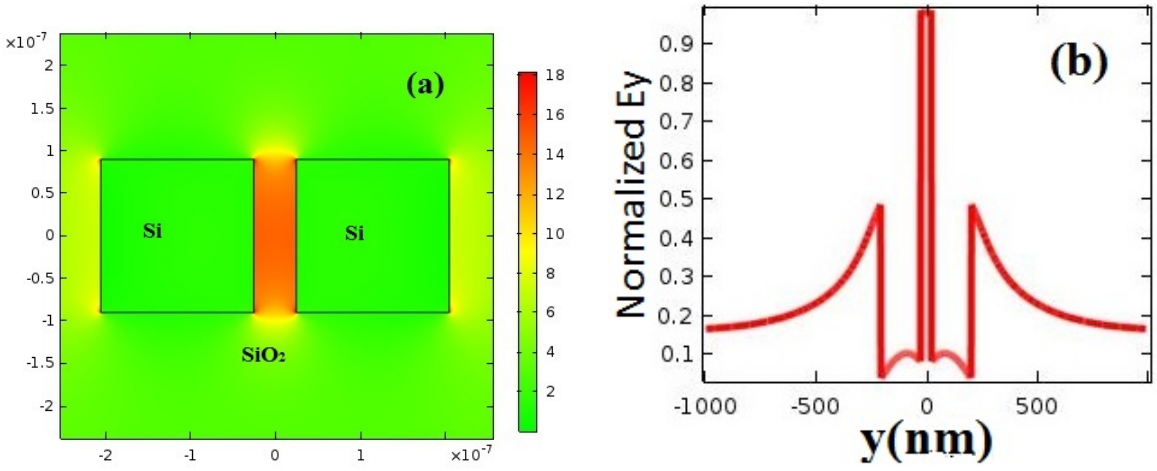

Figure 2.6: Slot waveguide geometry: a) single-slot structure showing mode distribution, b) E-field distribution in slot structure, exhibiting a high level of confinement in the low index slot region.

2.5.3 Hybrid Plasmonic Waveguide

There has been significant growth recently in theoretical and experimental work related to plasmonics. However, similarly to other technologies, the field of plasmonics still faces a critical challenge in relation to photonics. For example, the propagation loss might be very low (less than 1dB/cm) [11], but the mode size could be few hundred nanometers (which is high for a SOI waveguide); whereas the mode size of a plasmonic slot waveguide could

be less than 50*nm*, with a propagation loss exceeding 5000 dB/cm [11]. This indicates that there is a trade-off (i.e., between propagation loss and mode size), which poses a major challenge for researching plasmonics waveguides, and for their use in device and application designs. Hybrid Plasmonic Waveguides (HPWs) provide an approach for overcoming this dilemma.

Several different structures have been proposed [44, 15] in the optical range. For example, in [44], the hybrid mode is strongly confined, with sizes even smaller than 100 times the area of a limited diffraction. The subwavelength mode confinement in [44] shows that a strong interaction between the dielectric cylindrical waveguide mode and the long-range surface plasmon polariton mode of a thin metal film can be obtained.

A major contribution of this thesis, influencing its overall role in current research, is related to HPWs. The term "hybrid" here refers to the effective merging and simultaneous deployment of electronics technology, photonics, and surface plasmons or optical properties of a material [45, 46]. In other words, HPWs, where light is guided by a merging of the SPPs mode and dielectric waveguides, is likely to play a key role in the field of nanophotonics. However, in hybrid waveguides, the advantages of dielectric waveguides and the limitations of plasmonics are not easy to discern [47]. Work has been done in [15] (see Fig. 2.7) to show the relationship between mode confinement and propagation length in 2D. These researchers proposed a novel plasmonic waveguide geometry consisting of a high-permittivity semiconductor nanowire embedded in a low-permittivity dielectric near a metal surface, which constitutes a combination of a conventional dielectric slot waveguide and a plasmonic waveguide. Furthermore, they demonstrated subwavelength confinement and long-range propagation by controlling the dimensions of the geometry of a dielectric-metal interface. They also showed that strong confinement can occur in the gap between metal and nanowire, representing the coupling between the dielectric waveguide mode and

the SPP waveguide mode. For this reason, waveguides which support this type of mode are referred to as HPWs, and the optical mode is referred to as a hybrid mode.

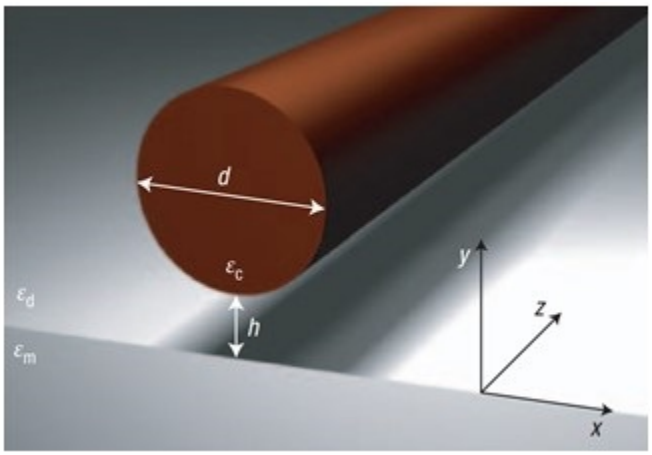

Figure 2.7: The hybrid optical waveguide [13].

A more accurate numerical approach to hybrid plasmonic waveguides (HPWGs) is presented in [47], as shown in Fig. 2.8(a) and Fig. 2.8(b). This illustrates the structure of HPWGs where there is a high-index medium separated from a metal plane by a low-index spacer. The numerical example is concerned primarily with the possibility of using HPWGs to obtain additional information about complex biological samples by analyzing the effects of various parameters of an HPWGs sensor in the Mach-Zehnder configuration. The relevant work, as shown in Fig. 2.8(c) [48], is a novel hybrid nanowedge SPP waveguide, consisting of two dielectric nanowires symmetrically located on the two sides of a thin metal film, with two identical patterned nanometer scale wedges. An ultra-deep-subwavelength mode confinement has thus been achieved.

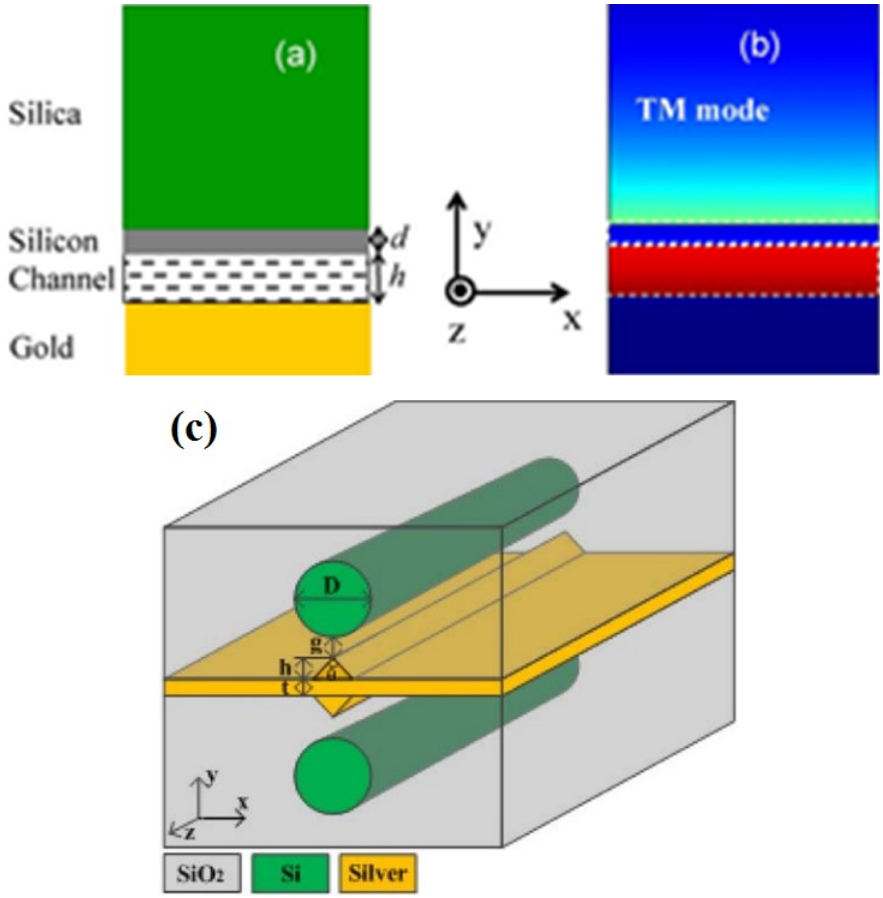

Figure 2.8: (a,b) Schematic of HPWG [44], and (c) schematic diagram of the cross-section of the proposed HNWSPP waveguide [45].

2.6 TERAHERTZ WAVES

Alternative waves that match our interests and goals is a Terahertz (THz) waves, which will be a topic of investigation in Chapters 4, 5, and 6. Structures for conventional waveguides are quite well-established, and advanced numerical tools for their analysis already exist, however THz waves are an alternative. Terahertz semiconductor plasmonics is currently attracting significant attention, and has a high potential for various technological and scientific research as well as industrial and commercial applications. Various electromagnetic spectrum frequencies are used, such as high frequency electronics microwaves,

long wavelength photonics infrared radiation, optical frequencies, etc. Terahertz bridges the gap between photonics and microwave frequencies, as shown in Fig. 2.9. In other words, the frequency of a THz wave is located in the electromagnetic spectrum between the microwave and infrared ranges [49, 46].

Moreover, THz normally refers to electromagnetic waves at frequencies ranging from 0.1 to 10 THz (corresponding to wavelengths from 30 μm to 3 mm). As a promising research area, THz technology has seen significant growth recently in theoretical and experimental work. In the optics field, the THz range corresponds to infrared rays, while in electronics, it is referred to as millimeter waves. The THz energy band is thus located between electronics and photonics. In terms of applications, terahertz waves have recently been used in various technologies [50], including plasmonics [51], and biosensors [52]. Chapters 4 and 5 will discuss in detail structures that use THz frequencies for a hybrid plasmonics waveguide. Specifically, they will present numerical solutions obtained for a novel hybrid terahertz plasmonic waveguide structure for both metals and semiconductors.

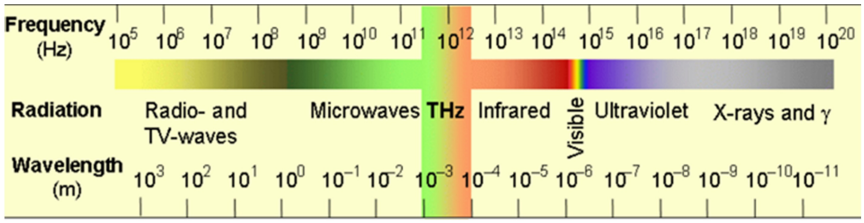

Figure 2.9: The electromagnetic spectrum.

2.6.1 Terahertz History

This band of the spectrum was investigated in 1923 by Ernest Nichols and J. D. Tear [53]. Their work succeeded in joining what they called the short electric wave spectrum to the infrared range. The possibility of using a THz technique can be found in both the microwave field and the optics field, including the nanophotonics area. The THz gap between

electronics and photonics remained unexplored until the 1980s [54]. More recently, extensive research of THz has achieved strongly confined modes in structures that use optical frequencies. For example, in [55] it is shown that shrinking the transverse size of a generic metallic structure leads to solutions with extreme field confinement. These researchers modeled and fabricated structures that support THz surface modes. The use of conventional 3D printing to create both planar and non-planar THz plasmonic waveguides is demonstrated in [56] where THz time-domain spectroscopy (THz-TDS) is used to characterize fully the propagation properties of the waveguides.

2.6.2 Applications of THz Frequencies

Before investigating the possible use of THz frequencies instead of optical frequencies, we need to address the question of why this would be beneficial. The reason is that this kind of electromagnetic wave, with frequencies that do not harm human skin, has many unique characteristics and potential applications [50].

The THz frequencies have attracted considerable attention in real-life applications. For example, THz has good penetrability for most dielectric materials, and many important processes in nature occur at THz frequencies [49, 46]. This has opened research avenues for a wide variety of applications.

This section gives examples of THz applications and briefly discusses the use of THz waves [54]. For example, biomedical and imaging applications of hybrid surface plasmon polariton (HSPPs) in the THz regime are described in [54], with spectral fingerprints, strong absorption by water, and excellent time and spatial resolution. In addition, THz-SPPs on a highly doped silicon surface that is patterned with periodic V-grooves has been experimentally demonstrated in [57]. These researchers observed that the grating structure

creates resonant modes that are confined near the surface. As well, hybrid plasmonic terahertz fibers for sensing applications [58] are described, where significant changes in modal losses can be used as a transduction mechanism.

2.7 Modeling Methods

Although the basics for SPPs is well-established, their structures are complex. Achieving an analytical solution that describes the operation of the devices is therefore problematic. To overcome this difficulty, numerical modeling should be applied to evaluate the more complex structures. There are several tools available to do this, including the Finite-Difference Time-Domain (FDTD) [59], and Finite Element Method (FEM) [60]. Here a brief discussion is provided of the most prevalent methods. The FDTD approach has rapidly become one of the most important computational methods in electromagnetics. since being proposed by Yee in 1966 [59].

2.7.1 Finite-Difference Time-Domain Method

As explained above, complex structural problems can be analyzed by using a numerical simulation. The FDTD method was developed to solve electromagnetic problems [61]. Fig. 2.10 shows the distribution of electric and magnetic field components in a Yee cell.

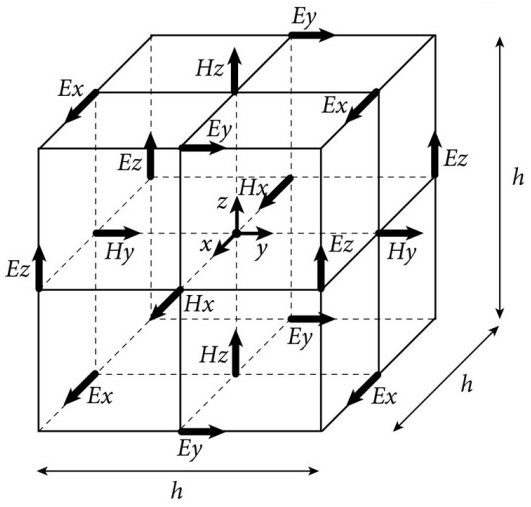

Figure 2.10: Distribution of electric and magnetic field components in a Yee cell.

In One-Dimensional (1D) free space, the time-dependent Maxwell's curl equation can be written as:

$$\frac{\partial E}{\partial t} = \frac{1}{\varepsilon_0}\nabla \times H \tag{2.26}$$

$$\frac{\partial H}{\partial t} = -\frac{1}{\mu_0}\nabla \times E \tag{2.27}$$

Starting with a simple 1D case using only E_x and H_y, Equations (2.26) and (2.27) become:

$$\frac{\partial E_x}{\partial t} = -\frac{1}{\varepsilon_0}\frac{\partial H_y}{\partial z} \tag{2.28}$$

$$\frac{\partial H_y}{\partial t} = -\frac{1}{\mu_0}\frac{\partial E_x}{\partial z} \tag{2.29}$$

It is interesting to note that the electric field is oriented in the x-direction, the magnetic field is oriented in the y-direction, and traveling is in the z-direction. Taking central difference approximations for both temporal and spatial derivations yields [59]:

$$\frac{E_x^{n+1/2}(k) - E_x^{n-1/2}(k)}{\Delta t} = \frac{1}{\varepsilon_0}\frac{H_y^n(k+1/2) - H_y^n(k-1/2)}{\Delta x} \tag{2.30}$$

$$\frac{H_y^{n+1}(k+1/2) - H_y^n(k+1/2)}{\Delta t} = \frac{1}{\mu_0}\frac{E_x^{n+1/2}(k+1) - E_x^{n+1/2}(k)}{\Delta x} \tag{2.31}$$

2.7.2 Finite Element Method

The Finite Element Method (FEM) is an alternative numerical analysis technique that can be adapted to approximate the solution to various partial differential equations. The term finite element was first used by Clough in 1960 [62]. Since then, engineers have used the method for approximate solutions of problems in several areas. Most commercial FEM software packages originated in the 1970s. The benefits of FEM are that the theory is well developed, and FEM can readily handle very complex geometry. It has been chosen for use in commercial software such as Comsol, which is used in this thesis. One of the most important features of FEM is that it can be based on structured or unstructured meshes. A structured mesh can have a grid-type topology, while an unstructured mesh is often computed by triangulation.

Let us take a two-dimensional Poisson problem with the function $u(x,y)$ to explain the fundamentals of FEM. The function $u(x,y)$ satisfies:

$$\begin{cases} -\nabla^2 u(x,y) = f(x,y) & \text{in } \Omega \\ u(x,y) = 0 & \text{in } \partial\Omega \end{cases} \tag{2.32}$$

where Ω is the simulation domain, and $\partial\Omega$ is the boundary of Ω. In addition, the function $u(x, y)$ can be expressed in the discretized form:

$$-\sum_{i=1}^{n} u_i \Phi\left(v_i, v_j\right) = \int_{\Omega} f v_i ds, \;\; j = 1, 2, \ldots n \tag{2.33}$$

The accuracy that can be obtained from any FEM is directly related to the mesh that is selected. Increasing or reducing the element order are complementary choices. Reduction is the easiest mesh refinement strategy, with element sizes reduced throughout the modeling domains [63]. For example, Fig. 2.11 shows a structure with two different mesh element sizes, a mesh with fewer elements, and the meshing sequence. Fig. 2.11 illustrates the two-dimensional (2D) geometry of the structure, which consists of a Si microwire placed on top of a ridge GaAs substrate, where the gap is assumed to be SiO_2. The blue area of the mesh indicates important design elements, remaining less dense for Si and GaAs. Fig. 2.11(a) shows a smaller number of mesh elements as a starting point. For a more a accurate result, a larger number of mesh elements is required, as shown in Fig. 2.11 (b). To obtain an accurate result, it is important to decrease the mesh size toward zero, by controlling the number of triangular elements used in the mesh, as shown in Fig. 2.11 (a, b).

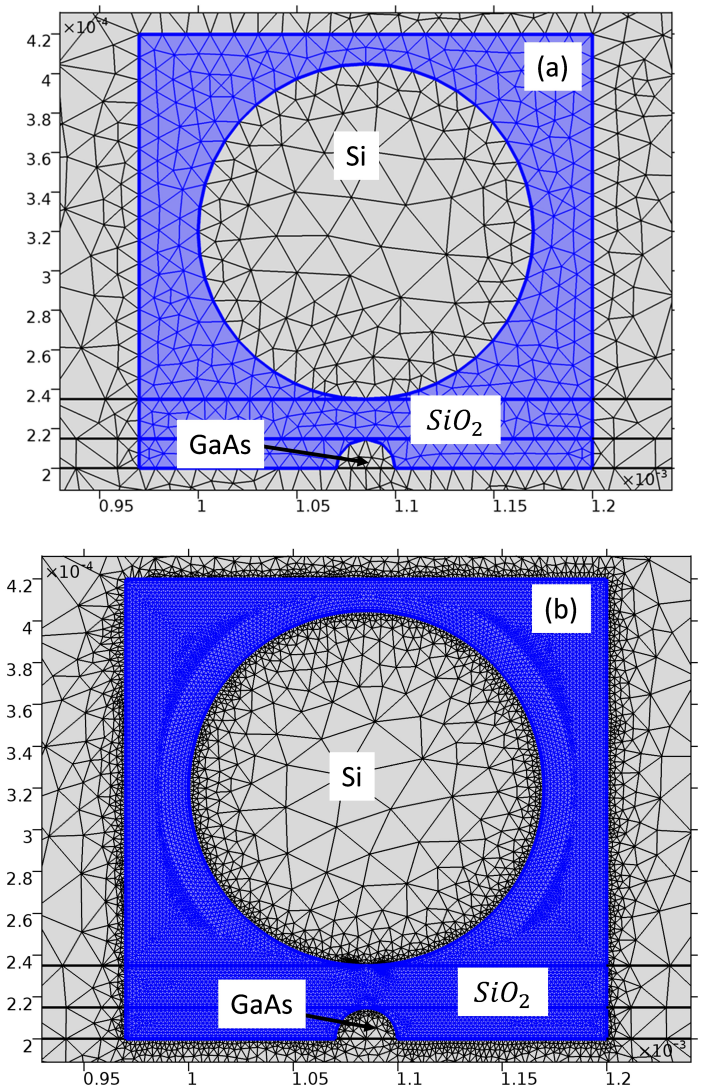

Figure 2.11: Finite element mesh (a) mesh with fewer elements., (b) more element mesh in a gap area.

Chapter 3

DRUDE-LORENTZ MODEL OF SEMICONDUCTOR OPTICAL PLASMONS

In this chapter, I use a combination method for the dielectric function, comprised of the best features (i.e., of the Drude and Lorentz models) to obtain the propagation of electromagnetic waves at optical frequencies along a semiconductor/dielectric interface. By including the loss term in both models, I am able to obtain numerical solutions for the plasmon dispersion curve of the semiconductor/dielectric interface. A detailed analysis was carried out to derive an expression for the dispersion of a silicon/air interface, by applying the new original approach[9]. This approach takes into account electromagnetic-field treatment of plasmons in semiconductor, makes it thus possible to include in the analysis that can be works other than metallic media.

This chapter discusses the equations derived for theoretical plasmon dispersion, with the aid of various models (i.e., the Drude and Drude Lorentz models). The approach described makes it possible to obtain a suitable model, which can be applied to semiconductors. Mathematically, the principal properties of propagating optical surface plasmon polaritons are represented, including the effect of a density profile of the plasma frequency in the Drude-Lorentz model, which includes losses. The Drude-Lorentz model is an improved version of the Drude model, showing strong dispersion around the resonant frequency, however, it is not an acceptable model for use with noble metals [38]. For this reason, only the Drude model will be discussed in the following chapters.

My contributions to this work consist of proposing the fundamental idea, carrying out numerical simulations and calculations of properties of the proposed dispersion, analyzing the data, and writing the first version of the manuscript. Finally, because the permission of IAENG Transactions on Engineering Technologies has been obtained, the paper itself is attached at the end of this thesis.

"Eldlio Mohamed, Franklin Che, and Michael Cada. "Drude-Lorentz model of semiconductor optical plasmons." IAENG Transactions on Engineering Technologies. Springer Netherlands, 2014. 41-49."

3.1 ABSTRACT

In this chapter a theoretical solutions are obtained for the propagation of electromagnetic waves at optical frequencies along a semiconductor/dielectric interface when losses are taken into account in the form of a complex dielectric function. A combination method for the dielectric function, comprised of the best features of the Drude and Lorentz models, is herein proposed. By including the loss term in both models, we were able to obtain numerical solutions for the plasmon dispersion curve of the semiconductor/dielectric interface. The surface plasmon waves, when excited, become short wavelength waves in the optical frequency or THz region. A silicon/air structure was used as our semiconductor/dielectric material combination, and comparisons were made to optical plasmons generated without losses. Our initial numerical calculation results show enormous potential for use in several applications.

3.2 INTRODUCTION

The fundamental optical excitation that is confined to a metal/dielectric interface is the Surface Plasmon Polariton (SPP), as described by Ritchie [23]. The term SPP comes from

coupled modes, which can be used to confine light and increase the electromagnetic fields at an interface between two media, of which at least one is conducting [1, 2, 31, 3]. Plasmonics in a semiconductor is taking an increasingly prominent role in the design of future silicon-based optoelectronic chips [30].

Optical plasmons have been shown to have many applications [1, 2] and are generally excited using metal/dielectric interfaces due to the high concentration of charge carriers in metals. SPP in semiconductor/dielectric interfaces have recently received considerable interest, and the use of a semiconductor/dielectric interface to support optical plasmons has been numerically shown in [9], albeit without the inclusion of losses. We therefore wish to take this a step further by including the loss contribution in the SPP dispersion relation. The loss is introduced through the complex dielectric function of the semiconductor. Little attention has thus far been paid to this phenomenon because it is generally very difficult to deal with. The SPP's dispersion and the resonance frequency depend on the interface configuration [1, 9].

Unlike metals, the semiconductor permittivity theory can be extremely complex, since it depends on the doping concentration of the semiconductor, which also determines the number of bound and free charge carriers in the material. In a semiconductor, plasma frequency can be determined by the effective carrier mass as well as the doping concentration. Two of the more difficult tasks are to confine light and increase the electromagnetic fields near the interfaces. The losses are related to the plasmon dispersion; however, they affect the shape of the plasmon dispersion curve near the plasma frequency.

Our goal is to develop a theoretical treatment to find a suitable model for the dielectric function of semiconductors. Starting with the Drude model, which is commonly used to describe the dielectric function of metals, we seek to modify and adapt it for semiconductors by adding the Lorentz model. We proceed by solving Maxwell's equation for the

interface between the dielectric and the semiconductor, and using the dielectric function described by the Drude-Lorentz model to obtain the dispersion relation.

This paper is organized as follows: A brief theory and background of models describing dielectric permittivity is addressed in Section 3.2. In Section 3.3, numerical results are presented and discussed, and Section 3.4 summarizes the results and draws conclusions. This is an extended and revised work of an earlier published conference paper [64].

3.3 THEORETICAL ANALYSIS

In this section, we briefly review different models, one of which is selected for our approach. The Drude model, Lorentz model, and a combination of both models (i.e., Drude-Lorentz model) are presented and discussed. Starting with a semiconductor/dielectric interface, we seek to obtain a surface plasmon wave traveling along that interface (z-axis) in the form [9]:

$$\mathbf{E}_{x,y} = \mathbf{E}_{x,y}^{d,s}\delta_{d,s} \tag{3.1}$$

$$\delta_{d,s} = e^{-j\omega t}e^{i\gamma_{d,s}}e^{j\beta z} \tag{3.2}$$

where ω is the angular frequency, and $\gamma_{d,s}$ and β are the transverse and longitudinal propagation constants, respectively. This assumed form of an evanescent wave is substituted in the Maxwell's equations:

$$\nabla\times\mathbf{H} = J_q + \varepsilon_0 + \frac{\partial\mathbf{E}}{\partial t} + \frac{\partial\mathbf{P}}{\partial t} \tag{3.3}$$

$$\nabla \times \mathbf{E} = -\mu_{\mathbf{0}} \frac{\partial \mathbf{H}}{\partial \mathbf{t}} \tag{3.4}$$

$$\nabla . \mathbf{H} = \mathbf{0} \tag{3.5}$$

$$\nabla . \left(\varepsilon_0 \frac{\partial \mathbf{E}}{\partial t} + \frac{\partial \mathbf{P}}{\partial t} \right) = \frac{\partial \mathbf{P}}{\partial t} \tag{3.6}$$

$$\mathbf{D} = \varepsilon \mathbf{E} \tag{3.7}$$

$$J = \sigma \mathbf{E} \tag{3.8}$$

To complete the development of optical plasmon in semiconductors theoretically, the notation of damping has to be described. From a basic perspective, the result of the surface plasmon dispersion equation becomes complex when losses are accounted for. This is directly related to the complex dielectric constant; in order to characterize the dispersion, damping, and excitation of the plasmon, its imaginary part needs to be included. Then the dielectric permittivity equation becomes complex. The dielectric constant is one of the most important factors to assess for future technology applications [30].

Applying the appropriate boundary conditions on both sides of the interface yields the dispersion equation below as:

$$\left(\varepsilon_S^2 - \varepsilon_D^2\right) \left[\frac{k^2 \varepsilon_S \varepsilon_D - \beta^2 \varepsilon_S - \beta^2 \varepsilon_D}{\varepsilon_S \varepsilon_D \left(\varepsilon_S + \varepsilon_D\right)} \right] = 0 \tag{3.9}$$

where,

$$k = \frac{\omega}{c} \tag{3.10}$$

ε_S is the dielectric permittivity of the semiconductor, ε_D is the dielectric permittivity of the dielectric, c is the speed of light, and k is the wavenumber. To be able to account for losses, we used a complex dielectric constant in the form:

$$\varepsilon_r = \varepsilon^{'} + j\varepsilon^{'''} \tag{3.11}$$

where, ε_r is the relative permittivity, $\varepsilon^{'}$ is a real part, and $\varepsilon^{''}$ is the imaginary part. ε_r can be represented by different models, so before presenting our proposed Drude-Lorentz model, we present the Drude model, which is commonly used for metals and highly doped semiconductors.

3.3.1 Drude Model

This model was proposed by Paul Drude in 1900 to explain the transport properties of electrons in metals [65, 66] and has also been adapted for semiconductors [12, 22]. To excite SPPs in the optical frequency range, in this work heavily doped semiconductors were used. This is because semiconductors with such heavily doped (e.g. Si) have a plasma frequency close to that of metals. The Drude dielectric function is given by:

$$\varepsilon_r = \varepsilon_\infty - \frac{\omega_p^2}{\omega\,(\omega + j\gamma)} \tag{3.12}$$

where ε_∞ is the high frequency permittivity, γ is the damping term, and ω_p is the plasma angular frequency given by [67]:

$$\omega_p = \sqrt{\frac{ne^2}{\varepsilon_0 m^*}} \tag{3.13}$$

$m*$, e, and n are the electron effective mass, the electron charge, and the carrier density, respectively, and ε_0 is the permittivity of free space.

The Drude model is the simplest classical treatment of optical properties of metals. It considers the valence electrons of the atoms to be free. In addition, it is used for semiconductors when free carrier density introduced through doping is sufficiently high to cause the semiconductor to behave similarly to a simple metal. However, in reality, this model has limitations. For example, it does not account for spatial dispersion, which exists when the dielectric constant depends on the wave-vector. Moreover, it does not account for the bound electrons and holes in semiconductors. On the other hand, it does if one replaces ε_0 with $\varepsilon_0\varepsilon_r$.

Additionally, recent work by Cada [9] shows that, for more general case, when $\varepsilon_S \neq \varepsilon_D \neq 1$, a new solution can exist only in a semiconductor/dielectric interface. This may be clearly seen in equations (5 and 6) in [9] which explain why it cannot appear in the metal. His approach, which focuses on an electromagnetic field treatment of plasmons in a semiconductor, thus makes it possible to include works in the analysis that involve semiconductor media rather than metallic media. From the derivation for a wave at an interface between two media, one dielectric and one with a concentration of free electrons, they obtained another solution for the semiconductor only. It can be shown that the solution is a constant with respect to β, as seen in the following equation (i.e., equation 5 in [9]) is:

$$\omega_3^2 = \frac{\omega_p^2}{\varepsilon_s - \varepsilon_d}, \tag{3.14}$$

and equation 6 in [9] which represents the two remaining roots in the form:

$$\omega_{1,2}^2 = \frac{\omega_p^2}{2\varepsilon_s} + \frac{\varepsilon_s + \varepsilon_d}{2\varepsilon_s\varepsilon_d}\beta^2 c^2 \pm \frac{1}{\varepsilon_s}\sqrt{\frac{\omega_p^2}{4} + \frac{\varepsilon_d - \varepsilon_s}{2\varepsilon_d}\omega_p^2\beta^2 c^2 + \frac{(\varepsilon_s + \varepsilon_d)^2}{4\varepsilon_d^2}\beta^4 c^2}. \tag{3.15}$$

3.3.2 Lorentz Model

The Lorentz model can be used to describe the frequency response of many materials and typically shows strong dispersion around the resonant frequency [21, 68, 69]. It is mostly suited for materials that have bound electrons, with the possibility of having many oscillators in a given system [65, 12, 20, 67]. The expression of the dielectric function for a single Lorentz oscillator is given by:

$$\varepsilon_r = \varepsilon_\infty + \frac{\Delta_\varepsilon \omega_p^2}{-\omega^2 + j\gamma\omega + \omega_0} \tag{3.16}$$

where ω_0 is the resonance frequency and is considered to be equal to an energy band gap of a semiconductor. Δ_ε is a weighting factor given by $\Delta_\varepsilon = \varepsilon_{st} - \varepsilon_\infty$, with ε_{st} being the static permittivity. As mentioned, the Lorentz model usually shows strong dispersion around the resonant frequency [67, 21] and is valid only when the photon energy is well below the band gap of the semiconductor. Thus, it cannot be used alone to describe the permittivity of semiconductors. To overcome this limitation, we propose the use of the Drude-Lorentz model to describe the dielectric function of semiconductors in the optical frequency range. The proposed dielectric function is given by:

$$\varepsilon_r = \varepsilon_\infty - \frac{\omega_p^2}{\omega(\omega + j\gamma)} + \frac{\Delta_\varepsilon \omega_p^2}{-\omega^2 + j\gamma\omega + \omega_0} \tag{3.17}$$

This model is chosen to enable us to take advantage of semiconductors at optical frequencies and search for a possibility of an optical plasmon existence in that range.

3.4 DISCUSSION AND RESULT

Matlab symbolic tool has been used to implement the above models. Using equation 3.9, we insert the desired model of the dielectric function and proceed to calculate the dispersion relation. Before we examine the possible development of the models that work for both materials (i.e. semiconductors and metals), we need to address the question of why it should even be done. The basic answer is to gauge the effect of the loss of plasmons, especially in semiconductors. The slight change in a dielectric permittivity and the damping values are taken into account.

We commence by discussing the details of all of the above models. To solve this dilemma, it is necessary to assume that the system is lightly damped. Based on this assumption, we can then ignore the damping term at first, and later add the loss term for comparison. Next, we recall equations 3.3 to 3.8 and substitute them in the model equation. Doing so, and satisfying the boundary conditions for fields in both media, one can find the dispersion equation for the Drude model without loss as [9]:

$$\begin{aligned} -\omega^6\left(\varepsilon_S\varepsilon_D-\varepsilon_S^2\varepsilon_D\right)+\omega^4\left(\beta^2c^2\varepsilon_S^2-\beta^2c^2\varepsilon_D^2+\varepsilon_D^2\omega_p^2-2\varepsilon_S\varepsilon_D\omega_p^2\right) \\ +\omega^2\left(2\varepsilon_d\beta^2c^2\omega_p^2+\varepsilon_d\omega_p^2\right)-\beta^2c^2\omega_p^2=0 \end{aligned} \tag{3.18}$$

where, ε_s is a semiconductor dielectric permittivity, ε_D is a dielectric permittivity, and ω_p is the plasma frequency. It may be noted that neglecting the losses in this equation and setting $\varepsilon_S = \varepsilon_D$=1[9] for a classical metal/air interface yields the well-known plasmon dispersion equation with well-known solution:

$$-\omega_p^2\omega^4-\omega^2(2\beta^2c^2\omega_p^2+\omega_p^4)+\beta^2c^2\omega_p^4=0 \tag{3.19}$$

Figure 3.1 shows the dispersion relation of surface plasmons propagating along a silicon/air boundary.

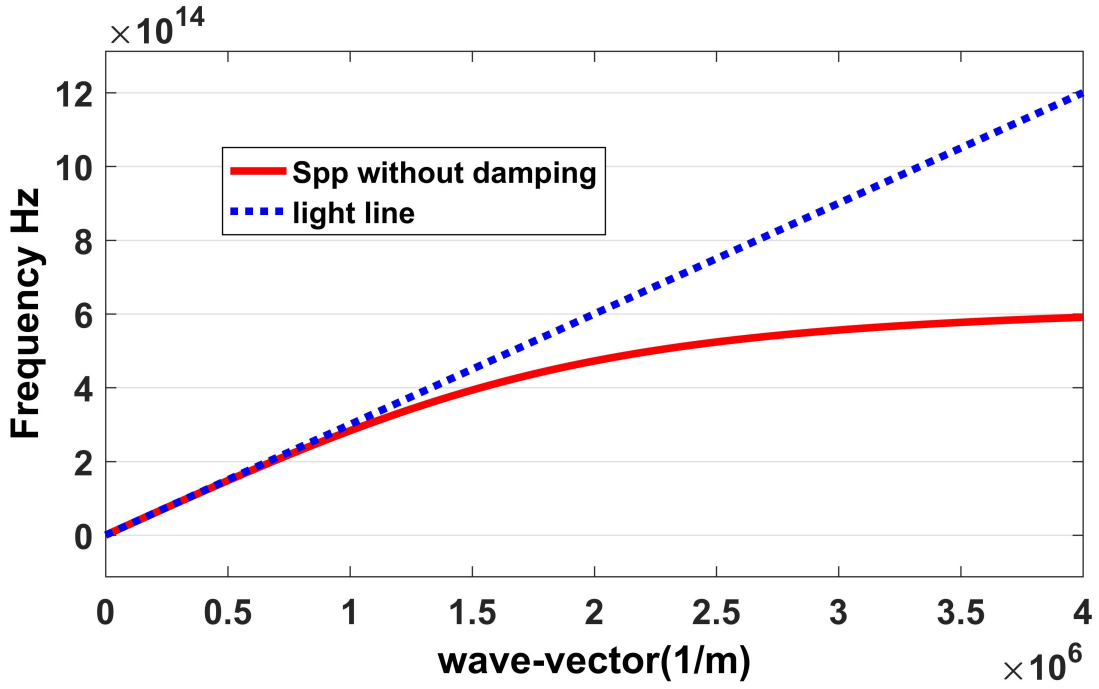

Figure 3.1: Plasmon dispersion without losses using a Drude model.

Employing the generalized Drude theory, the complex dispersion equation is obtained. Equation 3.20 below is the resulting plasmon dispersion equation obtained when losses are included in the Drude model, through the damping frequency, γ:

$$-\left(\omega^2\left((3c^2\omega_p^4\beta^2-2c^2\omega_p^2\beta^2\gamma^2+\omega_p^6)-\omega^4(2c^2\omega_p^2\beta^2+2\omega_p^4-\omega_p^2\gamma^2)\right)\right)$$
$$+\left(\omega_p^2\omega^6-c^2\omega_p^6\beta^2+c^2\omega_p^2\beta^2\gamma^2\right)=0 \tag{3.20}$$

For large values of the propagation constant, the surface plasmon frequency approaches a constant value, which can be obtained from equation 3.20 and is given by:

$$\omega_{\infty} = \left(\frac{\sqrt{9\omega p^4 - 12\omega p^2\gamma^2 - 8\omega p^2 + 4\gamma^4 + 8\gamma^2}}{4 + (3\omega p^2)/4 - \gamma^2/2} \right)^{1/2} \tag{3.21}$$

As can be seen from the dispersion relationship plotted in Fig. 3.2, when damping is taken into account, we observe a drop of the plasmon dispersion from 590 THz to about 432 THz for $\gamma > \omega_p$. However, when $\omega_p > \gamma$ the equation 3.21 yields an ω_{∞} value of 743 THz which is higher than what we obtain from Fig. 3.1. It is interesting to note that these plasmons are in the optical frequency range.

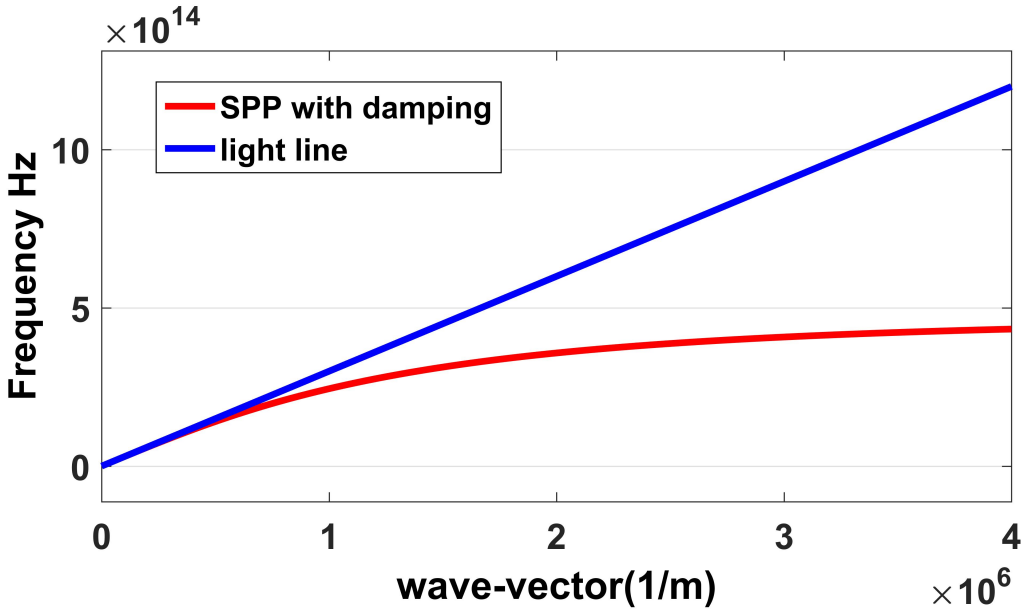

Figure 3.2: Plasmon dispersion with damping.

Following the same steps as previously and by inserting the Drude-Lorentz model function in equation 3.9 and rearranging the terms, one obtains:

$$-(\omega^2(\varepsilon_s^2\omega_p^2+\beta^2c^2\Delta_\varepsilon\omega_p^2+\varepsilon_s\Delta_\varepsilon^2\omega_p^4-2\varepsilon_s\Delta_\varepsilon\omega_p^4+\varepsilon_d\omega_p^4) \tag{3.22}$$
$$+\omega^6(\varepsilon_s\varepsilon_d^2-\varepsilon_s^2\varepsilon_d)+\omega^4(\varepsilon_s^2\omega_p^2+\beta^2c^2\varepsilon_s^2\omega_p^2-\beta^2c^2\varepsilon_d^2-2\varepsilon_s\varepsilon_d\omega_p^2-\varepsilon_s^2\Delta_\varepsilon\omega_p^2$$
$$+2\Delta_\varepsilon\varepsilon_s\varepsilon_d\omega_p^2)\beta^2c^2\omega_p^4+2\beta^2c^2\Delta_\varepsilon\omega_p^4-\beta^2c^2\Delta_\varepsilon^2\omega_p^4)=0$$

When losses are included in the Drude-Lorentz model, the following dispersion relation is obtained:

$$-\omega^4(2c^2\omega_p^2\beta^2\gamma^2+2\omega_p^4\gamma^2-\omega_p^4\gamma^2) \tag{3.23}$$
$$-\omega^2(3c^2\omega_p^4\beta^2\gamma^2+2\beta^2\gamma^4\omega_p^4c^2+\omega_p^6\gamma^2)$$
$$+\gamma^2\omega_p^2\omega^6-c^2\omega_p^4\beta^2\gamma^2+c^2\omega_p^6\beta^2\gamma^2=0$$

This dispersion relation of surface plasmon waves along silicon/air boundary including losses is shown in Fig. 3.3. *n*-doped silicon is used in the calculations, and all physical parameters are experimental values taken from [70]. To obtain the plasma frequency in the optical range, we had to use high carrier concentrations of the order of $10^{21}cm^{-3}$, which is feasible in silicon. By varying the plasma frequency parameter ω_p of the semiconductor, we obtained a different curve, which has a different surface plasmon frequency, as graphed in Fig. 3.3.

Figure 3.3 shows a different SPP curve than Fig. 3.2, depicting only the real part of the Drude-Lorentz model. When, $\omega_p > \gamma$, the surface plasmon frequency increases to approximately 723 THz,. It should be noted that the values of ω_p and γ for *n*-doped silicon change with doping concentration.

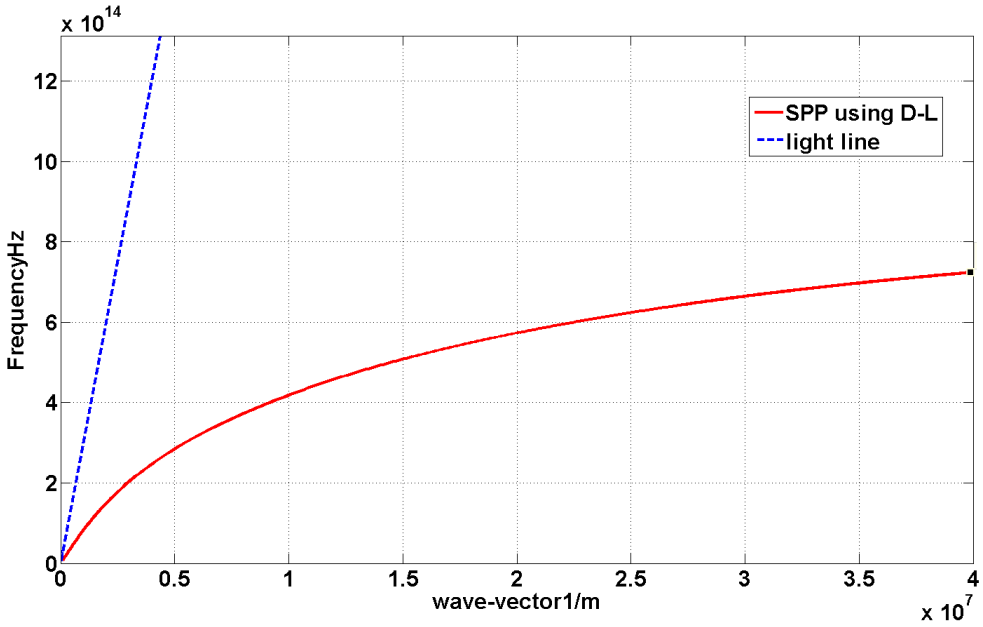

Figure 3.3: The model surface plasmon dispersion with damping -Drude- Lorentz.

Figure 3.4 compares all of the models, so that they can be understood more clearly. Physically, changing the model may have an influence on the plasma dispersion curves, which affect the optical properties of the structure. To address this point, the plasma dispersion was similuated at$1.55\,\mu m$ as shown in Fig. 3.4. Although the Drude-Lorentz model is an improvement over the Drude model, showing strong dispersion around the resonant frequency, it is not an acceptable model for use with noble metals [38].

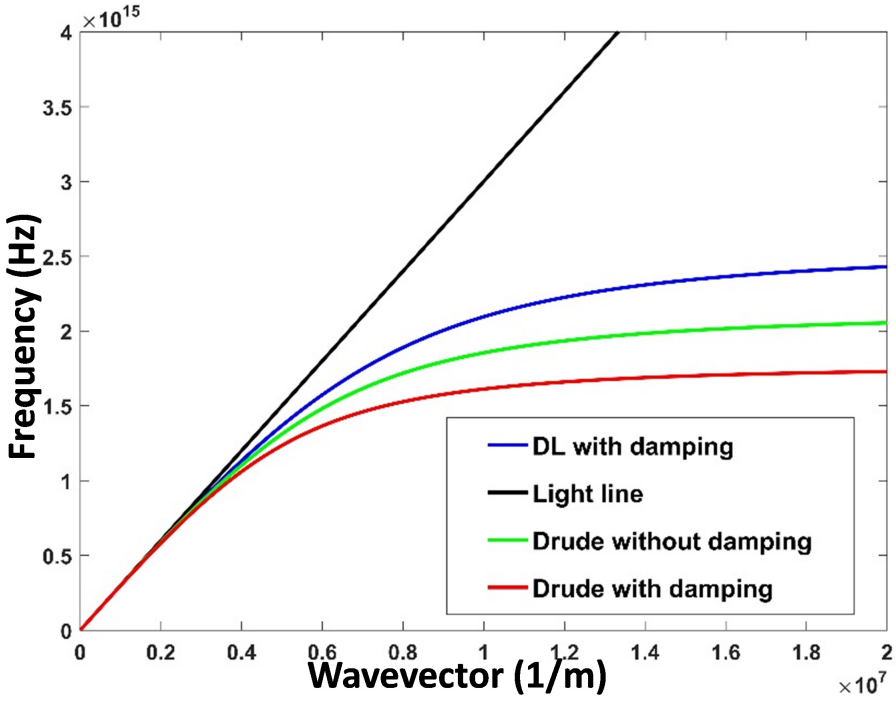

Figure 3.4: Comparison all models.

3.5 CONCLUSION AND FUTURE WORK

Theoretical and numerical studies were conducted on plasmonic interactions at a semiconductor/dielectric interface and a brief review of the basic model theory was presented. We have shown that the inclusion of losses reduces the surface plasmon frequency. As well, we have proposed the Drude-Lorentz model as a model for the dielectric function of semiconductors due to its ability to describe both free electron and bound systems simultaneously. The numerical results of the plasmon dispersion for a silicon/air interface were presented using the proposed model and were compared to the Drude model.

Future work involves the use of other types of semiconductors such as AlGaAs, InP or InGaAs with different and flexible optical properties. Different dielectric materials can also be used to tune the surface-plasmon frequency.

Chapter 4

A LONG RANGE HYBRID THZ PLASMONIC WAVEGUIDE WITH LOW ATTENUATION LOSS

This chapter investigates the modal properties of a hybrid plasmonic waveguide operating at 1 THz, composed of a silver film, in the vicinity of which two silicon rods are placed. A detailed analysis is made of the propagation length, the effective indices, and the model area of the supported modes. A preliminary investigation of a directional coupler is also made based on the proposed waveguides. The properties of long-range hybrid surface plasmon polaritons propagating along a symmetric silicon microwire and finite-width silver are studied. As a solution to the issue of propagation loss of LR-SPP at the terahertz frequency, I have proposed a novel waveguide, which I designate as a long-range hybrid THz plasmonic waveguide with low attenuation loss.

Finite Element Method (FEM) COMSOL commercial software was used to investigate the effects of structural parameters on the modal properties, in order to achieve an improved performance trade-off, and to calculate the propagation length for different gaps between Si and Ag, and different Si diameters. The structure under study outperforms existing hybrid plasmonic waveguides in terms of the figure of merit (FoM), and offers potential applications, for example in microsensors.

Efficient waveguide transmission is crucial for several applications. This analysis is therefore essential for the ongoing efforts to develop an efficient terahertz waveguide. The guiding properties of the hybrid terahertz surface plasmon polariton (HTSPP) waveguide

were analyzed numerically at the THz frequency, and double-structured comparisons were made of the best features of the terahertz plasmonic waveguide.

This work extends the study to double pairs of nanowire, as a step toward improving waveguiding properties. The aim is to investigate the interaction between wire pairs placed at a distance, and the advantage of adding an additional microwire to optimize the geometry to achieve the maximum possible propagation with low losses. This is useful for applications such as integrated photonic circuits (IPC-THz), to achieve package density.

In conclusion, I found that a long-range hybrid THz plasmonic waveguide with low attenuation loss (HTSPP) has a significant impact on the properties of SPPs. This result contributes to a better understanding of the HTSPP in practical applications.

My contributions to this work consist of proposing the idea for the HPTWG, determining the simulated and calculated properties of the proposed waveguide, analyzing the data, and writing the initial version of the manuscript. Finally, because permission of the Infrared Physics & Technology journal has been obtained, the paper itself is attached at the end of this thesis.

"Eldlio M., Ma Y. Q., Maeda H., & Cada., M. "A long-range hybrid THz plasmonic waveguide with low attenuation loss." Infrared Physics & Technology 80 (2017), 93-99."

4.1 ABSTRACT

Numerical solutions are obtained for the proposed novel hybrid terahertz plasmonic waveguide structure, namely the silicon metal silicon (SMS) waveguide. It is shown that the SMS waveguide can overcome the diffraction limit while still maintaining a sizeable propagation length. The geometric dependence of the mode characteristics of this structure

is analyzed in detail, showing strong confinement and low loss with propagation lengths exceeding $14mm$ at normalized mode areas of 1.72×10^{-2}. By using the FEM method (Comsol), the guiding properties of the hybrid terahertz surface plasmon polariton (HT-SPP) waveguide are numerically analyzed at the THz frequency, and a combination of double-structured comparisons of the best features of the terahertz plasmonic waveguide is made. Depending on the height used and how the mode confinement is measured, various modal designs, such as double microwire structures, are developed. The structures indicate that we verified the possibility of low attenuation loss of hybrid THz plasmonics propagation. The effective mode area A_{eff}, energy distribution, and propagation length L_p versus height for waveguides with Si microwire and SiO_2 are shown. The numerical calculation results reveal a potential for use in applications such as optical force in trapping and transporting biomolecules, and in high-density integrated circuits.

4.2 INTRODUCTION

There has been significant growth recently in theoretical and experimental work related to Hybrid Plasmonic Waveguides (HPW). The research studies have explored the plasmonic phenomenon within a low index nanogap between a high index waveguide and a conducting substrate. Numerous groups are presently investigating the interaction between a free carrier concentration and an electromagnetic field [1, 2, 3] giving rise to well-known surface plasmon polariton (SPP). These can be used to confine light and increase electromagnetic fields at an interface between two media where at least one is conducting [10].

The plasmonic waveguide is a good candidate for achieving large degrees of confinement and practical propagation lengths [71]; hence, sub-wavelength waveguides have been realized in various geometries for the next generation of integrated photonic circuits (IPC) [72, 48, 73, 15]. Different structures have been proposed [44, 74] in the optical range. For

example, in [44], the hybrid mode is shown to be strongly confined even in sizes smaller than 100 times the area of a diffraction-limited spot. Large subwavelength mode confinement in [74] shows that a strong interaction between a dielectric cylindrical waveguide mode and a long-range surface plasmon polaritons (LRSPP) mode of a thin metal film can be obtained.

It should be pointed out that the structure design in [44] was chosen primarily for optical frequency wavelength, which enabled the researchers to control the light in a small area over a typical propagation length ($434\mu m$), albeit without the inclusion of hybrid plasmonics in the THz regime. We therefore wish to take this a step further by including the hybrid THz contribution in the SPP waveguide. THz frequency shows great promise for use in high-resolution imaging, spectroscopy, and security applications such as biological agents or explosives [75]. A unique feature shown in [76] is the interaction with the material in ways that are diverse from other forms of electromagnetic radiation. For instance, plastics and papers are transparent to terahertz frequencies [77]. Various structures have been proposed as plasmonic waveguides in the THz range [78, 79].

Less attention has been paid, however, to a hybrid plasmonic terahertz (THz) waveguide (HPTWG) supporting hybrid plasmonic modes traveling through the microscale of a lossy material to achieve high mode confinement. The frequency of a THz wave occupies the electromagnetic spectra between microwave and infrared ranges [79]. To take advantage of this phenomenon, HPTWG has been the subject of much recent research [79, 72, 15].

Hybrid terahertz SPP can achieve high mode confinement in terms of longer amplitude propagation lengths [79] by merging the merits of an SPP waveguide, a slot waveguide, and a hybrid SPP waveguide. A long-range hybrid terahertz SPP (LR-HTSPP) is a combination of long-range SPP and dielectric waveguide modes. It offers the same degree of propagation length as LRSPP and similar mode confinement as HTSPP. In order to better

understand and distinguish between SPP and waveguide mode, intensive research has been proposed recently. For example, alternative plasmonic material, such as a graphene-based split-ring structure, has been investigated [80], along with micrometer-level graphene field effect transistors, which have high sensitivity and wide-band tunability throughout the entire THz domain [81]. The development of efficient THz sources and detectors has opened the THz frequency region (i.e., 0.1–10 THz) to numerous applications, including material analysis in microelectronics, non-invasive screening of cancer, label-free biomolecular analysis [79], and optical tweezers [82, 83, 84, 85].

In contrast, semiconductor microwire offers applications in nanophotonics, such as waveguides, sensors, photodetectors, and lasers [10, 71, 72]. However, the operating wavelength is much longer than the diameter of microwire and yields weak confinement due to a limited index-contrast. This dilemma arises from the difficulty in achieving subwavelengths on an optical scale, when small mode and wire diameters are desirable. To overcome this limitation, we propose using strong terahertz confinement to enhance the optical field strength and the gradient of light field and to determine the optimum size required for potential applications.

An important aspect that needs to be addressed in this work is confining and guiding long wavelength electromagnetic radiation into small-size structures by coupling them with HT-SPP, i.e., confining the light and increasing the electromagnetic fields at an interface between two media, of which at least one is conducting [3]. The structure under study outperforms existing hybrid terahertz plasmonic waveguides in terms of the figure of merit (FoM) that allows one to use it in real-life applications, such as optical force in trapping and transporting biomolecules [86] or in high density integrated circuits [1, 87]. It is worth mentioning that some works do not cover all aspects of hybrid plasmonic waveguides, such as coupled microwire at THz frequencies.

This paper is organized as follows: A brief theory and structure geometry are addressed in section 4.2. In section 4.3, numerical results are presented and discussed. Figures of merit are introduced in section 4.4, and section 4.5 summarizes the results and draws conclusions.

4.3 STRUCTURE GEOMETRY

To optimize the trade-off between mode confinement and propagation length in the THz frequency range, a novel structure was adopted [44], as shown in Fig. 4.1. The structure has the advantage of supporting a long propagation length, which consists of a thin metallic film (silver: Ag) sandwiched between two cylindrical silicon (Si) microwires with a diameter D and a gap distance h. The background material is assumed to be SiO_2. In order to verify the possibility of obtaining a low loss with a long propagation length for HTSPP mode, the complex dielectric function of Ag needs to be considered. The permittivity is described by the well-known Drude model as:

$$\varepsilon_r = \varepsilon_\infty - \frac{\omega_p^2}{\omega(\omega + j\gamma)} \tag{4.1}$$

where ε_∞ is the high frequency permittivity, γ is the damping term, and ω_p is the plasma angular frequency [2]:

$$\omega_p = \sqrt{\frac{ne^2}{\varepsilon_0 m^*}} \tag{4.2}$$

Here, $m*$, e, and n are the electron effective mass, the electron charge, and the carrier density, respectively, and ε_0 is the permittivity of free space. The parameters $\omega_p = 1.37 \times 10^{16}$ rad/s and $\gamma = 8.20 \times 10^{13}$ rad/s are taken from [88].

In this paper, the frequency considered is 1 THz, as this is within the critical range of the THz spectrum for spectroscopy, sensing applications, and networks [73]. We have carried out a detailed mode analysis using the commercial Finite Element Method (FEM) (Comsol) to investigate the effects of structural parameters on the modal properties to achieve an improved trade-off. To obtain an accurate result in our simulation, the minimum mesh size was set to $0.05\mu m$ and the sizes of the geometric structure domains were set sufficiently large that the fields would be small enough at the boundaries to be efficiently absorbed by a perfect magnetic boundary condition (PMC). Also, on the horizontal boundary, a set of perfect electric conductor boundary conditions (PECs) was used and in the convergence analysis, the calculation region in the *y*-direction (10λ) and x-direction (10λ) is assumed to be sufficiently large to ensure accurate eigenvalues. The mesh will not interfere in the calculations.

The proposed double-microwire structure in Fig. 4.1(b) is flexible and can be conveniently extended to a single microwire by adding a microwire. The new microwires, being the same as a single microwire in geometric dimensioning, are placed to the right of the single Si, and the distance between both is varied, as in the previous scenario. This design approach could be useful in a number of applications, such as in highly integrated optical circuits.

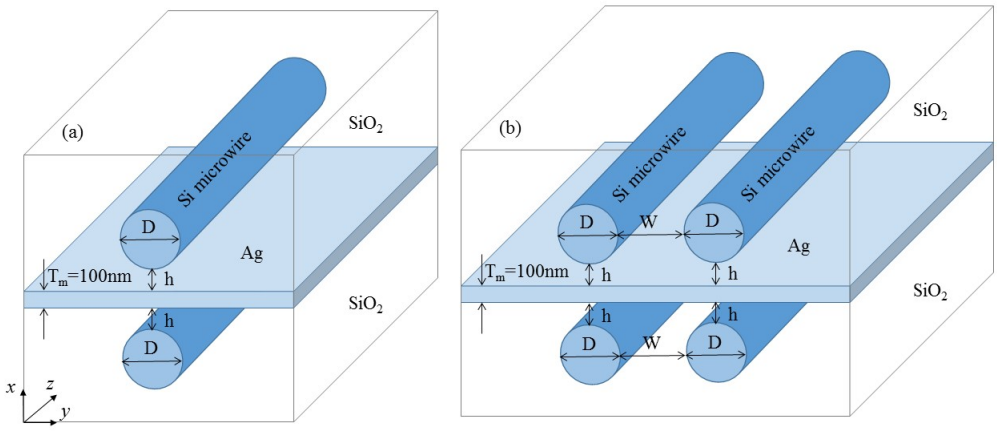

Figure 4.1: Schematic diagrams of HPTWG: (a) single pair of microwires, (b) double pair of microwires.

4.4 RESULTS AND DISCUSSION

Figures 4.1(a) and 4.1(b) show the schematic structures with symbols and an accepted coordinated system of the proposed work. Both configurations use a finite-width silver strip between Si microwire deposited at both interfaces of the lower and upper silver/ SiO_2. As will be discussed later in greater detail, the gap height in our case varies from 50 to 1000 nm, and the diameter D of Si varies from 10 to 60 μm.

It is worth mentioning that the performance of the HPTWG is evaluated by its normalized mode area, figure of merit (FoM), and propagation length. The normalized mode area is defined as A_m/A_0. Here, $A_0 = \lambda^2/4$ represents the diffraction-limited area in free space.:

$$A_m = \frac{W_m}{max\{W(r)\}} = \frac{1}{max\{W(r)\}} \iint W(r) d^2r \tag{4.3}$$

where W_m is the total mode energy, $W(r)$ is the energy density (per unit length along the direction of propagation), and r is a radius of Si microwire. The energy density can be written as [44, 89, 90]:

$$W(r) = \frac{1}{2}\left(\frac{(d(\varepsilon(r)\omega)}{d(\varepsilon(r)\omega)d\omega}|E(r|^2 + \mu_0|H(r)|^2\right) \tag{4.4}$$

To obtain the effective mode index, the complex propagation constant of the HTSPP mode propagating along the z-direction can be used. The propagation length (L_p) is calculated with regards to its propagation constant (β) [2]:

$$L_p = 1/2Im(\beta) \tag{4.5}$$

where $Im(\beta)$is the imaginary part of the complex propagation constant. The mode properties are affected by the waveguide size. Fig. 4.2 shows the HPTWG structure's normalized modal area $A = (A_m/A_0)$ as a function of the cylindrical diameter D for different gap distances h. Correspondingly, the general asymmetric HPTWG is given in Fig. 4.7(c) to compare how much this structure can support the LRSPP mode in symmetric and asymmetric hybrid THz plasmonic waveguides. This also will be shown later in greater detail. The parameters chosen as a high index refractive index microwire with dielectric were assumed to be a constant (i.e., ε_s=11.684) with a perfectly smooth sidewall. The substrate is made of SiO_2, with a refractive index of n_c=1.95 [91]. The parameters chosen were $D = 20\mu m$ and $h = 750nm$, and the Ag thickness is $T_m = 100nm$. Figs. 4.2(a) and 4.2(b) show the dependence of the normalized mode area A_m and the propagation length L_p on the Si microwire with height h. From Fig. 4.2, we can see that the normalized mode (A_m) initially decreases prior to $20\mu m$, after which it increases smoothly, indicating that it has a minimum value of

around $20\mu m$ of the Si diameter. This scenario occurs in all gaps between the metal and Si waveguide.

To better understand the meaning of this phenomenon, the normalized effective index was plotted versus the different Si microwire waveguide diameter D with a different height. In Fig. 4.2, when the diameter of Si is $20\mu m$ and the gap is $750nm$, the propagation length reaches a maximum of $12 \times 10^3 \mu m$. The corresponding normalized mode area is 1.36×10^{-2}. It is interesting to note that the geometry structure for the single-pair microwire of the HTSPP waveguide demonstrates a centimeter-scale propagation length with strong subwavelength confinement. As shown in Fig. 4.2(a) and 4.2(b), both the propagation length and the normalized mode area decrease with an increase in the gap at the beginning, followed by a further increase, which indicates that there is a minimum optimal value for both L_p and A_m at certain h values (i.e., around $20\mu m$). Figs. 4.2(a) and 4.2(b) clearly show that as the propagation length decreases monotonically, the normalized mode area at first decreases and then increases, displaying a minimum value (i.e., around $20\mu m$) for all of the considered gaps h. This could be because the varied Si microwire give rise to different values of the effective mode in Si microwire that will determine the mode hybridization character [48].

Figure 4.2(b) depicts the effect of the core diameter and the height on the propagation length. We can see that the propagation length decreases for smaller diameters and shorter separate distances due to an increase in confinement, as stated above. This indicates that our structure could feasibly control the propagation length of modes in a hybrid THz plasmonic waveguide. For optimally chosen parameters, the propagation length increases when the gap and diameter are increased. From Fig. 4.2(b), one can see that when D decreases, L_p increases, which is similar to well-known LRSPP in previous work [58]. It is essential to emphasize that obtaining this phenomenon is due to the possibility of designing optimal

parameters for long-distance propagation. For a microwire with $20\mu m$, the mode area is $487\mu^2$ with a propagation length of $14 \times 10^3 \mu m$.

Table 4.1 shows how the gap and diameter D of Si are affected by these parameters. It also shows that the hybrid mode has strong confinement even in sizes smaller than 20 times the area of a diffraction limit, which shows a good agreement with [44]. It is important to compare our results with respect to other THz (HPTW) waveguides [79]. The proposed HTSPP waveguide outperforms the existing HPTW with 1.2 times increased propagation length (long propagation length of HTSPP = $3300\mu m$), compared to those reported in [79] (long propagation length of HPTW= $2700\mu m$), with the same parameters of gap=$0.2\mu m$, D=$40\mu m$, and frequency 0.1 THz. Moreover, the structure in [79] is more complicated in terms of fabrication.

Table 4.1: Optimal parameters with various heights for $D = 20\mu m$.

h(nm)	mode area (μm^2)	A_m	Real n_{eff}	Im n_{eff}	$L_p(\mu m)$
50	172	7.66×10^{-3}	1.8402	1.472×10^{-3}	16×10^3
500	291	9.75×10^{-3}	1.8028	1.568×10^{-3}	17×10^3
750	370	1.36×10^{-2}	1.7861	1.820×10^{-3}	15×10^3
1000	487	1.72×10^{-2}	1.7714	1.901×10^{-3}	14×10^3

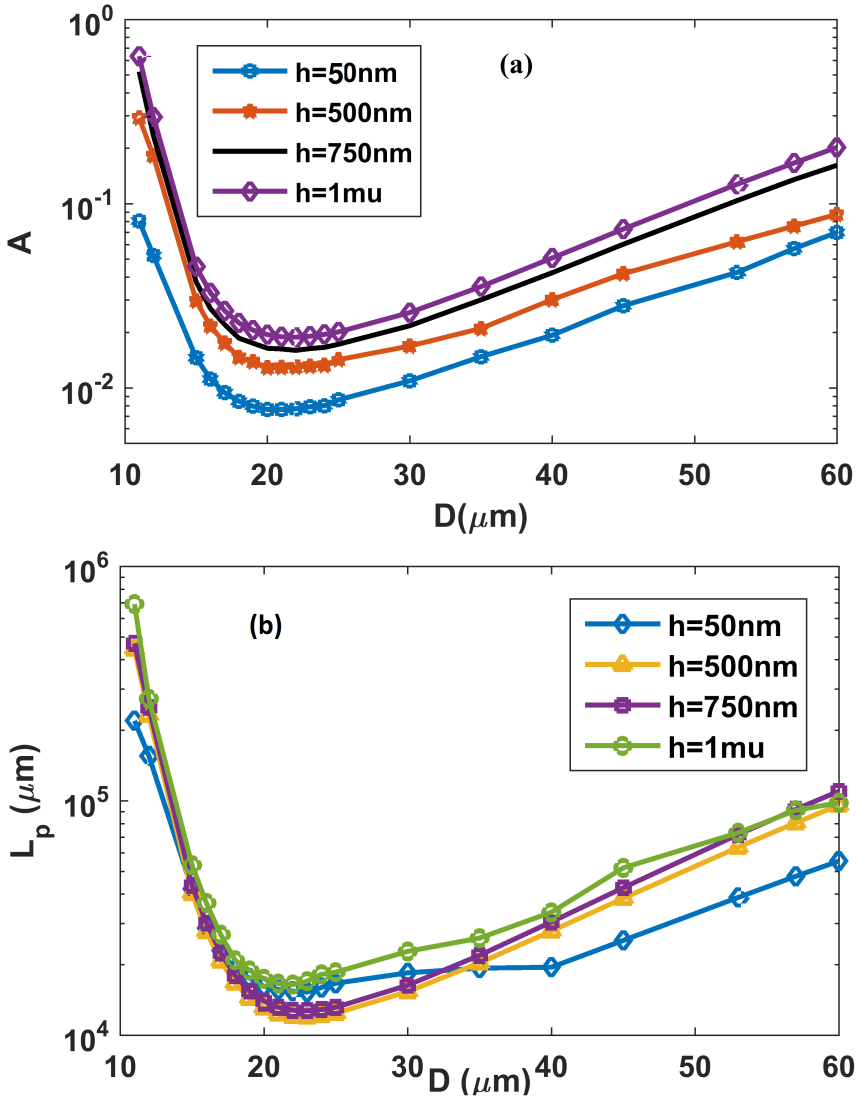

Figure 4.2: (a) Normalized mode area (A_m/A_0) as a function of cylindrical diameter of Si for different gaps. (b) The propagation length for various h as a function of D.

We have carried out a detailed mode analysis to investigate the energy density distributions, as shown in Figs. 4.3(a-d). In this simulation, the waveguide parameters are defined as the optimal values mentioned above. From the simulation, one can see that as the gap decreases, the EM field is highly localized at the interface between the Si microwire and Ag film, indicating that the structure acts as the LR-HTSPP waveguide, as shown in Fig. 4.3(a). On the other hand, the amount of EM field distributed in the vicinity of the Ag film

decreases as the gap increases, as shown in Fig. 4.3(b), leading to a smaller atteanuation loss and thus a longer propagation length. By selecting the appropriate parameters, the light is confined in the Si microwire and in the gap, as illustrated in Fig. 4.3(c), meaning that the hybrid mode is dominate. We can further infer from Fig. 4.3(d) that when increasing the gap, the majority of the EM field is located in the microwire, i.e., a standard dielectric mode waveguide.

The power confinement and the diameter of silicon have a proportional relationship. Hence, when more power can be confined in the core through increasing the silicon core size, weak mode confinement and a long propagation distance ensues. The gap confinement is achieved due to the core, which has a high index material. As we pointed out, decreasing the gap significantly enhances the electric fields, along with smaller mode dimensions affecting the modes in Si microwires. The propagation length and mode confinement can be tuned by varying the gap and Si diameter to achieve a trade-off between L_p and A. The intensity field becomes more confined in silicon for larger dimensions, so the field is relatively high in microwire Si only for large-size ($D = 40\mu m$). If the gap h between the silver and silicon waveguide continues to increase, the density drops due to a larger core.

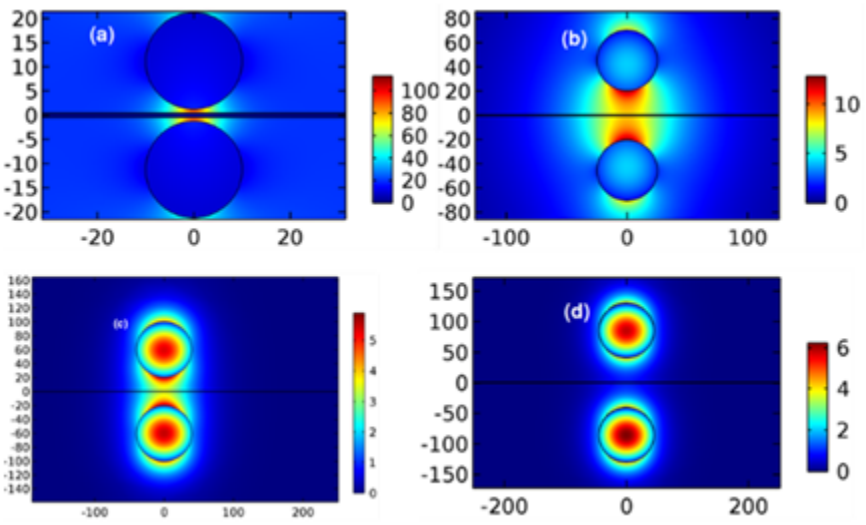

Figure 4.3: 2D energy density distributions of LR-HTSPP at 1 THz (a) SPP mode with D=20 μm and h=750 nm, (b) gap mode with D=50 μm and h=20 μm, (c) gap-microwire mode with D=20 μm and h=20 μm, and (d) microwire mode with D=90 μm and h=40 μm.

To get a clear view of the mode profile, Fig. 4.4 shows the 1D normalized energy density along $x = 0$ and $y = 0.5\mu m + h$ ($h = 750nm$ and $20\mu m$) at $D = 20\mu m$ for different gap distances h. In the HPTWG, a significant amount of electrical field intensity is confined in the low refractive-index material (i.e., SiO_2) between Si and high-index Ag. The dimensions affect the level of mode confinement. Fig. 4.4 shows the symmetric one as the long-range hybrid SPP mode. It can be happened when Ag has thickness $250nm$ and the Si microwire is $20\mu m$, two hybrid modes can exist through the coupling of the gap waveguide mode and the SPP mode. The existence within the gaps with lower index causes strong field enhancement in the gap region. Due to the fact of slot waveguide theory. When the Si microwire get closer to the Ag, the stronger mode coupling between the long-range SPP mode and the dielectric waveguide mode leads to an increase in n_{eff} and a decrease in L_p. In Fig. 4.4 it can be seen that when h is smaller than the characteristic decay length of the field, from the interface into the low-index region, a large fraction of the E-field distribution is tightly confined within the slot. Because the normal electric field undergoes a large discontinuity,

there is a high index contrast at the interfaces, resulting in a field enhancement in SiO_2, with a low refractive index. In addition, varying the power confinement factor [13, 43]in accordance with the ratio between the values of the electric field at both sides of the walls (see Eq. 4.3) affects the mode size of the slot waveguide.

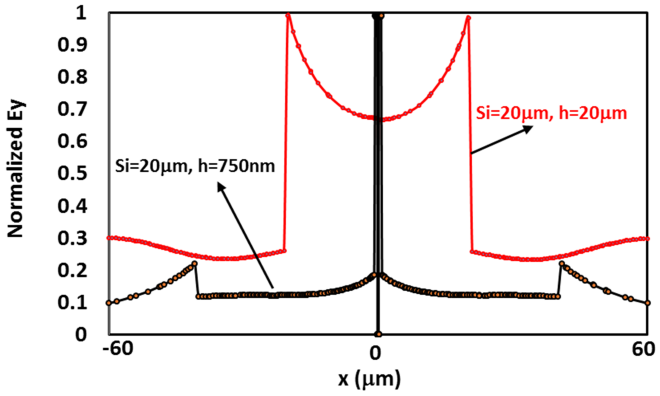

Figure 4.4: Normalized *Ex* distributions along the *x*-direction. The red (black) line represents the structure with h =20 μm (h=750 nm), while the cylindrical diameter D is set at 20 μm.

In order to verify the difference between the SPP and waveguide mode, the hybrid mode characteristics (HMC) should be introduced. This can easily be found by a superposition of the Si microwire mode and the LR-HTSPP mode:

$$HMC = \frac{\left(n_{eff1} - n_{eff2}\right)}{\left(n_{eff1} - n_{eff2}\right) + \left(n_{eff1} - n_{eff3}\right)} \tag{4.6}$$

where n_{eff1}, n_{eff2}, and n_{eff3} are the effective refractive indices of HPTWG, LR-HTSPP, and Si microwire, respectively. As shown in Fig. 4.5 (a), the mode effective index increases monotonically with increasing Si size. From the simulation, one can see that as the Si size increases, the n_{eff} becomes close to WGM, whereas decreasing the Si size results in n_{eff} becoming closer to LR-HTSPP. The values of the real part of n_{eff} vary in the range of 1.5–3 and for microwire sizes vary from 10 to 60 μm, which is considerably higher than

WGM, as shown in Fig. 4.5(a). This HMC is shown in Fig. 4.5(b). At the minimum, the long propagation distance is $D \tilde{} 20\ \mu m$ and HMC = 0.5, which agrees with previous works [92, 44]. One can used the HMC to gauge the degree to which the HPTWG mode is LR-HTSPP-like (i.e., $n_{eff3} < n_{eff2}$, i.e., HMC < 0.5) or WGM-like ($n_{eff3} > n_{eff2}$, i.e., HMC > 0.5). Thus, the LR-HTSPP mode characteristics are dependent on the Si waveguide and Ag parameters and are very important parameters related to HMC that can affect all results obtained in this work.

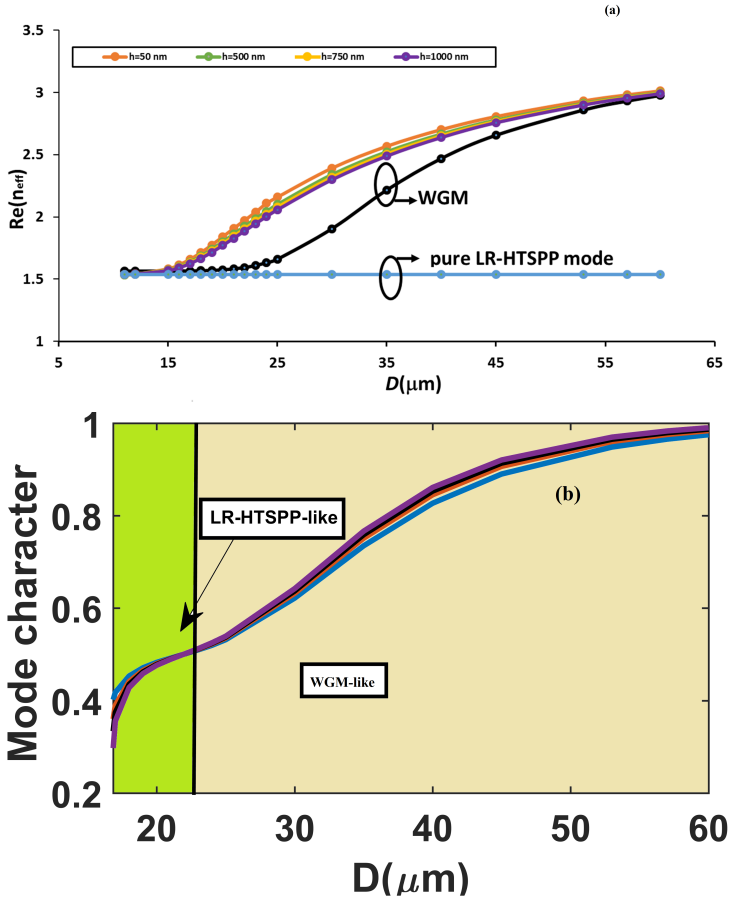

Figure 4.5: (a) Effective mode versus of Si size. (b) hybrid mode character HMC versus diameter of Si waveguide for different heights.

We now discuss the details of the double pair structure as seen in Fig. 4.6(a) and 4.6(b), which are the symmetric and antisymmetric mode, respectively. The double pair of microwires enhances waveguide transmission properties compared to the single wire. It has significantly improved coupling efficiency and has low light transmission with low group velocity [93]. The distance between the microwire (upper or lower) distance was chosen as a typical case. As shown in Figs. 4.6(a) and 4.6(b), the symmetric and asymmetric modes can be effectively confined in the low refractive region that is the SiO_2 area, even when our structures have large dimensions compared with the optical frequency regime in similar structures. In reality, there is less attention to investigating asymmetric coupling.

The relation between the coupling length and the size is plotted in Figs. 4.6(c) and 4.6(d). The coupling length (L_c) between two even and odd modes (symmetric and asymmetric, respectively) can be expressed as:

$$L_c = \frac{\pi}{Re\{\beta_e\} - Re\{\beta_o\}} = \frac{\lambda}{2\left(Re\left\{n_{eff}^{even}\right\} - Re\left\{n_{eff}^{odd}\right\}\right)} \tag{4.7}$$

Here, λ is the wavelength, and β_e and β_o are the propagation constants (basically effective indices) of the even and odd modes, respectively. One can clearly see that the optimal width is 75 μm. This makes it a good choice because the imaginary part of the effective index for symmetric and asymmetric modes at both heights (i.e., 750 nm and 1000 nm) is almost the same, indicating that both modes have the same decay as they propagate, leading to a perfect coupling. Moreover, one of the major advantages of this double Si microwire structure is that it is not sensitive to the gap h, making it have a large fabricate error tolerance. If the structure is sensitive to h, we need to take into account the gap for design purposes.

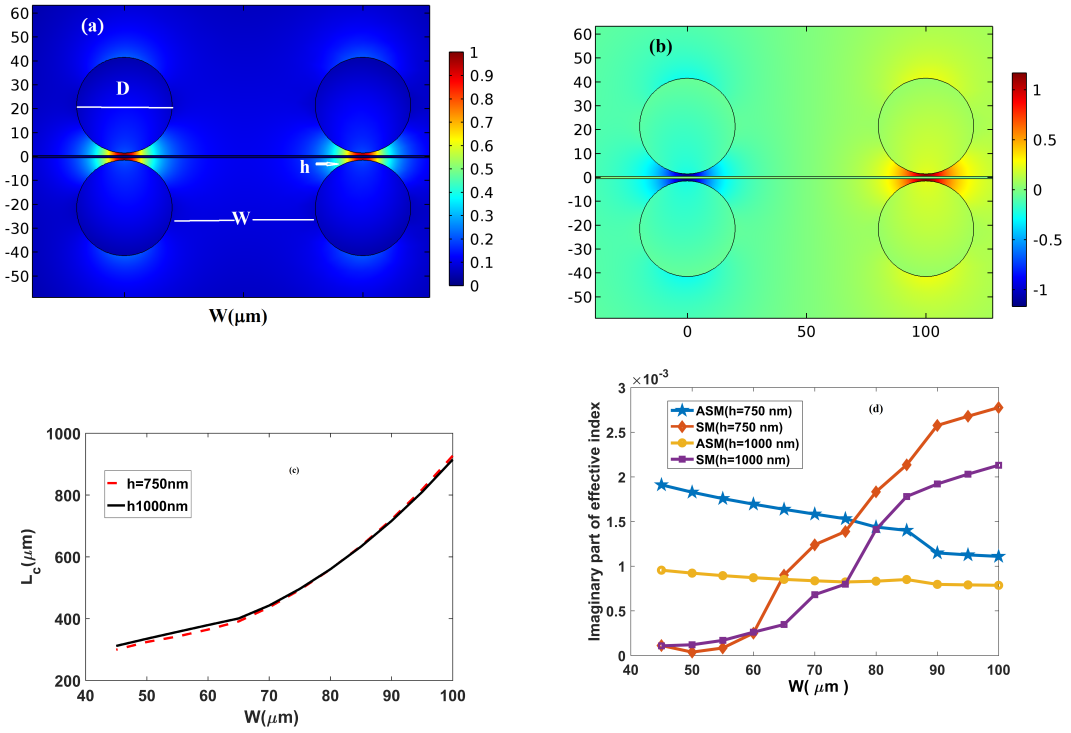

Figure 4.6: 2D energy density distributions of proposed structure for (a) symmetric mode and (b) antisymmetric mode. (c) Coupling length, and (d) imaginary part of effective index as a function of *W*.

4.5 FIGURE OF MERIT

Figure of merit (FoM) is another important parameter for evaluating waveguide performance. It is the ratio of the square root of the effective mode area to the propagation length and can be written as [44]:

$$FoM = \frac{L_p}{2\sqrt{\frac{A}{\pi}}} = \frac{\lambda}{4Im\left(n_{eff}\right)\sqrt{\pi A}} \tag{4.8}$$

We applied FoM in this work to gauge the trade-off of the symmetric mode propagation. It can be seen that the FoM for the hybrid mode at small heights is always larger than that for larger gaps in the whole range of microwire diameter *D*. For instance, Fig. 4.7(a)

illustrates the relationship between Si and FoM at various heights, showing the Si diameter as well as the height response in the FoM. Interestingly, decreases in FoM coincide with decreases in D until a minimum is reached (around D = 20 μm). Hence, with an increase in the Si diameter, the FoM first decreases and then increases when it reaches the optimal value. For smaller D, the mode extends deeper into the SiO_2. The FoM shows that when the guided wavelength decreases, confinement light increases, depending on the height. As mentioned above, a smaller diameter of the Si microwire (e.g., 20 μm) is preferable for achieving longer L_p with a higher FoM, whereas a larger diameter (e.g., 60 μm) is favorable for obtaining a smaller normalized mode area and a higher FoM.

From this, it is clear to see that, for a waveguide, a small h results in better performance. Figs. 4.7(a) and 4.7(b) show the FoM in two different structures: Si/SiO_2 /Ag/ SiO_2/Si and Si/ SiO_2/Ag. Comparing the structures, we see that the minimum of Si microwire diameter is similar in both cases. The difference, for example, for the same Si diameter of 20 μm for our proposal is that the structure with $h = 1\mu m$ in the gap has much better mode confinement ($A_m = \lambda^2/407$), with L_p at $11 \times 10^3 \mu m$ and FoM at 245. Compare this to a single structure $\left(A_m = \lambda^2/205\right)$, with $L_p$at $14 \times 10^3 \mu m$ and FoM at 117. However, FoM has almost the same order when the Si microwire size is $D = 20\mu m$, which can be acceptable for fabrication. A larger FoM means better performance of the HTSPP waveguide.

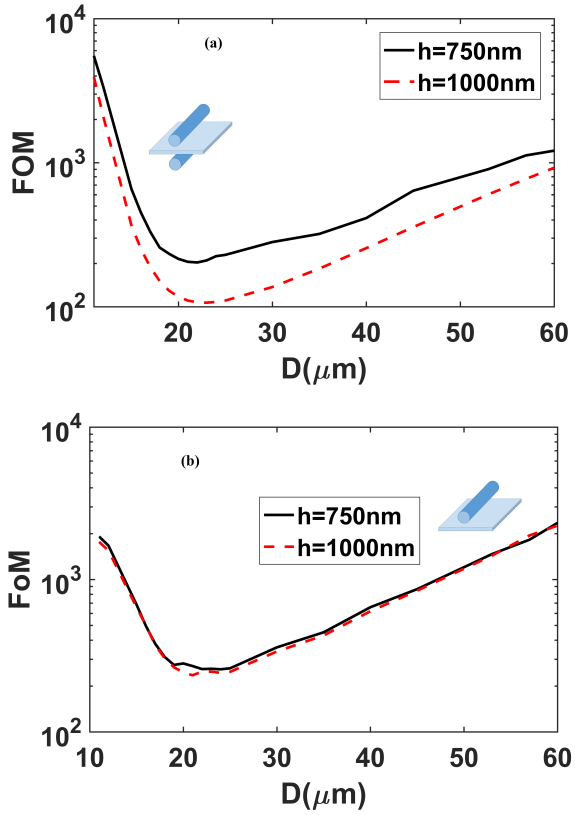

Figure 4.7: FoM (a) figure of merit as function of microwire size for various heights in single-pair microwire; (b) FoM in one Si microwire.

4.6 CONCLUSION

An approach for the simulation of a hybrid terahertz plasmonic waveguide structure by using the FEM method was presented. The guiding properties of the HTSPP waveguide were theoretically analyzed at the THz frequency and the concept of the HTSPP waveguide was established. In the proposed approach, a solution was presented for the propagation of electromagnetic waves at terahertz frequencies along a Si/ SiO_2/Ag interface. The above discussion suggested that the proposed HTSPP waveguide could offer enhanced capability for deep subwavelengths with low attenuation loss. We showed that a HTSPP waveguide has better performance compared to other conventional HSPP waveguides.

Furthermore, we provided a comprehensive analysis of a hybrid plasmonics waveguide in the THz regime. The plots of the effective mode area A_{eff}, energy distribution, and the propagation length L_p versus the height for waveguides with an Si microwire and SiO_2 were shown. A much larger mode area and propagation length were achieved when comparing our structure with a previous hybrid terahertz plasmonic waveguide that consisted of a single Si microwire deposited on Ag, resulting in enhanced FoM at THz frequency. The THz electric field amplitude in deep subwavelength confinement with low loss was significantly improved.

In our structure, we verified the possibility of low attention loss HTSPP propagation. Correspondingly, our analysis demonstrated how to facilitate the development and design of hybrid terahertz plasmonic high-density integrated circuits or bio-sensors. We also investigated in detail the effects of the wavelength, the waveguide dimensions, and the material properties on hybrid mode characteristics. The modal effective index $\left(n_{eff}\right)$, along with the FoM of the HPTWG mode of the proposed structure with various gaps and diameters, was shown. The modes supported by both structures have deeper subwavelength confinement within the range of the parameters chosen.

The work provides a better understanding of the mode confinement effect. The guiding properties of the asymmetric and symmetric modes of a hybrid plasmonic waveguide were investigated by using the FEM method. Due to the extraordinary guiding properties of the proposed hybrid, the terahertz plasmonic waveguide has the possibility to become a basic structure for the design of new types of integrated photonic circuits.

Chapter 5

A THz SEMICONDUCTOR HYBRID PLASMONIC WAVEGUIDE WITH FABRICATION-ERROR TOLERANCE

This chapter describes my design of a novel semiconductor THz hybrid SPP (STHSPP) waveguide to optimize the trade-off between mode confinement and propagation length. The designed STHSPP has a high extinction ratio and low insertion loss. I have considered not only mode properties and performance of the effect of structural perturbations, but also simplicity of fabrication.

This chapter presents an extension of the previous work described in Chapter 4. The approach is to combine Si microwire techniques with the advantages of a THz micro-plasmonic structure consisting of semiconductor GaAs instead of a metal. The trade-off previously described is explored by using a semiconductor at the THz frequency.

Numerical solutions were obtained for a novel semiconductor THz hybrid SPP (STHSPP) waveguide structure, by using FEM COMSOL software. The guiding properties of the STHSPP waveguide was analyzed numerically at the THz frequency, demonstrating that the STHSPP waveguide could surpass the diffraction limit while still maintaining large propagation lengths. The geometric dependence of the mode characteristics of the proposed structure were analyzed in detail, showing strong confinement with large propagation lengths. The numerical results indicate the potential for use in several applications, including biosensors.

The work also considered properties of the SPPs guided in a SiO_2 gap between heavily doped GaAs materials and Si microwire at a THz frequency. Energy density distributions and intensity fields were calculated by using the FEM method. Better confinement is achieved at a cost of a higher propagation losses in the STHSPP.

My contributions to this work include generating the fundamental ideas, performing the analytical description and necessary analyses, and carrying out numerical simulations. I also wrote the initial version of the manuscript. Finally, because permission of the Japanese Journal of Applied Physics has been obtained, the paper itself is attached at the end of this thesis.

"Eldlio Mohamed, Youqiao Ma, Franklin Che, Hiroshi Maeda, and Michael Cada. "A THz semiconductor hybrid plasmonic waveguide with fabrication-error tolerance." Japanese Journal of Applied Physics 56, (2017), 010306."

5.1 ABSTRACT

In this letter, a novel waveguide based on semiconductor THz hybrid surface plasmon polariton (STHSPP) is proposed and numerically analyzed. The structure under study can confine light in the ultradeep-subwavelength region $\left(\text{ranging from } \lambda^2/360 \text{ to } \lambda^2/156\right)$ with a large propagation length ranging from 374 to $506\mu m$. Compared with a conventional hybrid SPP (HSPP) waveguide without a ridge, our proposed structure with the same propagation length has a much higher mode confinement with a one order of magnitude smaller normalized mode area.

5.2 INTRODUCTION

There has recently been a significant increase in theoretical and experimental work related to surface plasmon polaritons (SPP) [1, 2]. SPP can be used to confine light and increase electromagnetic (EM) fields at an interface between two media, at least one of which is conducting [1, 2, 3]. SPP have already excited widespread interest for various applications [64, 71]. They are a very promising and powerful technology with enormous potential for advanced SPP applications, such as V-grooves in metals [72] and plasmonic wire waveguides [1] involving high-sensitivity biosensors; however, the large propagation losses induced by the intrinsic Ohmic loss in the metal limit the use of plasmonic waveguides, which poses a challenge. In reality, the usefulness of metal/dielectric interfaces originates from the high concentration of charge carriers in metals, although the concentration is limited by losses. A critical issue in using SPP is the high losses in metal optics while maintaining nanoscale mode confinement. Several solutions to overcome these limitations based on the prominent features of SPP have been proposed in recent years. For example, THz hybrid integration using a semiconductor instead of a metal [9] could enable a more accurate and precise deep confinement with a low loss [93]. Terahertz semiconductor plasmonics is currently attracting significant attention in both scientific research and industry. Numerous THz semiconductor hybrid plasmonic waveguides have been proposed [57, 94, 15], with immense effort being dedicated towards overcoming losses [57] in order to enable potential applications of THz semiconductor plasmonics, such as structured semiconductor surfaces [95]. Many important processes in nature occur at THz frequencies [96], which has opened research avenues in numerous applications such as microtweezers, as these frequencies do not harm skin.

The frequency of a THz wave occupies the EM spectrum between the microwave and infrared ranges [49], acting as a bridge between these ranges. To take advantage of this

fact, hybrid terahertz plasmonic waveguides (HTPWGs) have recently been the subject of intense research [49, 97, 94, 9, 57]. There are different designs of subwavelength THz plasmonic waveguides based on metal/dielectric wire structures [98, 79] and spoof surface plasmons on corrugated metal surfaces [79]. TPWGs can achieve a high mode confinement and larger propagation lengths [49, 57] by merging the merits of an SPP waveguide, a slot waveguide, and a hybrid SPP waveguide, including semiconductor materials.

Thus, in this Letter, we propose and design a novel semiconductor THz hybrid SPP (STH-SPP) structure to optimize the trade-off between the mode confinement and the propagation length (L_p). The examination of the geometric dependence of the mode characteristics reveals that the structure can provide a strong confinement in the wavelength region of $\lambda^2/360$ to $\lambda^2/156$ and a low loss with a propagation length ranging from 374 to $506\mu m$.

5.3 RESULT AND DISCUSION

Figure. 5.1 shows the three-dimensional (3D) geometry of the structure, which consists of a Si microwire (n_{si} = 3.415) placed on top of a GaAs substrate with a half-cylinder ridge. This structure is deposited directly onto a second SiO_2 substrate, where the cladding is assumed to be SiO_2 with a refractive index of 1.95 [99]. Numerical simulation results show that the maximum coupling between the Si waveguide mode and the SPP mode induces hybridization when the diameter of the Si microwire, D, is equal to $20\mu m$. The structure under study outperforms existing HTPWGs, with the former having twice and half the propagation length and mode area, respectively, of those reported in Ref. [94], thus allowing it to be used in applications such as biomolecular tweezers [100, 101] and high-density integrated circuits [49, 94].

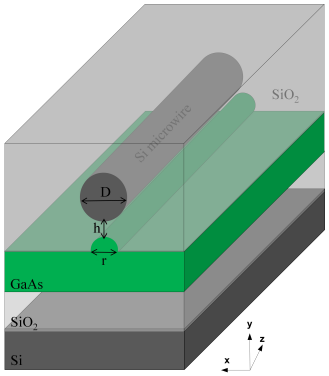

Figure 5.1: Schematic diagram of cross section of proposed STHSPP waveguide.

We have carried out a detailed mode analysis using COMSOL commercial finite element method (FEM) software to investigate the effects of structural parameters on modal properties to achieve an improved trade-off by adopting two important evaluation factors (i.e., propagation length and mode area) to describe the propagation loss and mode confinement, respectively.

In order to verify the possibility of obtaining a large propagation length with a low loss, the complex dielectric function of GaAs needs to be considered. In the case of homogeneously doped GaAs, the dielectric function $\varepsilon(\omega)$ is determined by free-charge carriers, and the classical Drude equation is valid for its description, which is expressed as [49]:

$$\varepsilon_r = \varepsilon^{'} + j\varepsilon^{''} = \varepsilon_\infty - \frac{\omega_p^2}{(\omega^2 + \Gamma^2)} + j\frac{\omega_p^2 \Gamma}{(\omega^2 + \Gamma^2)\,\omega} \tag{5.1}$$

where, ε_∞ is the high-frequency permittivity and ω_p is the plasma angular frequency. The damping term is given by $\Gamma = \frac{e}{(m_{eff} m_0 \mu}$, where μ is the mobility of the carriers, which has been phenomenologically approximated as [71] $\mu = \frac{9400}{1+\sqrt{N(10^{-17})}} \left(cm^2 V^{-1} S^{-1}\right)$. The parameters used are ε_∞= 10.89 and m_{eff}=0.0153 [102].

The propagation length is calculated from its propagation constant (β) as $L_p = 1/2Im(\beta)$, where $Im(\beta)$is the imaginary part of the complex propagation constant. The normalized mode area is defined as A/A_0, where $A_0 = \left(\lambda^2/4\right)$ represents the diffraction-limited area in free space [49] and can be expressed as [103]:

$$A = \frac{\iint W(r)d^2r}{W(r_0)} = \frac{\iint W(r)d^2r}{max[W(r)]} \tag{5.2}$$

where $W(r)$ is the electric field energy density and $W(r_0)$ is the energy density at the position where the highest field is observed, i.e., $max[W(r)]$.

The mode properties are affected by the geometric parameters of the waveguide. For example, by increasing the gap between the Si microwire and the GaAs ridge r, the propagation length can be further increased at the expense of a weaker mode confinement. To examine this in detail, the effect of the parameter r on the normalized mode area A and the propagation length L_p while keeping D fixed at 20 μm is plotted in Fig.5.2(a). We can infer from Fig. 5.2 (a) that, when increasing the diameter of the ridge r, the propagation length decreases monotonically, while the normalized mode area first decreases and then increases, displaying a minimum value at around $r = 2\,\mu m$. The propagation length reaches maxima of 3.48×10^2, 5×10^2 , and 6.58×10^2 μm for the three considered heights h ,i.e., 1, 5, and 10 μm, respectively. This could be due to the fact that varying$r$ gives rise to different values of the effective mode index in the Si microwire, which determines the mode hybridization character [49]. Therefore, the parameter r will be fixed at $2\mu m$ in the following discussion to maintain a low propagation loss.

To clarify the physical mechanisms of the behavior of L_p depicted in Figs. 5.2 (a) and Figs. 5.2(b) ($r = 250nm$, $h = 5\mu m$, and $D = 20\mu m$), Fig. 5.2(c) ($r = 2\,\mu m$, $h = 5\mu m$, and $D = 20\mu m$), and Fig. 5.2(d) ($r = 20\,\mu m$, $h = 5\mu m$, and $D = 20\mu m$) show their related EM energy

patterns. Generally, a smaller r means that the SPP mode dominates the hybrid mode, whereas a large r means that the coupling gives rise to a strongly confined mode. Also, decreasing the gap distance significantly enhances the electric field within the gap owing to small mode dimensions. Furthermore, most of the energy density will be distributed inside the Si waveguide if the height h is further increase.

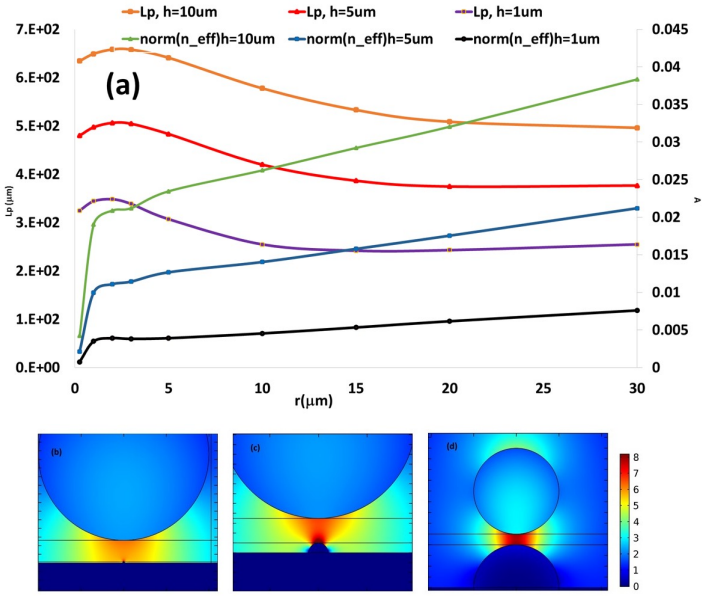

Figure 5.2: Dependences of modal properties of proposed structure at 1 THz. (a) Large propagation length and normalized mode area as a function of ridge r. (b) Field distribution of SPP mode with $r = 250nm$, $h = 5\mu m$, and $D = 20\mu m$, (c) field distribution of gap mode with $r = 2\mu m$, $h = 5\mu m$, and $D = 20\mu m$, and (d) field distribution of hybrid mode with $r = 20\mu m$, $h = 5\mu m$, and $D = 20\mu m$.

The numerical simulation results show that the proposed STHSPP waveguide has the capability of controlling the hybridization, which can be achieved by adjusting the diameter of the Si microwire, D, until one obtains an optimal value. Fig. 5.3 shows L_p and n_{eff} as a function of D with $h = 10\mu m$. It can be seen that the normalized mode area decreases exponentially as D increases until it reaches the optimal value (i.e., $20\mu m$). This scenario occurs for all gaps between the GaAs ridge and the waveguide.

Regarding the propagation length, when D increases from 5 to 55 μm, it slightly depends on the parameter D. This is followed by a further increase as D varies from 55 to 100 μm, which indicates that there is an optimal value of D, i.e., around 20 μm. For example, the propagation length increases from about 1273 to 2955 μm and the normalized mode area decreases from 0.45 to 0.099 as D increases from 5 to 40 μm, as illustrated in Fig. 5.3. This can be understood as follows: when D is small, the EM field is highly localized at the interface between GaAs and SiO_2, meaning that the structure acts as a pure SPP waveguide, resulting in a larger mode area and a smaller propagation length. On the other hand, when D is sufficiently large, a waveguide mode with a low loss in the Si microwire emerges and the propagation length begins to increase. The corresponding field distributions are also plotted in the insets of Fig. 5.3, showing the hybrid mode and SPP localization. It is worth noting that the selection of the values of h, r , and D is important because appropriate values give rise to the strongest mode confinement and largest propagation length.

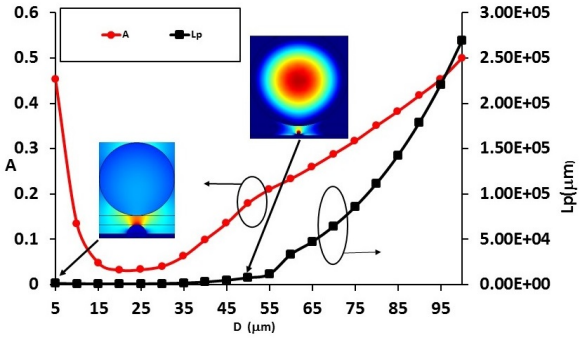

Figure 5.3: Normalized mode area A and propagation length L_p as a function of diameter of Si waveguide at a frequency of 1 THz. Insets: EM energy density patterns with different values of D.

The carrier concentration n of a semiconductor is an important parameter for designing plasmonic waveguides in the THz regime. In this simulation, the waveguide parameters are defined as the optimal values mentioned above. From the simulation, one can see that as n increases from 0.5×10^{17} to 2×10^{17} cm^{-3}, the normalized mode area increases from

0.0081 to 0.0126 and the propagation length increases from 115 to 483 μm. This can be physically explained by the fact that the real part of the dielectric permittivity of GaAs increases with n, which means that the penetration depth into GaAs decreases, resulting in a decreased attenuated loss, i.e., a larger propagation length. In other words, by varying the carrier concentration, one can tune the propagation loss of the STHSPP mode as well as the degree of mode confinement.

Let us now turn our attention to the fabrication process and fabrication error tolerance, which can be used to demonstrate the fabrication feasibility. For example, a precise alignment in the horizontal direction between the Si microwire and the GaAs ridge is a challenge, so the investigation of misalignment is highly desired. The centers of the Si microwire and the GaAs ridge have to be aligned with each other, i.e., there should be no shift S. When both centers are not aligned (off-center), there is a misalignment shift, which affects the normalized mode area and propagation length, as shown in Fig. 5.4. According to Fig. 5.4, however, there is no significant change in mode area or propagation length when S changes from 1 to 5 μm. For example, the calculations show that the normalized mode area increases by less than 10% when the shift increases from 0 to 5 μm. Conversely, for the propagation length, the error is less than only 3% for the same shift compared with that in an ideal case. The results suggest that the proposed STHSPP waveguide exhibits a good tolerance to fabrication errors.

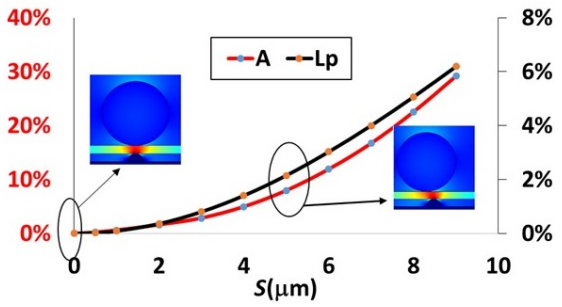

Figure 5.4: Fabrication errors of propagation length and mode area as a function of shift S. Insets: TM energy density patterns for structures with shift and without shift.

We found that, in terms of the gap size corresponding to the shift error, the main loss mechanism is radiation leakage into free space. This allows one to control the mode confinement and L_p. The simulation results show that the proposed STHSPP waveguide has a strong mode confinement within the gap, which indicates that the overlap between the field of the STHSPP and the dielectric within the gap is large. This gives it great potential in biosensing applications.

In this work, one can use the microfluidic channel to guide the sample liquid into the gap. It should be noted that a feasible method to pump the reagents and samples into the microfluidic channel is required [104]. Such a method for fabricating the on-chip microfluidics is explained in detail in Ref. [103]. Also, a review of the fabrication techniques and applications of microfluidics can be found in Ref. [105]. In order to verify the optimal parameters, the simulation result is depicted in Fig. 5.5 for a gap size of 5 μm. One can clearly observe that L_p and A are affected by the refractive index as it varies between 1.33 and 1.38. From Fig. 5.5, one can conclude that A and L_p show a highly linear decrease with an increase in liquid refractive index. Knowing this, one can predict the values of $A$and L_p for other values of the refractive index.

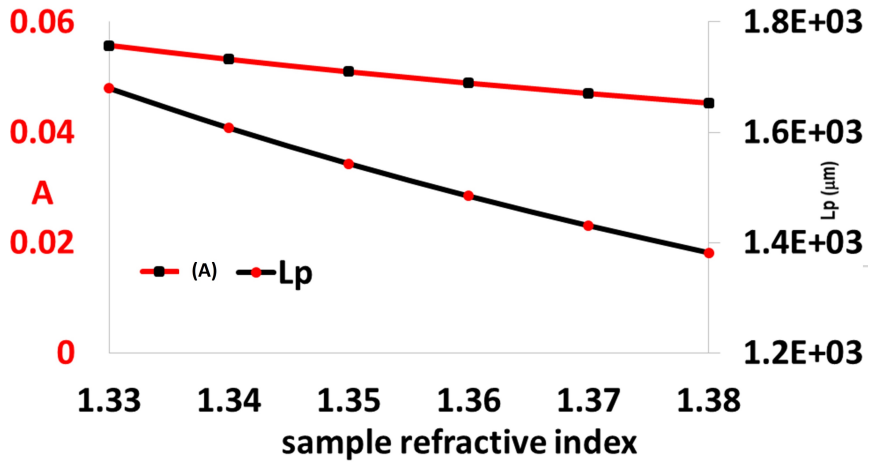

Figure 5.5: Propagation length and mode area as a function of refractive index.

A more important issue is to compare our result with the THz waveguide (plasmonic waveguide using doped GaAs) waveguide in Ref. [94]. The proposed STHSPP waveguide outperforms the existing THz plasmonic waveguide using doped GaAs, having a propagation length of $1147\mu m$, 2.5 times that of the waveguide $(430\mu m)$ in Ref. [94], with the same gap of $20\mu m$, a Si diameter of $20\mu m$, a frequency of 0.9 THz, the same refractive index, and $N = 0.6 \times 10^{17} cm^{-3}$.

The other essential parameter, the carrier concentration doping level, also plays an important role in waveguide performance. Physically, changing the doping level may influence the coupling of surface plasmons, thus affecting the optical properties of the STHSPP. To address this point, the mode size was simulated as a function of the doping level at 1 THz, as shown in Fig. 5.6. Here it can be clearly seen that the mode properties are affected by changing the doping level. As a result, decreasing the concentration decreases the mode area. This result indicates that it is possible to adjust the mode area of the STHSPP mode by varying the concentration.

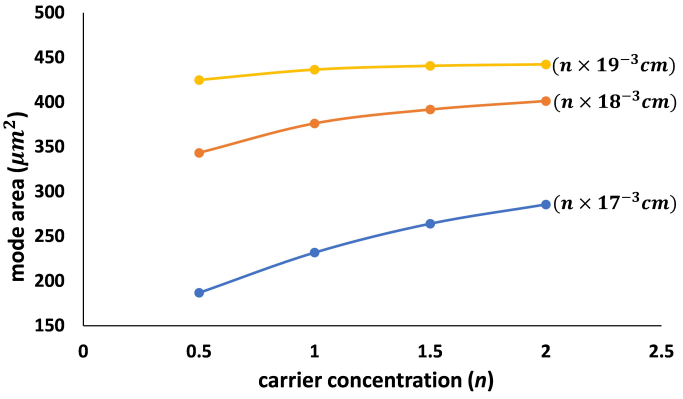

Figure 5.6: Mode size of propagation length as a function of doping level at 1 THz.

Finally, Fig. 5.7 shows the suggested fabrication steps for the experimental verification of the proposed structure. The process is described as follows. (a) The structure composed of

SiO_2, GaAs, and Si layers is deposited on a silica substrate. (b) The GaAs ridge is formed by the Electron beam lithography technique [93]. (c) The microfluidic channel is deposited. In a real fabrication proces, we would use materials such as silica or quartz owing to their excellent THz properties. (d) To produce the Si microwire with precise dimensions, the vapor-liquid-solid method can be used [106]. (e) The SiO_2 layer is dissolved in acetone, leaving the GaAs exposed, at which point the proposed structure is complete.

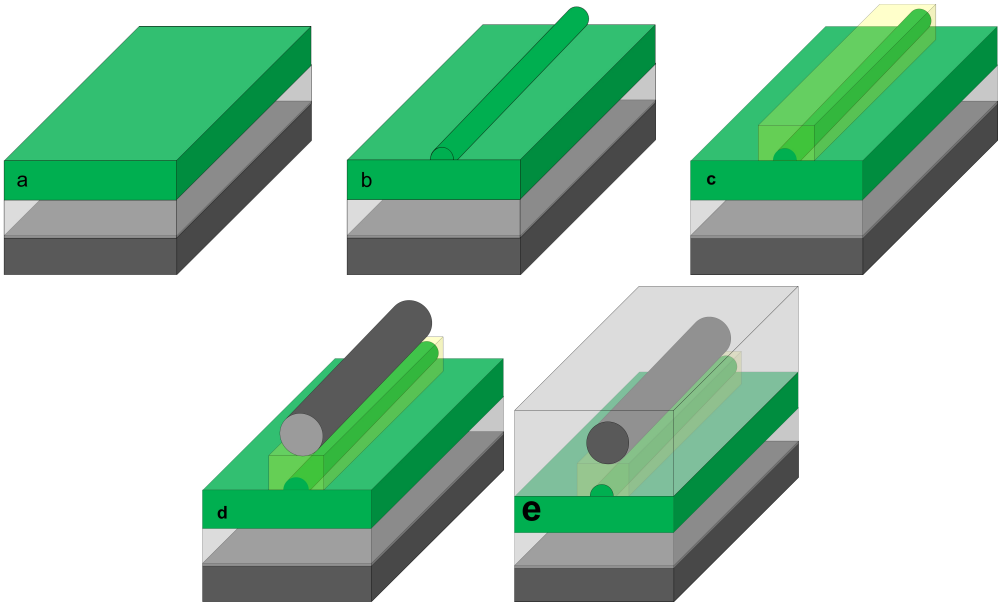

Figure 5.7: Schematic diagrams of fabrication process.

5.4 CONCLUSION

In conclusion, we have proposed and numerically investigated an STHSPP waveguide that is compatible with standard processes for silicon-on-insulator (SOI) technology. The simulation results reveal that the structure has very good tolerance to fabrication errors. We showed that different carrier concentrations in GaAs can be used to tune the propagation length L_p and the mode area A. We also showed that the STHSPP waveguide exhibits

a higher performance than other conventional HSPP waveguides. The deep mode confinement and the large propagation length suggest great potential for use in several THz semiconductor devices, such as microtweezers and highly integrated circuits.

Chapter 6

PLASMONIC PROPERTIES OF SUPERCONDUCTOR-INSULATOR-SUPERCONDUCTOR WAVEGUIDE

This chapter presents a theoretical study of a superconductor-insulator-superconductor waveguide at both THz and telecommunication frequencies. Yttrium-Barium-Copper-Oxide has been chosen as the superconductor, since Yttrium-Barium-Copper-Oxide exhibits better plasmonic behavior in the THz range, as compared to other telecommunication frequencies. The numerical results indicate a strong potential for use in several applications, such as biosensing and quantum information technology.

My contributions include proposing part of the idea, simulating and calculating properties of the proposed waveguide, analyzing the data, and writing the initial manuscript. Finally, because permission of the Applied Physics Express journal has been obtained, the paper itself is attached at the end of this thesis.

" Ma, Youqiao, Mohamed Eldlio, Hiroshi Maeda, Jun Zhou, and Michael Cada. "Plasmonic properties of superconductor–insulator–superconductor waveguide." Applied Physics Express 9, (2016), 072201."

6.1 ABSTRACT

The simultaneous realization of low propagation loss and subwavelength mode localization remains one of the critical challenges in plasmonics. Aiming to simultaneously realize

low propagation loss and subwavelength mode localization in plasmonics, we introduce a class of low-loss and deeply confined guiding schemes utilizing an alternative plasmonic material, i.e., a superconductor (SC). The optical properties of a SC-insulator-SC (SCISC) waveguide are analyzed both at terahertz (THz) and telecommunication (TC) frequencies. The SCISC waveguide features a deep-subwavelength confinement with mode length as small as $\lambda/6000$ $(\lambda/18)$ for THz (TC) frequency, while the propagation length can be extended up to $400mm$ $(1mm)$.

6.2 INTRODUCTION

Surface plasmon polaritons (SPPs) are electromagnetic waves coupled to electron oscillations and propagating along the interface between a conductor and a dielectric. As one of the most fascinating areas of Photonics, SPPs have attracted significant research interest for applications in subwavelength light guiding, slow light, and biosensing [107]. However, the prospects of SPPs are hindered by their large dissipative losses, and what is worse is that such losses will further increase if the mode size is downscaled to a subwavelength level. As a result, intensive research has been carried out to reduce the losses, such as by designing the hybridized SPP (HSPP) waveguide [44, 15] and using the gain medium to compensate for the propagation loss [108]. Although the propagation length up to 2 mm for the HSPP mode has recently been reported, it suffers from a complicated fabrication process [48]. On the other hand, the usage of the gain medium could mitigate the propagation loss, but it is found that even the best gain materials available are barely enough to compensate for the metallic loss [12].

Note that such loss is inherent to materials; thus, to search alternative plasmonic materials with lower losses, for example, semiconductors [109], graphene [110] and superconductors [111] seems a promising solution. Very high doping levels are necessary for

semiconductors to exhibit a negative real permittivity at optical frequencies, but achieving such extremely high doping levels is challenging [112]. Graphene is another good alternative plasmonic material owing to its zero band-gap and high carrier mobility, which has been demonstrated for THz applications [113]. However, its losses are still comparable to those of noble metals at near-infrared (NIR) frequencies [12]. On the contrary, the zero-resistance superconductor (SC), in principle, offers a practical approach to eliminate the dissipative loss [111]; thus, it has attracted rapidly growing interest. In recent years, many SC plasmonic structures, including low-loss propagating terahertz SC SPPs [114] and the extraordinary transmission from the perforated SC films [115, 116] have been proposed and investigated. However, very little attention has thus far been paid to analyze the optical properties of the SC-insulator-SC (SCISC) waveguide at both terahertz (THz) and telecommunication (TC) frequenciesor to comparing it with its counterpart structure, i.e., the metal–insulator–metal (MIM) waveguide. Therefore in this paper, the plasmonic properties of the SCISC waveguide are discussed at both THz and TC frequencies.

6.3 RESULT AND DISCUSSION

Numerical results show that the SCISC waveguide features a large propagation length (ranging from 55 mm to 400 mm) and a deep-subwavelength mode confinement (ranging from $\lambda/6000$to $\lambda/300$) for THz frequency. Albeit the superconductivity will eliminate if SC operates at TC frequency, the SCISC (strictly it cannot be named as SC) waveguide still possesses a fivefold enhanced figure of merit (FoM) compared to the MIM waveguide [115].

Figure 6.1 depicts the schematic diagram of two-dimensional (2D) SCISC waveguide, consisting of a dielectric core sandwiched between two identical semi-infinite SC claddings.

The core width is noted as d, the permittivities of the core and cladding are respectively assumed as ε_1 and ε_2.

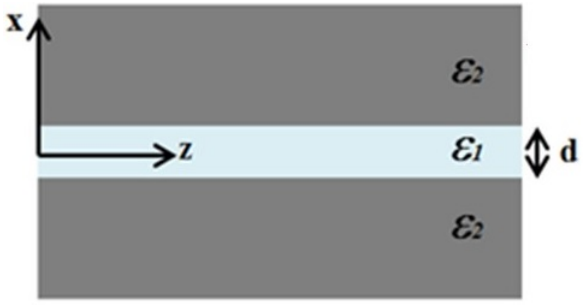

Figure 6.1: Schematic diagram of the SCISC heterostructure waveguide.

Assuming the SPP wave travels along z-direction with a propagation constant β, then the electromagnetic field for the TM mode can be expressed as follows [117]:

$$\begin{cases} H_y = Ae^{j\beta z}e^{-k_2 x} \\ E_x = -\frac{A\beta e^{j\beta z}e^{-k_2 x}}{\omega\varepsilon_1\varepsilon_2} \\ E_z = j\frac{k_2 A e^{j\beta z}e^{j\beta z}e^{-k_2 x}}{\omega\varepsilon_1\varepsilon_2} \end{cases} \quad \text{for } |x| > d/2 \tag{6.1}$$

$$\begin{cases} H_y = 2Be^{j\beta z}\cosh(k_1 x) \\ E_x = -\frac{2B\beta e^{j\beta z}\cosh(k_1 x)}{\omega\varepsilon_1\varepsilon_2} \\ E_z = -j\frac{2Bk_1 e^{j\beta z}sinh(k_{1x})}{\omega\varepsilon_1\varepsilon_2} \end{cases} \quad \text{for } |x| < d/2 \tag{6.2}$$

Here, $k_1 = \sqrt{\beta^2 - k_0^2\varepsilon_1}$ and $k_2 = \sqrt{\beta^2 - k_0^2\varepsilon_2}$. The dispersion relation is obtained from the boundary condition [2]:

$$\tanh\left(\frac{k_1 d}{2}\right) = -\frac{k_1\varepsilon_2}{k_2\varepsilon_1} \tag{6.3}$$

In this study, Yttrium-Barium-Copper-Oxide (YBCO) was selected as the SC because it possesses a better plasmonic behavior in the THz range [114]. For comparison, the chosen metal was silver (Ag) owing to its relatively low loss. The temperature-dependent permittivity of YBCO (ε_{2YBCO}) and Ag (ε_{2Ag}) are described by Drude models [114, 2]. For example, the permittivity ε_{2YBCO} can be expressed as:

$$\varepsilon_{2YBCO} = \frac{\omega^2\tau^2(\omega^2-\omega_s^2-\omega_n^2)+(\omega^2-\omega_s^2)}{\omega^2(\omega^2\tau^2+1)} + j\frac{(\omega_n^2\tau)}{\omega^2\tau^2+\omega} \tag{6.4}$$

where τ is the relaxation time, ω_s is the plasma frequency, and ω_n is the normal electron plasma resonant frequency, which are given as:

$$\tau = \frac{t^{\xi}+at(1-t^{\xi})}{t^{(}(1+\xi)\gamma_c}, \omega_s = \sqrt{\frac{N_s e^2}{\varepsilon_0 m_0}}, \omega_n = \sqrt{\frac{N_n e^2}{\varepsilon_0 m_0}} \tag{6.5}$$

Here, ξ and a are the fitting parameters, e is the electron charge, m_0 is the mass of a free electron, $t = T/T_c$ (T_c is the critical temperature and T is the operating temperature), γ_c is the scattering rate at T_c, $N_s = N[1-t^4]$ and $N_n = Nt^4$ are respectively the superconducting electron and normal electron densities, where N is the temperature-independent total density of free carriers. In addition, the permittivity (ε_{2Ag}) is obtained by $\varepsilon_{2Ag} = \varepsilon_{\infty} - \frac{\omega_p^2}{\omega(\omega+j\omega_c)}$, where ω_p is the temperature-dependent plasmon frequency and ω_c is the collision frequency of the free electrons, with forms as:

$$\omega_p = \frac{\omega_{pT_0}}{\sqrt{1+3\gamma(T-T_0)}}, \omega_c = \frac{0.012\pi^4\left[(TK_B)^2+\left(\frac{\hbar\omega}{2\pi}\right)^2\right]+E_F\Lambda}{\hbar E_F} \tag{6.6}$$

where ω_{pT_0} is the plasmon frequency at room temperature T_0, γ is the thermal linear expansion coefficient, $\hbar$ is the Plank's constant, $\Lambda = \hbar\omega_{eph}$ (ω_{eph} is the electron-photon scattering coefficient), E_F is Fermi level energy and K_B is the Boltzmann constant.

Before examining the plasmonic properties of the SCISC waveguide, the material properties of the YBCO and Ag at T = 40 K were analyzed. Fig. 6.2 shows their permittivities around the (a) 1 THz and (b) TC frequencies. Generally, the wavelength will be used rather than the frequency for the TC range. The parameters of Drude model for YBCO are [118]: $T_c = 88\,K$, $\xi = 1.5$, $a = 10$, $N = 1.255 \times 1027 m^{-3}$ and $\gamma_c = 0.28 \times 1014$ Hz, while those for Ag are [2]: $\varepsilon_\infty = 3.67$, $\gamma = 1.5 \times 10^{-15} K^{-1}$, $E_F = 2980$ THz, and $\Lambda = 4$ THz. As shown in Fig. 6.2, within the frequency range of interest, both the YBCO and Ag exhibit negative Real(ε) values, making them essential plasmonic materials. However unlike the optical properties at TC frequency, the Real (ε) values of YBCO and Ag are very large at THz frequency, giving rise to the negligible field penetration into the conductor. In addition, YBCO exhibits a smaller imaginary part of permittivity, indicating a lower loss for YBCO compared with Ag.

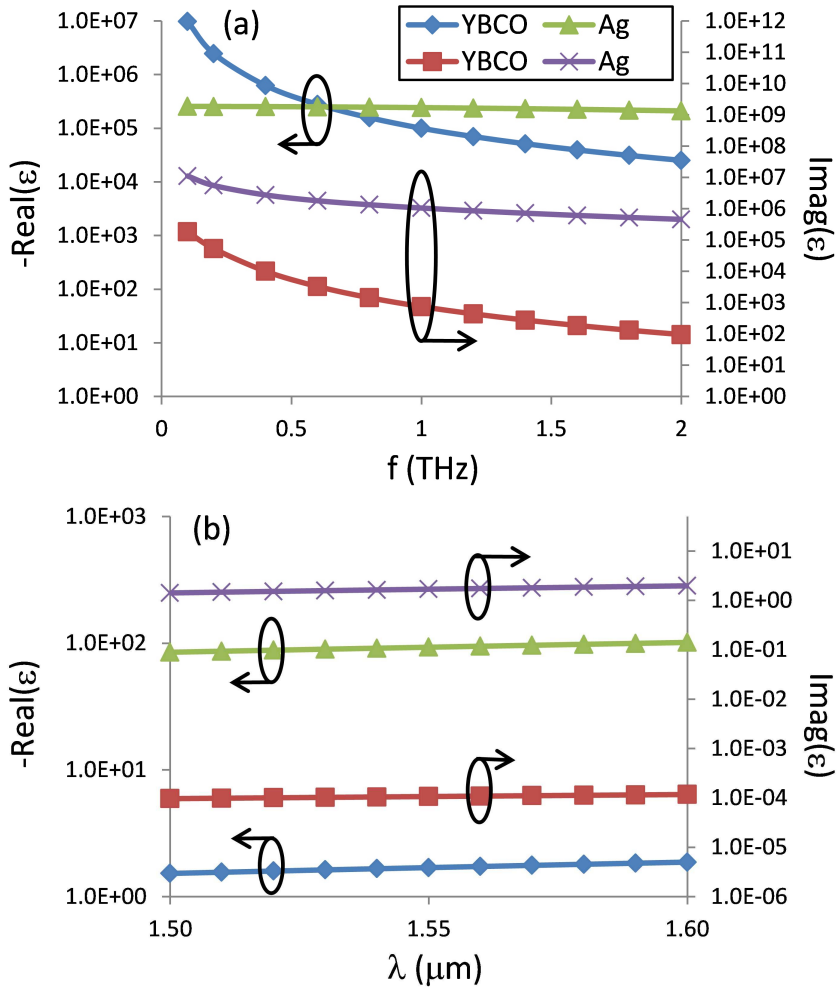

Figure 6.2: Real and imaginary parts of permittivity of the YBCO and Ag around (a) THz and (b) TC frequencies.

Then, the dispersion relations for the SCISC and MIM waveguides were investigated and are shown in Fig. 6.3 (a). Air was chosen as the core insulator, and other parameters were T =40 K and $d = 500nm$. It should be mentioned that some other materials can be used as the core insulator for the practical fabrication, such as Silica (SiO_2), Polymethylpentene (TPX) and Teflon, owing to their excellent transparency and relatively low reflectivity at THz frequency [91]. From Fig. 6.3 (a) it is found that the SCISC waveguide plot lies on the right side of that for the MIM waveguide with d = 50 nm, that is, the SPP wavelength for the SCISC waveguide is shorter than that for the MIM waveguide. Figs. 6.3 (b) and 6.3 (c)

respectively show the E_x distributions for the SCISC waveguide at 1 THz and 193.4 THz (i.e., 1550 nm). Compared with TC frequency, the electric field is highly distributed in the insulator core and negligibly penetrated into the YBCO, indicating that YBCO behaves as a perfect electrical conductor (PEC) at THz frequencies.

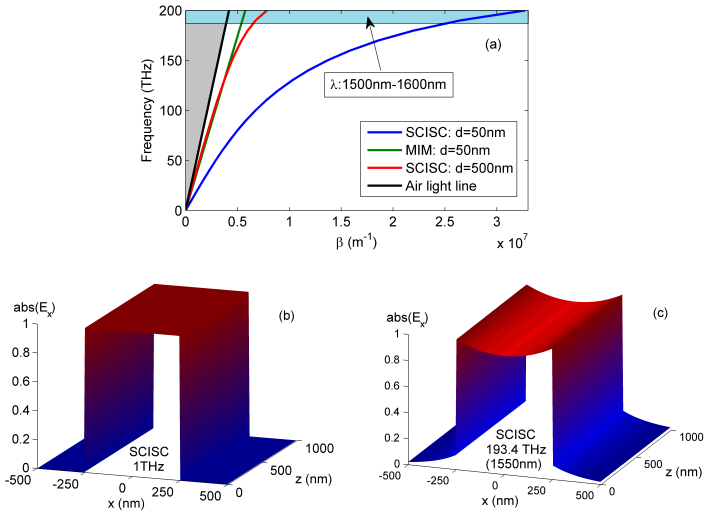

Figure 6.3: (a) Dispersion relations for the SCISC and MIM waveguides. Electric field profiles for the SCISC waveguide at (b) 1 THz and (c)1550*nm*.

The field profile depicted in Fig. 6.3 (b) is mainly the same as that of the TEM-like mode of a parallel-plate waveguide (PPWG) reported in [119]. To better distinguish the mode of the SCISC waveguide, Fig. 6.4 shows the contour plots of the normalized cross-sectional electric field (Ex) distribution versus the incident frequency for different core widths. As expected, the profiles are similar to the results in Ref. [119]. The field is located in the insulator core at low frequencies ($<$ 2 THz), which is corresponds to the TEM-like mode, while it is distributed at the edges for higher frequencies ($>$ 2 THz), which corresponds to the plasmonic mode. From Fig. 6.4, it is also noted that this mode transition is also determined by the core width. The coupling between the surface waves propagating on the two SC plates becomes stronger for the smaller core width; thus, the field is nearly constant

in the insulator core and vice versa. The SCISC waveguide operates in the plasmonic regime if the core width and frequency are larger than $300\mu m$ and 2 THz, respectively.

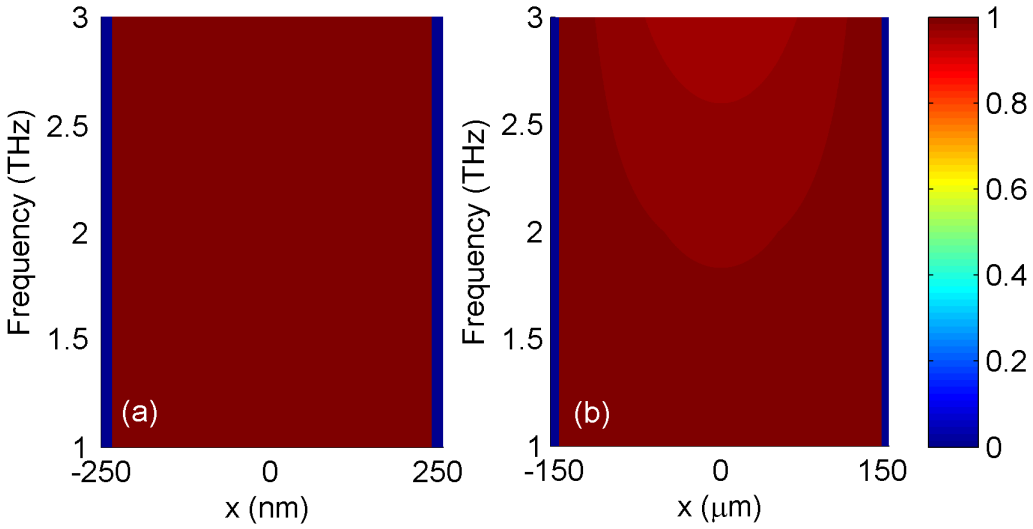

Figure 6.4: Contour plots of the normalized cross-sectional electric field profile as a function of frequency with different core widths of (a) $d = 500nm$ and (b) $d = 300\mu m$.

It is well known that the SPP waveguides could offer a subwavelength mode size beyond the diffraction limit but suffer from a small propagation length; thus, two key factors, propagation length (L_p) and mode length (L_m), need to be considered to characterize the performance of the SCISC waveguide [72]. The propagation length is calculated as $L_p = \lambda/([4\pi Im(n_{eff})])$, where $Im(n_{eff})$ is the imaginary part of the mode effective index n_{eff}, while the mode length L_m is defined as [120]:

$$L_m = \frac{\int W(z)dz}{max\{W(z)\}} \tag{6.7}$$

where W(z) is the electric field energy density. In addition, the normalized propagation length L_{NP} and normalized mode length L_{Nm} were also defined by $L_{Np} = {}^{L_p}/\lambda$ and $L_{Nm} = {}^{L_m}/L_0$, respectively, where $L_0 = \lambda/2$ is the diffraction-limited mode length. It should be noted that to overcome the diffraction limit requires $L_m < L_0$, which is $L_{Nm} < 1$.

Figure 6.5 shows the mode properties of the SCISC waveguide versus the core width d with $\varepsilon_1 = 1$ and $T = 40$ K. d was selected by considering the decay length of SPP mode at a single SC-I interface, for example, the decay lengths in the insulator are 15 mm at f=1 THz and 405 nm at λ=1550 nm, indicating that the respective maximum d values are around $30mm$ and $810nm$. As seen from Figs. 6.5 (a) and 6.5 (b), the mode length reasonably decreases with decreasing core width, suggesting a higher electromagnetic energy near the SC surface; thus, the propagation length decreases. On the other hand, it is also found that both L_{Nm} and L_{NP} increase with frequency. For lower frequencies, the larger real and imaginary parts of permittivity respectively give rise to smaller penetration depth and higher propagation loss, thus smaller mode and propagation lengths. What is important is that, as shown in Figs. 6.5 (a) and 6.5 (b), the mode lengths are far beyond the diffraction limit (depicted by a red solid arrow).

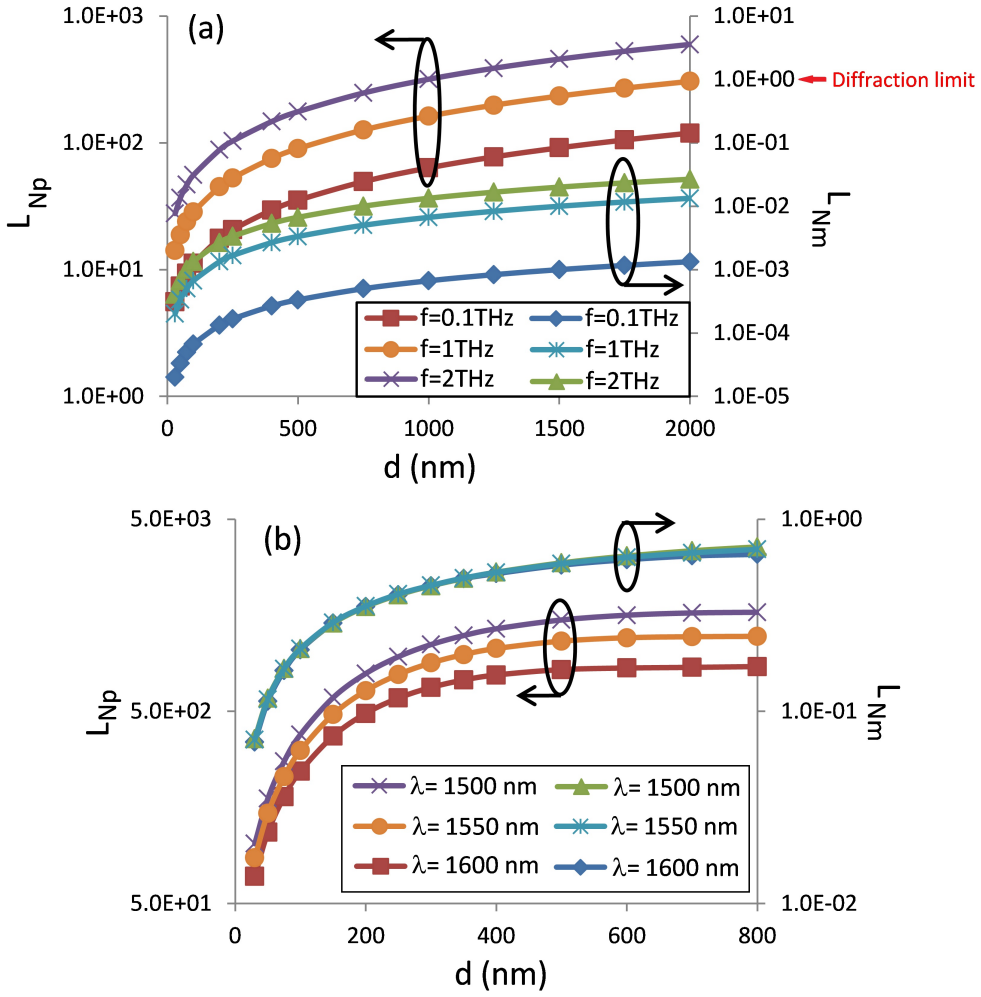

Figure 6.5: Mode characteristics of the SCISC waveguide as functions of the core width d around (a) THz and (b) TC frequencies.

The mode properties of the SCISC waveguide are also depend on the core insulator permittivity ε_1 and operating temperature T. Fig. 6.6 shows the mode properties depending on $\varepsilon_1$and T with d = 100 nm at (a) f=1 THz and (b) λ=1550 nm. The permittivity $\varepsilon_1$was considered from 1 to 13 for f=1 THz, while it was selected from 1 to 1.6 for λ=1550 nm owing to the fact that the real part of the permittivity of YBCO is 1.69 at $\lambda = 1550nm$. From Figs. 6.6 (a) and 6.6 (b), it is found that L_{NP} increases with decreasing ε_1. The physical mechanism can be explained in accordance with the electric field boundary condition, the continuity of normal component of electric displacement D (i.e. $\varepsilon_1 E_{1\perp} = \varepsilon_2 E_{2\perp}$). The

ratio of the electric field distributed in the insulator increases with decreasing ε_1, resulting in an extended L_{NP}. For the influence of ε_1 on L_{Nm}, we can see that variations are insignificant for f=1 THz, owing to the PEC-like character. However, for smaller $\varepsilon_1$at λ=1550 nm, the enhanced field in the insulator gives rise to the decreased penetration depth into the YBCO; thus, L_{Nm} decreases with decreasing ε_1. From Fig. 6.6 (a) and 6.6 (b), it is also found that the variations of L_{NP} are more sensitive to the operating temperature temperature T than those of L_{Nm}, suggesting a vital solution to the well-known tradeoff between the mode propagation length and mode confinement. For example, with $\varepsilon_1 = 1$ and f=1THz, the propagation length operating at T= 20 K (i.e., $L_{NP} = 1549$ and $L_p = 464mm$) is at least 55-fold-greater than that for $T = 40$ K ($L_{NP} = 28$ and $L_p = 8mm$) without sacrificing the mode size.

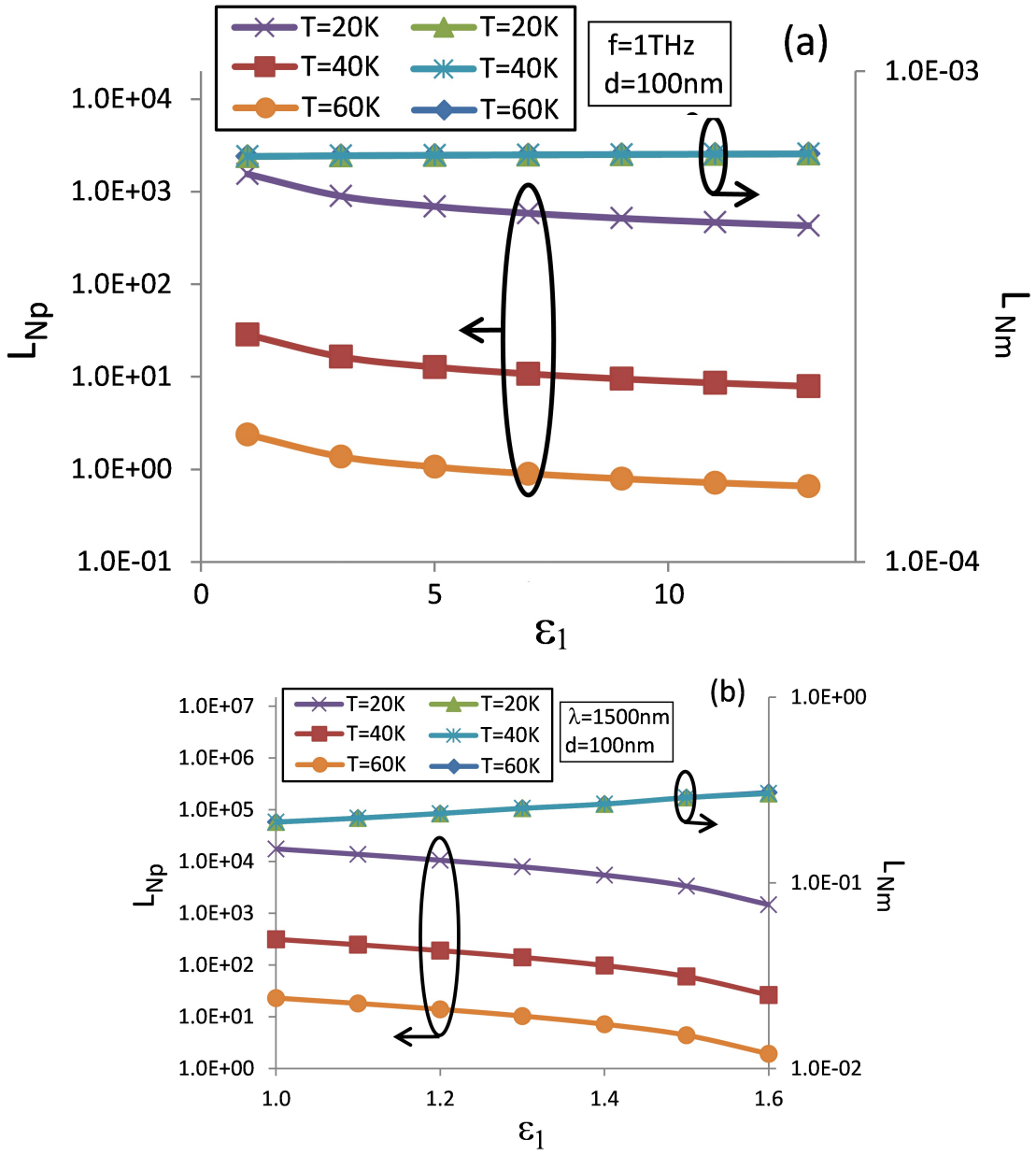

Figure 6.6: Mode characteristics of the SCISC waveguide as functions of ε_1 and T at (a) 1 THz and (b) TC frequencies.

The results discussed above indicate that the SCISC waveguide has a superior capability for low-loss subwavelength light guiding. To quantitatively demonstrate the superiority of the SCISC waveguide, Figs. 6.7 (a) and 6.7 (b) show the results for the SCISC and MIM

waveguides with $\varepsilon_1 = 1$ and $T = 40K$. Here, two types of SC are considered: the conventional SC Niobium (Nb) and unconventional SC YBCO. The parameters of the Drude model for Nb are [121]: $T_c = 9.26K, N = 9.4 \times 10^{27} m^{-3}$ and $\tau = 7.3 \times 10^{-10} s$. It illustrates that the mode lengths are almost the same; however, the propagation lengths of the SCISC waveguide are much larger than those of the MIM waveguide. For example, at d = 100 nm and λ=1550 nm, the propagation length for the SCISC: YBCO waveguide is increased at least eightfold compared with that of the MIM waveguide ($L_p = 485\mu m$ for SCISC: YBCO waveguide and $L_p = 55\mu m$ for MIM waveguide). At $d = 100nm$ and f=1 THz , the propagation length for the SCISC: YBCO waveguide is increased at least 80-fold compared with that of the MIM waveguide ($L_p = 85mm$ for SCISC: YBCO waveguide and $L_p = 1mm$ for MIM waveguide). Furthermore, it also illustrates that the SCISC: YBCO waveguide outperforms the SCISC: Nb waveguide, which shows a twofold greater propagation length. Fig. 6.7 (c) shows the FoM, which is defined as L_{Np}/L_{Nm} for the SCISC and MIM waveguides. From Fig. 6.7 (c) it is observed that the FoM for the SCISC waveguide are always larger than those for the MIM waveguide. Compared with that for the MIM waveguide, the FoM for the SCISC: YBCO waveguide demonstrates an improvement of at least 50-fold (5-fold) at d = 100 nm and f=1 THz (λ=1550 nm).

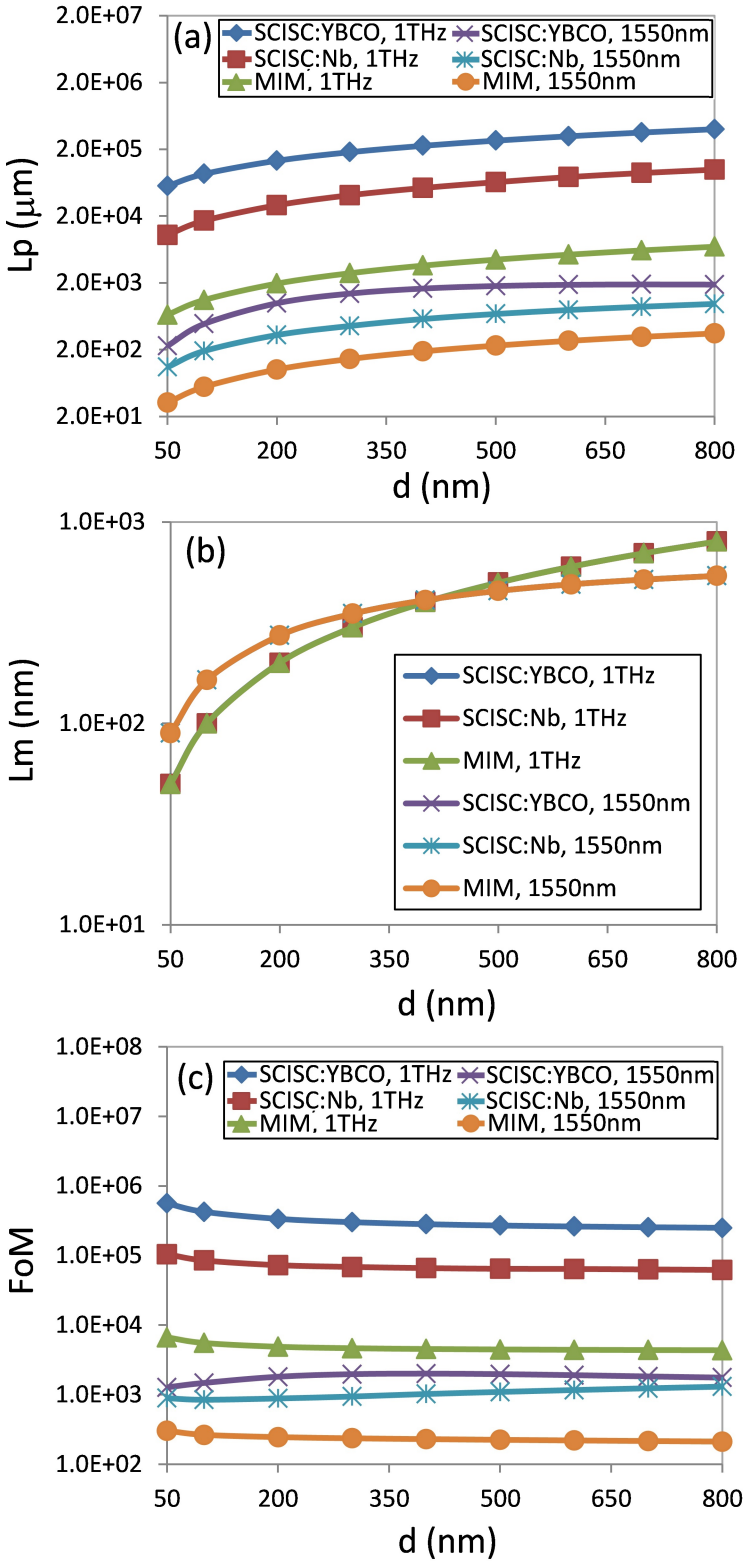

Figure 6.7: (a) Propagation length (b) mode lengths of SCISC (YBCO and Nb) and MIM waveguides, and (c) FoMs for the SCISC (YBCO and Nb) and MIM waveguides.

6.4 CONCLUSION

In summary, we have numerically investigated the optical properties of a SCISC waveguide and shown that the SCISC waveguide allows SPP transport on the subwavelength scale with a very large propagation length. The mode length can be as small as thousandths (tenths) of the vacuum diffraction limited size, and the propagation length can be extended up to hundreds of millimeters (micrometers) at THz (TC) frequencies. Compared with the MIM waveguide, a much larger propagation length, as well as a comparable mode length, greatly improves the FoM for the SCISC waveguide. The promising guiding properties of the SCISC waveguide could open up exciting avenues in the fields of plasmonic circuits, biosensing, and quantum information technology.

Chapter 7

CONCLUSION

This chapter summarizes the results obtained by the thesis and also proposes suggestions for future work as an extension of this Ph.D. study. The geometries that are the primary focus of attention in this thesis are the THz semiconductor-based hybrid plasmonic waveguides, which exhibit the capability of supporting SPPs.

7.1 Conclusions From The Research

Due primarily to their ability to confine light within the nanoscale in metal/semiconductors, plasmonic waveguides form the focus of this thesis work, which demonstrates their potential to become a basic structure for designs that require small sizes. This thesis presents the fundamental principles of waveguides, and then describes the modeling, investigation, design and analysis of plasmonic devices and their applications.

The purpose of this work was to build upon the understanding of surface plasmonics by investigating them further in the terahertz regime. However, plasmonic waveguides in THz/optical regimes remain problematic. One challenge is the trade-off between mode size and propagation length. This challenge limits the advantages of plasmonic devices and has delayed the use of plasmonic waveguides in practical applications, thus impacting the progress of plasmonic technology. In this thesis, the design of novel THz hybrid plasmonic waveguides has achieved an enhanced balance of deep confinement against low attenuation loss.

The overall research achievements and main contributions of this thesis can be summarized as follows:

1. Finding a suitable model that works for semiconductors instead of metal.
2. Designing structures that can support SPPs with low attenuation losses.
3. Using semiconductors instead of metals to increase the degree of freedom in the models and thus heighten the possibility of successful engineering for different plasmonic applications.
4. Investigating the effect of different parameters for superconductors at optical and THz frequencies.

In this work, the choices made were mainly designed to enable practical device applications. They are discussed in further detail below.

Drude-Lorentz model of semiconductor optical plasmons

In chapter 3, the study focused on finding a suitable model for semiconductors [10]. The main contribution of this work is the derivation of a generalized dispersion relation for semiconductors, with the aid of the Drude-Lorentz model. My approach, which is entirely different from those previously discussed, was primarily to explore interactions of the electromagnetic fields produced by using semiconductors at wavelengths within the optical range. By studying the experimental results of Dr. Cada's photonics lab report, I was able to consolidate it with the original model, draw conclusions, provide feedback, and propose

a new round of experiments for further validation of the model used, taking into consideration possible engineering applications. The new model developed for optical plasmon semiconductor behavior in materials with losses is a realistic and practical solution for future application devices. From the studies, it can be concluded that:

- The dispersion relation with respect to the wave vector when losses are taken into account shows that the plasmon dispersion dropped from 590 THz to about 432 THz, with identically strong dispersion around the resonant frequency.
- If losses are taken into account, according to the Drude-Lorentz model, the dispersion relation with respect to the wave vector is valid when the photon energy is well below the band gap of the semiconductor, including losses.
- It is possible to engineer an additional degree of freedom in this model to suit different plasmonic applications.

A long-range hybrid THz plasmonic waveguide with low attenuation loss.

This thesis establishes the concept of long-range hybrid plasmonics. In chapter 4 [45], by numerically examining a hybrid terahertz plasmonic waveguide using two silicon microwires separated by a thin metal film (Ag), I extended this study to double pairs of microwire as a step to improve waveguiding properties. The effects of various parameters on propagation length and normalized mode area were examined in order to achieve optimal parameters. Efficient waveguide transmission is crucial for several applications, and

we therefore believe this analysis is essential to the ongoing efforts of developing efficient terahertz waveguides. The guiding properties of the hybrid terahertz surface plasmon polariton (HTSPP) waveguide were numerically analyzed at the THz frequency, and double-structured comparisons were made of the best features of the terahertz plasmonic waveguide. This implementation made it possible to study hybrid waveguide properties in detail, including slot waveguide, symmetric mode and asymmetric mode properties. The key conclusions from this are as follows:

- The simulation results demonstrate that the propagation length and mode area can be obtained by adjusting the geometry characteristics of the microwire.
- For a single microwire pair, this structure shows a good balance between mode area and propagation length (i.e., for a microwire with 20 μm, the mode area is 487 μm^2 with a propagation length of $14 \times 10^3 \mu m$).
- Compared to the THz (HPTW) waveguide reported in [79], the proposed HTSPPs waveguide outperforms the existing HPTW, exhibiting a 1.2 increase in propagation length with the same parameters.
- The calculations clearly show that the normalized mode area and propagation length decreased when the frequency increased. Such frequency/thickness dependency offers a possibility of controlling the trade-off by selecting the appropriate parameters.

A THz semiconductor hybrid plasmonic waveguide with fabrication-error tolerance.

To mitigate the trade-off between the propagation length and mode confinement further, in chapter 5 [46], I proposed a novel waveguide based on semiconductor hybrid plasmonic

waveguide surface plasmon polaritons (STHSPPs), with a numerical investigation to examine 1D and 2D confinement. This structure showed good tolerance for fabrication errors. Although the proposed structure can be expected to exhibit unique light confinement and propagation length properties, only a suggestion of experimental results could be obtained. The numerical results of this work are nonetheless relevant to well-established THz hybrid plasmonic waveguide technologies. The structure benefits from low propagation loss at the microchannel, which has a low refractive index sandwiched between Si microwire and a GaAs ridge, as well as increased field confinement. I found that the semiconductor has a significant impact on the properties of SPPs. Moreover, it permits the use of a THz hybrid plasmonic waveguide using doped GaAs, indicating that GaAs plasmonic waveguides offer promising solutions to enhance the mode area while managing loss at an acceptable level. This has great potential for the realization of biosensor and integrated photonic circuits such as micro-tweezers. With an appropriate selection of structural parameters, it can be concluded that:

- The STHSPPs could be very useful for confining light in the ultra-deep-subwavelength region (ranging from $\lambda^2/360$ to $\lambda^2/156$), with a long propagation length ranging from 374 to 506 μm.
- The fabrication steps suggested for an experimental verification of the proposed structure include some micro-fabrication techniques such as Electron beam lithography and vapor-liquid-solid methods.
- STHSPPs have an acceptable level of tolerance for fabrication. For example, the calculations show that the normalized mode area increases by less than 10% when the shift of microwire increases from 0 to 5 μm. Conversely, for the propagation

length, the error is less than 3% for the same shift, as compared to that in an ideal case.

- With the same parameters of gap = 20 μm, Si diameter = 20 μm, frequency = 0.9 THz, and the concentration $n = 0.6 \times 10^{17} cm^{-3}$, the proposed STHSPP waveguide can improve propagation length significantly, by at least 2.5 times, in comparison to the conventional THz plasmonic waveguide proposed in [94].

Plasmonic properties of superconductor-insulator-superconductor waveguide.

Simulation work concerning a plasmonic waveguide with superconductor claddings in a planar waveguide geometry is investigated theoretically in chapter 6 [49]. The main finding is the long plasmonic mode propagation length in SC-dielectric-SC waveguide geometry, the main contribution of which is to eliminate propagation loss. With the appropriate selection of structural parameters, it can be concluded that:

- A propagation length exceeding 400 mm for YBCO claddings was achieved at a temperature of T = 20 K and an operating frequency of about 1THz.
- Numerical results show that the SCISC waveguide features a long propagation length (ranging from 55 mm to 400 mm) and a deep-subwavelength mode confinement (ranging from $\lambda/6000$ to $(\lambda)/300$) for the THz frequency.
- Compared to the propagation length of (˜ tenth of mm) in [15], the improvement of propagation length is about forty-fold, which is very important for this field of research.

- Although the superconductivity pair breaks if the SC works at a TC frequency, the SCISC waveguide (which cannot be referred to as an SC) still has a five-fold enhanced Figure of Merit (FoM) in comparison with the MIM waveguide.

7.2 Future Work

More work needs to be done on the design of newer types of plasmonic devices before it can be seen which applications will ultimately benefit from plasmonics. For example:

1. Experimental evidence is needed to show the effectiveness of the ideas proposed above. Numerous techniques have been investigated, such as classical THz microscopy, aperture [122] and terahertz near-field microscopy [123, 124], as well as the use of nano/microfabrication tools and measurement of optical characteristics at THz frequencies by utilizing near-field microscopy techniques.

2. To implement a microfluidic channel for the above proposal, due to the need for fluid control, the microfluidic channel should be explored in more depth by choosing appropriate materials. The choice of materials depends upon the requirements and conditions, such as the properties of semiconductors (e.g., the refractive index).

3. Practical applications of the structures proposed above have been attracting increased attention in many fields; they should be considered for use in micro-tweezers, for example. The proposed semiconductor hybrid plasmonic waveguide surface plasmon polaritons (SHPSPPs) offer some advantages for fabricating new types of devices and could become one of the field's great discoveries.

4. Plasmonic waveguides cannot realize zero loss propagation, due to Ohmic loss. Therefore, a gain medium could address such a critical loss challenge, as guiding light beyond the diffraction limit is possible through promising technological developments that shrink the scale and frequency of Integrated Photonic Circuits (IPCs). However, there are still some limitations, the most important of which is that SPPs suffer significant propagation loss. To overcome this limitation, a medium with gain should be introduced. Some recent research has explored the possibility of loss compensation by using a gain material [125]. The gain medium can be introduced within the gap region, to increase propagation significantly [126]. Therefore, compensation through the use of a gain medium to obtain an ultra-deep subwavelength in small areas could be a promising approach for future work.

Bibliography

[1] H. Raether, *Surface plasmons on smooth surfaces*. Springer, 1988.

[2] S. A. Maier, *Plasmonics: fundamentals and applications*. Springer Science & Business Media, 2007.

[3] L. Novotny and B. Hecht, *Principles of nano-optics*. Cambridge university press, 2012.

[4] S. Yushanov, J. Crompton, and K. Koppenhoefer, "Plasmonic waveguide analysis," 2015.

[5] E. Ozbay, "Plasmonics: merging photonics and electronics at nanoscale dimensions," *science*, vol. 311, no. 5758, pp. 189–193, 2006.

[6] J. M. Luther, P. K. Jain, T. Ewers, and A. P. Alivisatos, "Localized surface plasmon resonances arising from free carriers in doped quantum dots," *Nature materials*, vol. 10, no. 5, pp. 361–366, 2011.

[7] J. Jung and T. G. Pedersen, "Analysis of plasmonic properties of heavily doped semiconductors using full band structure calculations," *Journal of Applied Physics*, vol. 113, no. 11, p. 114904, 2013.

[8] W. L. Barnes, "Surface plasmon–polariton length scales: a route to sub-wavelength optics," *Journal of optics A: pure and applied optics*, vol. 8, no. 4, p. S87, 2006.

[9] M. Cada and J. Pistora, "Optical plasmons in semiconductors," in *ISMOT conference, June*, 2011, pp. 20–23.

[10] M. Eldlio, F. Che, and M. Cada, "Drude-lorentz model of semiconductor optical plasmons," in *IAENG Transactions on Engineering Technologies*. Springer, 2014, pp. 41–49.

[11] M. Z. Alam, J. S. Aitchison, and M. Mojahedi, "A marriage of convenience: Hybridization of surface plasmon and dielectric waveguide modes," *Laser & Photonics Reviews*, vol. 8, no. 3, pp. 394–408, 2014.

[12] P. R. West, S. Ishii, G. V. Naik, N. K. Emani, V. M. Shalaev, and A. Boltasseva, "Searching for better plasmonic materials," *Laser & Photonics Reviews*, vol. 4, no. 6, pp. 795–808, 2010.

[13] V. R. Almeida, Q. Xu, C. A. Barrios, and M. Lipson, "Guiding and confining light in void nanostructure," *Optics letters*, vol. 29, no. 11, pp. 1209–1211, 2004.

[14] B. Min, E. Ostby, V. Sorger, E. Ulin-Avila, L. Yang, X. Zhang, and K. Vahala, "High-q surface-plasmon-polariton whispering-gallery microcavity," *Nature*, vol. 457, no. 7228, pp. 455–458, 2009.

[15] R. F. Oulton, V. J. Sorger, D. Genov, D. Pile, and X. Zhang, "A hybrid plasmonic waveguide for subwavelength confinement and long-range propagation," *Nature Photonics*, vol. 2, no. 8, pp. 496–500, 2008.

[16] A. J. Baragwanath, A. J. Gallant, and J. M. Chamberlain, "Terahertz plasmonic structures," in *Terahertz Spectroscopy and Imaging*. Springer, 2012, pp. 539–568.

[17] X. Wang, Y. Deng, Q. Li, Y. Huang, Z. Gong, K. B. Tom, and J. Yao, "Excitation and propagation of surface plasmon polaritons on a non-structured surface with a permittivity gradient," *Light: Science & Applications*, vol. 5, no. 12, p. e16179, 2016.

[18] P. Berini, "Long-range surface plasmon polaritons," *Advances in Optics and Photonics*, vol. 1, no. 3, pp. 484–588, 2009.

[19] J. Homola and M. Piliarik, "Surface plasmon resonance (spr) sensors," in *Surface plasmon resonance based sensors*. Springer, 2006, pp. 45–67.

[20] C. Janke, J. G. Rivas, P. H. Bolivar, and H. Kurz, "All-optical switching of the transmission of electromagnetic radiation through subwavelength apertures," *Optics letters*, vol. 30, no. 18, pp. 2357–2359, 2005.

[21] J. G. Rivas, J. Sánchez-Gil, M. Kuttge, P. H. Bolivar, and H. Kurz, "Optically switchable mirrors for surface plasmon polaritons propagating on semiconductor surfaces," *Physical Review B*, vol. 74, no. 24, p. 245324, 2006.

[22] M. Kuttge, H. Kurz, J. G. Rivas, J. Sánchez-Gil, and P. H. Bolivar, "Analysis of the propagation of terahertz surface plasmon polaritons on semiconductor groove gratings," *Journal of applied physics*, vol. 101, no. 2, p. 023707, 2007.

[23] R. Ritchie, "Plasma losses by fast electrons in thin films," *Physical Review*, vol. 106, no. 5, p. 874, 1957.

[24] A. Sommerfeld, "Ueber die fortpflanzung elektrodynamischer wellen längs eines drahtes," *Annalen der Physik*, vol. 303, no. 2, pp. 233–290, 1899.

[25] J. Zenneck, "Über die fortpflanzung ebener elektromagnetischer wellen längs einer ebenen leiterfläche und ihre beziehung zur drahtlosen telegraphie," *Annalen der Physik*, vol. 328, no. 10, pp. 846–866, 1907.

[26] R. Wood, "Xlii. on a remarkable case of uneven distribution of light in a diffraction grating spectrum," *The London, Edinburgh, and Dublin Philosophical Magazine and Journal of Science*, vol. 4, no. 21, pp. 396–402, 1902.

[27] U. Fano, "The theory of anomalous diffraction gratings and of quasi-stationary waves on metallic surfaces (sommerfeldï¿œs waves)," *JOSA*, vol. 31, no. 3, pp. 213–222, 1941.

[28] A. Otto, "Excitation of nonradiative surface plasma waves in silver by the method of frustrated total reflection," *Zeitschrift für Physik*, vol. 216, no. 4, pp. 398–410, 1968.

[29] E. Kretschmann and H. Raether, "Notizen: radiative decay of non radiative surface plasmons excited by light," *Zeitschrift für Naturforschung A*, vol. 23, no. 12, pp. 2135–2136, 1968.

[30] B. Yao, Z. Fang, Y. Zhu, T. Ji, and G. He, "A model for the frequency dispersion of the high-k metal-oxide-semiconductor capacitance in accumulation," *Applied Physics Letters*, vol. 100, no. 22, p. 222903, 2012.

[31] A. V. Zayats, I. I. Smolyaninov, and A. A. Maradudin, "Nano-optics of surface plasmon polaritons," *Physics reports*, vol. 408, no. 3, pp. 131–314, 2005.

[32] C. F. Guo, T. Sun, F. Cao, Q. Liu, and Z. Ren, "Metallic nanostructures for light trapping in energy-harvesting devices," *Light: Science and Applications*, vol. 3, no. 4, p. e161, 2014.

[33] O. Krupin, W. R. Wong, P. Beland, F. R. M. Adikan, and P. Berini, "Long-range surface plasmon-polariton waveguide biosensors for disease detection," 2016.

[34] S. V. Boriskina, H. Ghasemi, and G. Chen, "Plasmonic materials for energy: From physics to applications," *Materials Today*, vol. 16, no. 10, pp. 375–386, 2013.

[35] N. C. Lindquist, P. Nagpal, K. M. McPeak, D. J. Norris, and S.-H. Oh, "Engineering metallic nanostructures for plasmonics and nanophotonics," *Reports on Progress in Physics*, vol. 75, no. 3, p. 036501, 2012.

[36] Y. Ma, N. Nguyen-Huu, J. Zhou, H. Maeda, Q. Wu, M. Eldlio, J. Pistora, and M. Cada, "Mach-zehnder interferometer-based integrated terahertz temperature sensor," *IEEE Journal of Selected Topics in Quantum Electronics*, vol. 23, Issue: 4, pp. 1–7, July/August 2017.

[37] K. H. Lee, I. Ahmed, R. S. M. Goh, E. H. Khoo, E. P. Li, and T. G. G. Hung, "Implementation of the fdtd method based on lorentz-drude dispersive model on gpu for plasmonics applications," *Progress In Electromagnetics Research*, vol. 116, pp. 441–456, 2011.

[38] L. Rayleigh, "Xviii. on the passage of electric waves through tubes, or the vibrations of dielectric cylinders," *The London, Edinburgh, and Dublin Philosophical Magazine and Journal of Science*, vol. 43, no. 261, pp. 125–132, 1897.

[39] K. S. Packard, "The origin of waveguides: A case of multiple rediscovery," *IEEE Transactions on Microwave Theory and Techniques*, vol. 32, no. 9, pp. 961–969, 1984.

[40] O. Mitrofanov, R. James, F. A. Fernández, T. K. Mavrogordatos, and J. A. Harrington, "Reducing transmission losses in hollow thz waveguides," *IEEE Transactions on Terahertz Science and Technology*, vol. 1, no. 1, pp. 124–132, 2011.

[41] M. Ahmadi-Boroujeni, M. Shahabadi, and K. Altmann, "Thz plasmonic devices based on an array of metallic posts in a parallel-plate waveguide," in *2013 38th International Conference on Infrared, Millimeter, and Terahertz Waves (IRMMW-THz)*. IEEE, 2013, pp. 1–2.

[42] C. Yeh and F. I. Shimabukuro, *The essence of dielectric waveguides*. Springer, 2008.

[43] Q. Xu, V. R. Almeida, R. R. Panepucci, and M. Lipson, "Experimental demonstration of guiding and confining light in nanometer-size low-refractive-index material," *Optics letters*, vol. 29, no. 14, pp. 1626–1628, 2004.

[44] L. Chen, T. Zhang, X. Li, and W. Huang, "Novel hybrid plasmonic waveguide consisting of two identical dielectric nanowires symmetrically placed on each side of a thin metal film," *Optics express*, vol. 20, no. 18, pp. 20 535–20 544, 2012.

[45] M. Eldlio, Y. Ma, H. Maeda, and M. Cada, "A long-range hybrid thz plasmonic waveguide with low attenuation loss," *Infrared Physics & Technology*, 2016.

[46] M. Eldlio, Y. Ma, F. Che, H. Maeda, and M. Cada, "A thz semiconductor hybrid plasmonic waveguide with fabrication-error tolerance," *Japanese Journal of Applied Physics*, vol. 56, no. 1, p. 010306, 2017.

[47] M. Alam, F. Bahrami, J. Aitchison, and M. Mojahedi, "Analysis and optimization of hybrid plasmonic waveguide as a platform for biosensing," *IEEE Photonics Journal*, vol. 6, no. 4, pp. 1–10, 2014.

[48] Y. Ma, G. Farrell, Y. Semenova, and Q. Wu, "Hybrid nanowedge plasmonic waveguide for low loss propagation with ultra-deep-subwavelength mode confinement," *Optics letters*, vol. 39, no. 4, pp. 973–976, 2014.

[49] Y. Ma, M. Eldlio, H. Maeda, J. Zhou, and M. Cada, "Plasmonic properties of superconductor–insulator–superconductor waveguide," *Applied Physics Express*, vol. 9, no. 7, p. 072201, 2016.

[50] B. Ferguson and X.-C. Zhang, "Materials for terahertz science and technology," *Nature materials*, vol. 1, no. 1, pp. 26–33, 2002.

[51] T. Otsuji, V. Popov, and V. Ryzhii, "Active graphene plasmonics for terahertz device applications," *Journal of Physics D: Applied Physics*, vol. 47, no. 9, p. 094006, 2014.

[52] A. Menikh, "Terahertz-biosensing technology: progress, limitations, and future outlook," in *Optical Guided-wave Chemical and Biosensors II*. Springer, 2010, pp. 283–295.

[53] M. F. Kimmitt, "Restrahlen to t-rays–100 years of terahertz radiation," *Journal of biological physics*, vol. 29, no. 2-3, pp. 77–85, 2003.

[54] X. Yang, X. Zhao, K. Yang, Y. Liu, Y. Liu, W. Fu, and Y. Luo, "Biomedical applications of terahertz spectroscopy and imaging," *Trends in biotechnology*, 2016.

[55] D. Gacemi, J. Mangeney, R. Colombelli, and A. Degiron, "Subwavelength metallic waveguides as a tool for extreme confinement of thz surface waves," *Scientific reports*, vol. 3, p. 1369, 2013.

[56] S. Pandey, B. Gupta, and A. Nahata, "Terahertz plasmonic waveguides created via 3d printing," *Optics express*, vol. 21, no. 21, pp. 24 422–24 430, 2013.

[57] S. Li, M. M. Jadidi, T. E. Murphy, and G. Kumar, "Terahertz surface plasmon polaritons on a semiconductor surface structured with periodic v-grooves," *Optics express*, vol. 21, no. 6, pp. 7041–7049, 2013.

[58] A. Markov and M. Skorobogatiy, "Hybrid plasmonic terahertz fibers for sensing applications," *Applied Physics Letters*, vol. 103, no. 18, p. 181118, 2013.

[59] K. S. Yee *et al.*, "Numerical solution of initial boundary value problems involving maxwellï¿œs equations in isotropic media," *IEEE Trans. Antennas Propag*, vol. 14, no. 3, pp. 302–307, 1966.

[60] J.-M. Jin and D. J. Riley, *Finite element analysis of antennas and arrays*. John Wiley & Sons, 2009.

[61] D. M. Sullivan, *Electromagnetic simulation using the FDTD method*. John Wiley & Sons, 2013.

[62] S. Chakravorti, *Electric field analysis*. CRC Press, 2015.

[63] [Online]. Available: http://fab.cba.mit.edu/classes/S62.12/docs/COMSOL_Multiphysics.pdf

[64] M. Eldlio, F. Che, and M. Cada, "Optical semiconductor surface-plasmon dispersion including losses using the drudelorentz model," in *World Congress on Engineering and Computer Science 2012 (WCECS 2012)*. Newswood Limited, 2012.

[65] M. Fox, *Optical properties of solids*. Oxford university press, 2010, vol. 3.

[66] S. L. Chuang, *Physics of photonic devices*. John Wiley & Sons, 2012, vol. 80.

[67] I. Ahmed, E. H. Khoo, O. Kurniawan, and E. P. Li, "Modeling and simulation of active plasmonics with the fdtd method by using solid state and lorentz–drude dispersive model," *JOSA B*, vol. 28, no. 3, pp. 352–359, 2011.

[68] Y. Huang and S.-T. Ho, "Computational model of solid-state, molecular, or atomic media for fdtd simulation based on a multi-level multi-electron system governed by pauli exclusion and fermi-dirac thermalization with application to semiconductor photonics," *Optics express*, vol. 14, no. 8, pp. 3569–3587, 2006.

[69] A. Hryciw, Y. C. Jun, and M. L. Brongersma, "Plasmonics: Electrifying plasmonics on silicon," *Nature materials*, vol. 9, no. 1, pp. 3–4, 2010.

[70] M. Van Exter and D. Grischkowsky, "Optical and electronic properties of doped silicon from 0.1 to 2 thz," *Applied Physics Letters*, vol. 56, no. 17, pp. 1694–1696, 1990.

[71] A. H. Yang, S. D. Moore, B. S. Schmidt, M. Klug, M. Lipson, and D. Erickson, "Optical manipulation of nanoparticles and biomolecules in sub-wavelength slot waveguides," *Nature*, vol. 457, no. 7225, pp. 71–75, 2009.

[72] W. L. Barnes, A. Dereux, and T. W. Ebbesen, "Surface plasmon subwavelength optics," *Nature*, vol. 424, no. 6950, pp. 824–830, 2003.

[73] J. Tian, C. Zhang, X. Liang, and H. Li, "Mode analysis of a symmetric hybrid surface plasmonic waveguide for photonic integration," *IEEE Journal of Quantum Electronics*, vol. 49, no. 3, pp. 331–334, 2013.

[74] M. J. Fitch and R. Osiander, "Terahertz waves for communications and sensing," *Johns Hopkins APL technical digest*, vol. 25, no. 4, pp. 348–355, 2004.

[75] M. Tonouchi, "Cutting-edge terahertz technology," *Nature photonics*, vol. 1, no. 2, pp. 97–105, 2007.

[76] M. Pereira and O. Shulika, *Terahertz and Mid Infrared Radiation: Detection of Explosives and CBRN (using Terahertz)*. Springer, 2014.

[77] R. Mendis, V. Astley, J. Liu, and D. M. Mittleman, "Terahertz microfluidic sensor based on a parallel-plate waveguide resonant cavity," *Applied Physics Letters*, vol. 95, no. 17, p. 171113, 2009.

[78] T. Ohkubo, M. Onuma, J. Kitagawa, and Y. Kadoya, "Micro-strip-line-based sensing chips for characterization of polar liquids in terahertz regime," *Applied physics letters*, vol. 88, no. 21, p. 212511, 2006.

[79] C. Gui and J. Wang, "Wedge hybrid plasmonic thz waveguide with long propagation length and ultra-small deep-subwavelength mode area," *Scientific reports*, vol. 5, 2015.

[80] W. Tang, L. Wang, X. Chen, C. Liu, A. Yu, and W. Lu, "Dynamic metamaterial based on the graphene split ring high-q fano-resonnator for sensing applications," *Nanoscale*, vol. 8, no. 33, pp. 15 196–15 204, 2016.

[81] L. Wang, X. Chen, A. Yu, Y. Zhang, J. Ding, and W. Lu, "Highly sensitive and wide-band tunable terahertz response of plasma waves based on graphene field effect transistors," *Scientific reports*, vol. 4, 2014.

[82] H. Tyagi and J. G. Rivas, "Photo-generated thz plasmonic waveguides," *Journal of Optics*, vol. 16, no. 9, p. 094011, 2014.

[83] L. Novotny, R. X. Bian, and X. S. Xie, "Theory of nanometric optical tweezers," *Physical Review Letters*, vol. 79, no. 4, p. 645, 1997.

[84] M. Righini, G. Volpe, C. Girard, D. Petrov, and R. Quidant, "Surface plasmon optical tweezers: tunable optical manipulation in the femtonewton range," *Physical review letters*, vol. 100, no. 18, p. 186804, 2008.

[85] A. Grigorenko, N. Roberts, M. Dickinson, and Y. Zhang, "Nanometric optical tweezers based on nanostructured substrates," *Nature Photonics*, vol. 2, no. 6, pp. 365–370, 2008.

[86] X. Yang, Y. Liu, R. F. Oulton, X. Yin, and X. Zhang, "Optical forces in hybrid plasmonic waveguides," *nano Letters*, vol. 11, no. 2, pp. 321–328, 2011.

[87] S. Mandal, X. Serey, and D. Erickson, "Nanomanipulation using silicon photonic crystal resonators," *Nano letters*, vol. 10, no. 1, pp. 99–104, 2009.

[88] W. Cao, C. Song, T. E. Lanier, R. Singh, J. F. O'Hara, W. M. Dennis, Y. Zhao, and W. Zhang, "Tailoring terahertz plasmons with silver nanorod arrays," *Scientific reports*, vol. 3, 2013.

[89] R. Oulton, G. Bartal, D. Pile, and X. Zhang, "Confinement and propagation characteristics of subwavelength plasmonic modes," *New Journal of Physics*, vol. 10, no. 10, p. 105018, 2008.

[90] J. Zhang, L. Cai, W. Bai, Y. Xu, and G. Song, "Hybrid plasmonic waveguide with gain medium for lossless propagation with nanoscale confinement," *Optics letters*, vol. 36, no. 12, pp. 2312–2314, 2011.

[91] [Online]. Available: www.tydexoptics.com/en/products/thzoptics_thzmaterials

[92] Y. Ma, G. Farrell, Y. Semenova, and Q. Wu, "A hybrid wedge-to-wedge plasmonic waveguide with low loss propagation and ultra-deep-nanoscale mode confinement," *Journal of Lightwave Technology*, vol. 33, no. 18, pp. 3827–3835, 2015.

[93] T. Ogawa, D. Pile, T. Okamoto, M. Haraguchi, M. Fukui, and D. Gramotnev, "Numerical and experimental investigation of wedge tip radius effect on wedge plasmons," *Journal of Applied Physics*, vol. 104, no. 3, p. 033102, 2008.

[94] H. Amarloo and S. Safavi-Naeini, "Slot plasmonic waveguide based on doped-gaas for terahertz deep-subwavelength applications," *JOSA A*, vol. 32, no. 11, pp. 2189–2194, 2015.

[95] G. Kumar, S. Li, M. M. Jadidi, and T. E. Murphy, "Terahertz surface plasmon waveguide based on a one-dimensional array of silicon pillars," *New Journal of Physics*, vol. 15, no. 8, p. 085031, 2013.

[96] T. Gric, M. S. Wartak, M. Cada, J. Wood, O. Hess, and J. Pistora, "Spoof plasmons in corrugated semiconductors," *Journal of Electromagnetic Waves and Applications*, vol. 29, no. 14, pp. 1899–1907, 2015.

[97] D. F. Pile and D. K. Gramotnev, "Channel plasmon–polariton in a triangular groove on a metal surface," *Optics Letters*, vol. 29, no. 10, pp. 1069–1071, 2004.

[98] K. Wang and D. M. Mittleman, "Metal wires for terahertz wave guiding," *Nature*, vol. 432, no. 7015, pp. 376–379, 2004.

[99] D. Grischkowsky, S. Keiding, M. Van Exter, and C. Fattinger, "Far-infrared time-domain spectroscopy with terahertz beams of dielectrics and semiconductors," *JOSA B*, vol. 7, no. 10, pp. 2006–2015, 1990.

[100] J. Choi, W. S. Kwon, K.-S. Kim, and S. Kim, "Nondestructive material characterization in the terahertz band by selective extraction of sample-induced echo signals," *Journal of Nondestructive Evaluation*, vol. 34, no. 1, pp. 1–9, 2015.

[101] F. M. Weinert, C. B. Mast, and D. Braun, "Optical fluid and biomolecule transport with thermal fields," *Physical Chemistry Chemical Physics*, vol. 13, no. 21, pp. 9918–9928, 2011.

[102] S. Adachi, *Handbook on physical properties of semiconductors*. Springer Science & Business Media, 2004, vol. 2.

[103] O. Madelung, *Semiconductors: data handbook*. Springer Science & Business Media, 2012.

[104] G. M. Whitesides, "The origins and the future of microfluidics," *Nature*, vol. 442, no. 7101, pp. 368–373, 2006.

[105] S. Prakash, M. Pinti, and B. Bhushan, "Theory, fabrication and applications of microfluidic and nanofluidic biosensors," *Philosophical Transactions of the Royal Society of London A: Mathematical, Physical and Engineering Sciences*, vol. 370, no. 1967, pp. 2269–2303, 2012.

[106] T. Kuykendall, P. J. Pauzauskie, Y. Zhang, J. Goldberger, D. Sirbuly, J. Denlinger, and P. Yang, "Crystallographic alignment of high-density gallium nitride nanowire arrays," *Nature materials*, vol. 3, no. 8, pp. 524–528, 2004.

[107] D. K. Gramotnev and S. I. Bozhevolnyi, "Plasmonics beyond the diffraction limit," *Nature photonics*, vol. 4, no. 2, pp. 83–91, 2010.

[108] C. Hahn, S. H. Song, C. H. Oh, and P. Berini, "Plasmonic gain in long-range surface plasmon polariton waveguides bounded symmetrically by dye-doped polymer," *Applied Physics Letters*, vol. 107, no. 12, p. 121107, 2015.

[109] G. V. Naik and A. Boltasseva, "A comparative study of semiconductor-based plasmonic metamaterials," *Metamaterials*, vol. 5, no. 1, pp. 1–7, 2011.

[110] A. Grigorenko, M. Polini, and K. Novoselov, "Graphene plasmonics," *Nature photonics*, vol. 6, no. 11, pp. 749–758, 2012.

[111] R. Singh and N. Zheludev, "Materials: Superconductor photonics," *Nature Photonics*, vol. 8, no. 9, pp. 679–680, 2014.

[112] G. V. Naik and A. Boltasseva, "Semiconductors for plasmonics and metamaterials," *physica status solidi (RRL)-Rapid Research Letters*, vol. 4, no. 10, pp. 295–297, 2010.

[113] A. K. Geim and K. S. Novoselov, "The rise of graphene," *Nature materials*, vol. 6, no. 3, pp. 183–191, 2007.

[114] K. S. Novoselov, V. Fal, L. Colombo, P. Gellert, M. Schwab, K. Kim *et al.*, "A roadmap for graphene," *Nature*, vol. 490, no. 7419, pp. 192–200, 2012.

[115] A. Tsiatmas, A. Buckingham, V. Fedotov, S. Wang, Y. Chen, P. De Groot, and N. Zheludev, "Superconducting plasmonics and extraordinary transmission," *Applied Physics Letters*, vol. 97, no. 11, p. 111106, 2010.

[116] Z. Tian, R. Singh, J. Han, J. Gu, Q. Xing, J. Wu, and W. Zhang, "Terahertz superconducting plasmonic hole array," *Optics letters*, vol. 35, no. 21, pp. 3586–3588, 2010.

[117] Y. Kurokawa and H. T. Miyazaki, "Metal-insulator-metal plasmon nanocavities: Analysis of optical properties," *Physical Review B*, vol. 75, no. 3, p. 035411, 2007.

[118] A. Tsiatmas, V. A. Fedotov, F. J. G. de Abajo, and N. I. Zheludev, "Low-loss terahertz superconducting plasmonics," *New Journal of Physics*, vol. 14, no. 11, p. 115006, 2012.

[119] J. Liu, R. Mendis, and D. M. Mittleman, "The transition from a tem-like mode to a plasmonic mode in parallel-plate waveguides," *Applied Physics Letters*, vol. 98, no. 23, p. 231113, 2011.

[120] S. V. Jayanti, J. H. Park, A. Dejneka, D. Chvostova, K. M. McPeak, X. Chen, S.-H. Oh, and D. J. Norris, "Low-temperature enhancement of plasmonic performance in silver films," *Optical Materials Express*, vol. 5, no. 5, pp. 1147–1155, 2015.

[121] K. K. Mei and G.-C. Liang, "Electromagnetics of superconductors," *IEEE transactions on microwave theory and techniques*, vol. 39, no. 9, pp. 1545–1552, 1991.

[122] A. J. L. Adam, "Review of near-field terahertz measurement methods and their applications," *Journal of Infrared, Millimeter, and Terahertz Waves*, vol. 32, no. 8-9, pp. 976–1019, 2011.

[123] A. Bitzer, A. Ortner, and M. Walther, "Terahertz near-field microscopy with subwavelength spatial resolution based on photoconductive antennas," *Applied optics*, vol. 49, no. 19, pp. E1–E6, 2010.

[124] F. Blanchard, A. Doi, T. Tanaka, H. Hirori, H. Tanaka, Y. Kadoya, and K. Tanaka, "Real-time terahertz near-field microscope," *Optics express*, vol. 19, no. 9, pp. 8277–8284, 2011.

[125] Y. Ma, J. Zhou, J. Pištora, M. Eldlio, N. Nguyen-Huu, H. Maeda, Q. Wu, and M. Cada, "Subwavelength insb-based slot wavguides for thz transport: concept and practical implementations," *Scientific Reports*, vol. 6, p. 38784, 2016.

[126] M. Z. Alam, J. Meier, J. Aitchison, and M. Mojahedi, "Gain assisted surface plasmon polariton in quantum wells structures," *Optics express*, vol. 15, no. 1, pp. 176–182, 2007.

Appendix A

Copyright Permission

A.1 Applied Physics Express's Permission

JJAP-Michiya Takekawa <takekawa@jsap.or.jp> Sun 6/19 permission@jsap.or.jp Dear Mohamed Eldlio,

Thank you for your e-mail. You can use the final version of the manuscript of this article as a part of the PhD thesis. The usage of the publisher version which appears on JJAP Online is not allowed.

Best regards,

Michiya Takekawa (Dr.) APEX/JJAP Copyright Division

A.2 IAENG Transactions on Engineering Technologies's Permission

Dear IAENG, I am the first author of the following book, while I was working toward my PhD degree. Now, I am preparing my PhD thesis for submission to the Faculty of Graduate Studies at Dalhousie University, Halifax, Nova Scotia, Canada. I am seeking your permission to include a manuscript version of the following chapter as a chapter in the thesis: 1. Mohamed Eldlio, Franklin Che, and Michael Cada, "Drude-Lorentz Model of Semiconductor Optical Plasmons", IAENG Transactions on Engineering Technologies, Lecture Notes in Electrical Engineering, Chapter 4, 41-49,(2014). 2. Mohamed Eldlio,

Franklin Che, and Michael Cada, “Optical Semiconductor Surface-Plasmon Dispersion Including Losses Using the Drude-Lorentz Model” Proceedings of the World Congress on Engineering and Computer Science 2012 Vol II ,WCECS 2012, October 24-26, 2012, San Francisco, USA Full publication details and a copy of this permission letter will be included in the thesis.

Best Regards,

Mohamed Eldlio

SPRINGER LICENSE TERMS AND CONDITIONS Mar 22, 2017

This Agreement between mohamed Eldlio (”You”) and Springer (”Springer”) consists of your license details and the terms and conditions provided by Springer and Copyright Clearance Center. License Number 4074320538718 License date Licensed Content Publisher Springer Licensed Content Publication Springer eBook Licensed Content Title Drude-Lorentz Model of Semiconductor Optical Plasmons Licensed Content Author Mohamed Eldlio, Licensed Content Date Jan 1, 2014; Type of Use Thesis/Dissertation Portion. Full text Number of copies 1. Author of this Springer article Yes and you are the sole author of the new work. Order reference number Dr. M. Cada . Title of your thesis / dissertation SEMICONDUCTOR-BASED HYBRID PLASMONICS. Expected completion date May 2017 Estimated size(pages) 133. Requestor Location mohamed Eldlio 1459 Oxford Street, Halifax, NS

Halifax, NS B3H 4R2 Canada Attn: Mohamed Eldlio Billing Type Invoice Billing Address Mohamed Eldlio 1459 Oxford Street, Halifax, NS

Halifax, B3H 4R2 Canada Attn: Mohamed Eldlio Total 0.00 CAD Terms and Conditions

by CCC) as provided in CCC's Billing and Payment terms and conditions. If full payment is not received by the date due, then any license preliminarily granted shall be deemed automatically revoked and shall be void as if never granted. Further, in the event that you breach any of these terms and conditions or any of CCC's Billing and Payment terms and conditions, the license is automatically revoked and shall be void as if never granted. Use of materials as described in a revoked license, as well as any use of the materials beyond the scope of an unrevoked license, may constitute copyright infringement and Springer reserves the right to take any and all action to protect its copyright in the materials. Copyright Notice: Disclaimer You must include the following copyright and permission notice in connection with any reproduction of the licensed material: "Springer book/journal title, chapter/article title, volume, year of publication, page, name(s) of author(s), (original copyright notice as given in the publication in which the material was originally published) "With permission of Springer" In case of use of a graph or illustration, the caption of the graph or illustration must be included, as it is indicated in the original publication. Warranties: None Springer makes no representations or warranties with respect to the licensed material and adopts on its own behalf the limitations and disclaimers established by CCC on its behalf in its Billing and Payment terms and conditions for this licensing transaction. Indemnity You hereby indemnify and agree to hold harmless Springer and CCC, and their respective officers, directors, employees and agents, from and against any and all claims arising out of your use of the licensed material other than as specifically authorized pursuant to this license. No Transfer of License This license is personal to you and may not be sublicensed, assigned, or transferred by you without Springer's written permission. No Amendment Except in Writing This license may not be amended except in a writing signed by both parties (or, in the case of Springer, by CCC on Springer's behalf). Objection to Contrary Terms Springer hereby objects to any terms contained in any purchase order, acknowledgment, check endorsement or other writing prepared by you, which terms are

inconsistent with these terms and conditions or CCC's Billing and Payment terms and conditions. These terms and conditions, together with CCC's Billing and Payment terms and conditions (which are incorporated herein), comprise the entire agreement between you and Springer (and CCC) concerning this licensing transaction. In the event of any conflict between your obligations established by these terms and conditions and those established by CCC's Billing and Payment terms and conditions, these terms and conditions shall control. Jurisdiction All disputes that may arise in connection with this present License, or the breach thereof, shall be settled exclusively by arbitration, to be held in the Federal Republic of Germany, in accordance with German law. Other conditions: V 12AUG2015 Questions? customercare@copyright.com or +1-855-239-3415 (toll free in the US) or +1-978-646-2777.

A.3 Infrared Physics & Technology Journal's Permission

Wed 12/28, 1:32 PM

journals@mail.elsevier.com;

Dear Editor-in-Chief

Infrared Physics & Technology,

I am the first author of the following journal, while I was working toward my PhD. degree. Now, I am preparing my PhD. thesis for submission to the Faculty of Graduate Studies at Dalhousie University, Halifax, Nova Scotia, Canada.

I am seeking your permission to include a manuscript version of the following paper as a chapter in the thesis:

M. Eldlio, Y. Ma, H. Maeda, and M. Cada, “A long-range hybrid TH plasmonic waveguide with low attenuation loss,” Infrared Physics & Technology, 2016.

Full publication details and a copy of this permission letter will be included in the thesis.

Best Regards,

Mohamed Eldlio

meldlio@dal.ca

Permission Letter PH Permissions

Helpdesk <permissionshelpdesk@elsevier.com>

12:24 PM

Mohamed Eldlio

Dear Mohamed,

As an Elsevier journal author, you retain the right to Include the article in a thesis or dissertation (provided that this is not to be published commercially) whether in part or in total, subject to proper acknowledgment; see http://www.elsevier.com/about/company-information/policies/copyright/personal-use for more information.

As this is a retained right, no written permission from Elsevier is necessary. As outlined in our permissions licenses, this extends to the posting to your university’s digital repository of the thesis provided that if you include the published journal article (PJA) version, it is embedded in your thesis only and not separately downloadable:

19. Thesis/Dissertation: If your license is for use in a thesis/dissertation your thesis may be submitted to your institution in either print or electronic form. Should your thesis be

published commercially, please reapply for permission. These requirements include permission for the Library and Archives of Canada to supply single copies, on demand, of the complete thesis and include permission for Proquest/UMI to supply single copies, on demand, of the complete thesis. Should your thesis be published commercially, please reapply for permission. Theses and dissertations which contain embedded PJAs as part of the formal submission can be posted publicly by the awarding institution with DOI links back to the formal publications on ScienceDirect.

Best of luck with your thesis and best regards,

Laura Laura Stingelin

Permissions Helpdesk Associate

ELSEVIER | Global E-Operations Books

+1 215-239-3867 office

l.stingelin@elsevier.com

Contact the Permissions Helpdesk

+1 800-523-4069 x3808 | permissionshelpdesk@elsevier.com

A.4 Japanese Journal of Applied Physics's Permission

JJAP-Michiya Takekawa <takekawa@jsap.or.jp>

10:11 PM Mohamed Eldlio;

jjap_edit@jsap.or.jp

Dear Dr. Mohamed Eldlio,

The Japan Society of Applied Physics (JSAP) gives you the permission to reproduce the material(s) you have requested under the condition that you follow the Copyright Policy of JSAP.

[Copyright Policy of JSAP]

http://www.jsap.or.jp/english/copyright_policy.html

Please indicate that the material is the reproduction from APEX/JJAP with volume number, issue number, page number/manuscript ID, published year, name of authors, and so on.

Sincerely yours,

Kazuo Hotate, Ph. D.,

President, the Japan Society of Applied Physics

(sent by APEX/JJAP copyright division)

Appendix B

LIST OF PUBLICATIONS

B.1 Book Edit

1. **Mohamed Eldlio**, Franklin Che, Michael Cada, "Drude-Lorentz Model of Semiconductor Optical Plasmons", Book Chapter(4), IAENG Transactions on Engineering Technologies, pp 41-49, 2014.

B.2 Papers Published in Peer-reviewed Journals

1. **Mohamed Eldlio**, Franklin Che, Michael Cada, "Optical Semiconductor Surface Plasmon Dispersion Including losses Using Drude-Lorentz Model", Journal Lecture Notes in Engineering and Computer Science, 2012.

2. Gric Tatjana, **Mohamed Eldlio**, Michael Cada, and Jaromír Pištora, "Analytic Solution to Field Distribution in Two-Dimensional Inhomogeneous Waveguides" Journal of Electromagnetic Waves and Applications, 29, 1068—1081, 2015.

3. **Mohamed Eldlio**, Youqiao Ma , Maeda Hiroshi, and Michael Cada, "A Long-Range Hybrid THz Plasmonic Waveguide with Low Attenuation Loss", Infrared Physics & Technology, 80 , PP. 93–99, 2017.

4. Youqiao Ma, **Mohamed Eldlio**, Maeda Hiroshi, Zhou Jun, and Michael Cada, " Plasmonic properties of Superconductor-Insulator-Superconductor waveguide", Applied Physics Express, 9, 072201, 2016.

5. **Mohamed Eldlio**, Youqiao Ma , Franklin Che, Maeda Hiroshi, and Michael Cada, "A THz Semiconductor Hybrid Plasmonic Waveguide with Suitable Fabrication-Error-Tolerance", Japanese Journal of Applied Physics, 56, 010306, 2017.

6. Youqiao Ma, Jun Zhou, Jaromír Pištora, **Mohamed Eldlio**, Nghia Nguyen-Huu, Hiroshi Maeda, Qiang Wu and Michael Cada; "Subwavelength InSb-based Slot wavguides for THz transport: concept and practical implementations", Scientific Reports, 6, 38784, 2016.

7. Youqiao Ma, Nghia Nguyen-Huu, Jun Zhou, Hiroshi Maeda, Qiang Wu, **Mohamed Eldlio**, Jaromír Pištora and Michael Cada, "Mach-Zehnder Interferometer-based Integrated Terahertz Temperature Sensor", Journal of Selected Topics in Quantum Electronics, Vol. 33, Issue 4, PP. 1-7, 2017.

8. Youqiao Ma, Yousef Alattar, Jun Zhou, **Mohamed Eldlio**, Hiroshi Maeda, Jaromir Pistora, Michael Cada, "Semiconductor-Based Plasmonic Interferometers for Ultrasensitive sensing in Terahertz Regime", Optics Letters 42, PP.2338-2341, 2017.

B.3 Conference Proceedings

1. **Mohamed Eldlio**, Franklin Che, Michael Cada, "Optical Semiconductor Surface Plasmon Dispersion Including losses Using Drude-Lorentz Model", World Congress on Engineering and Computer Science, (WCECS 2012) II: 1078-81, 2012.

2. Tatjana Gric , **Mohamed Eldlio**, and Michael Cada, “Challenge of Inhomogeneous Waveguides Analysis”, SPIE 9288, Photonics North, 2014.

3. **Mohamed Eldlio**, Tatjana Gric, D. Blazek, Michael Cada, “Surface Plasmon Polariton Dispersion in Inhomogeneous Semiconductors”, Photonics North, 2015.

4. Youqiao Ma, **Mohamed Eldlio**, Hiroshi Maeda, and Michael Cada, “Analysis of Superconductor based Waveguide at THz and Telecommunication frequencies”, Photonics North, 2016.

5. **Mohamed Eldlio**, Youqiao Ma, Hiroshi Maeda, and Michael Cada., “Analysis of inhomogeneous semiconductor-based hybrid plasmonic slot waveguide”, Photonics North, 2016.

6. Youqiao Ma, Yousef Alattar, **Mohamed Eldlio** , Nghia Nguyen-Huu, Hiroshi Maeda, and Michael Cada, “Plasmonic Semiconductor-Based Interferometers for Ultrasensitive THz Biosensing”, IEEE International Conference on Computational Electromagnetics, Kumamoto Japan, March 2017.